(6)

A TWO-HYDROPHONE TECHNIQUE FOR MEASURING THE COMPLEX REFLECTIVITY OF MATERIALS IN WATER-FILLED TUBES

Scott Sutherland Corbett III

Technical Memorandum
File No. TM 82-246
September 27, 1982
Contract No. NOOO24-79-C-6043

Copy No. 6

The Pennsylvania State University
Intercollege Research Programs and Facilities
APPLIED RESEARCH LABORATORY
Post Office Box 30
State College, PA 16801

NAVY DEPARTMENT

NAVAL SEA SYSTEMS COMMAND

UNCLASSIFIED

SECURITY CLASSIFICATION OF THIS PAGE (When Data Entered)

REPORT DOCUMENTATION PAGE		READ INSTRUCTIONS BEFORE COMPLETING FORM
1. REPORT NUMBER 82-246	2. GOVT ACCESSION NO. AD-A138 613	3. RECIPIENT'S CATALOG NUMBER
4. TITLE (and Subtitle) A Two-Hydrophone Technique for Measuring the Complex Reflectivity of Materials in Water-Filled Tubes		5. TYPE OF REPORT & PERIOD COVERED M.S. Thesis, May 1983 6. PERFORMING ORG. REPORT NUMBER 82-246
7. AUTHOR(s) Scott Sutherland Corbett III		8. CONTRACT OR GRANT NUMBER(s) N00024-79-C-6043
9. PERFORMING ORGANIZATION NAME AND ADDRESS The Pennsylvania State University Applied Research Laboratory, P.O. Box 30 State College, PA 16801		10. PROGRAM ELEMENT, PROJECT, TASK AREA & WORK UNIT NUMBERS
11. CONTROLLING OFFICE NAME AND ADDRESS Naval Sea Systems Command Department of the Navy Washington, DC 20362		12. REPORT DATE Sept. 27, 1982 13. NUMBER OF PAGES 160 pp.
14. MONITORING AGENCY NAME & ADDRESS(if different from Controlling Office)		15. SECURITY CLASS. (of this report) Unclassified, Unlimited 15a. DECLASSIFICATION/DOWNGRADING SCHEDULE

16. DISTRIBUTION STATEMENT (of this Report)

Approved for public release, distribution unlimited, per NSSC (Naval Sea Systems Command), 24 February 1983

17. DISTRIBUTION STATEMENT (of the abstract entered in Block 20, if different from Report)

18. SUPPLEMENTARY NOTES

19. KEY WORDS (Continue on reverse side if necessary and identify by block number)

hydrophone, measurement, reflectivity, thesis

20. ABSTRACT (Continue on reverse side if necessary and identify by block number)

A two-microphone technique has been developed by Blaser, Chung, Seybert, and others for measuring the complex reflection factor, and through it the complex acoustic imedance, of a material surface in tubes containing air. The procedure consists of simultaneously sampling the stationary acoustic field at two locations in front of an ensonified sample. This thesis describes an extension of this technique to measure the same characteristics in water-filled tubes. However, because of the close acoustic coupling between the water and

DD FORM 1 JAN 73 1473 EDITION OF 1 NOV 65 IS OBSOLETE UNCLASSIFIED

SECURITY CLASSIFICATION OF THIS PAGE (When Data Entered)

the tube walls, a number of modifications were needed in order to implement the technique. These included the development, after several attempts, of a two-hydrophone system that did not perturb the acoustic field and yet was isolated from any structure-borne noise, and the development of more elaborate signal processing procedures in which pulses of sound rather than a continuous sound field were projected to ensonify the tube. Subsequent measurements indicated that the technique could be performed in water using both pulsed and continuous sound fields. A comparison of measured values of the complex reflection factor of three different simple terminations (air, steel, rubber), using the two-hydrophone technique and the more conventional standing wave ratio procedure, indicates good agreement over the frequency range of interest, with the added advantage of a considerable savings in time and experimental effort.

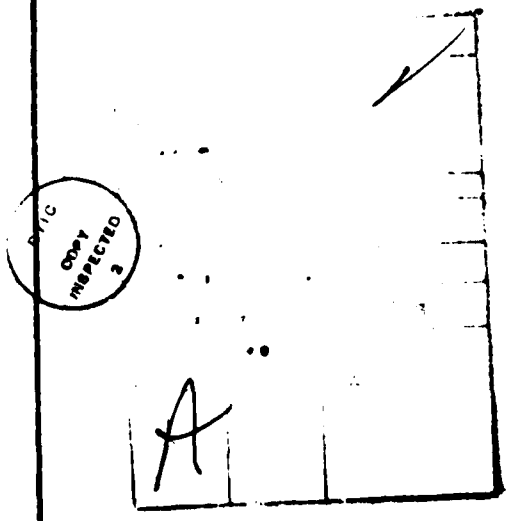

Abstract

A two-microphone technique has been developed by Blaser, Chung, Seybert, and others for measuring the complex reflection factor, and through it the complex acoustic impedance, of a material surface in tubes containing air. The procedure consists of simutaneously sampling the stationary acoustic field at two locations in front of an ensonified sample. This thesis describes an extension of this technique to measure the same characteristics in water-filled tubes. However, because of the close acoustic coupling between the water and the tube walls, a number of modifications were needed in order to implement the technique. These included the development, after several attempts, of a two-hydrophone system that did not perturb the acoustic field and yet was isolated from any structure-borne noise, and the development of more elaborate signal processing procedures in which pulses of sound rather than a continuous sound field were projected to ensonify the tube. Subsequent measurements indicated that the technique could be performed in water using both pulsed and continuous sound fields. A comparison of measured values of the complex reflection factor of three different simple terminations (air, steel, rubber), using the two-hydrophone technique and the more conventional standing wave ratio procedure, indicates good agreement over the frequency range of interest, with

the added advantage of a considerable savings in time and experimental effort.

TABLE OF CONTENTS

	Page
ABSTRACT	iii
LIST OF FIGURES	viii
NOMENCLATURE	xii
ACKNOWLEDGEMENTS	xvi
Chapter	
1. BACKGROUND	1
1.1 Introduction	1
1.2 Impedance Measuring Methods	3
1.3 Tube Techniques	4
1.3.1 In-Air Measurements	5
1.3.2 In-Water Measurements	9
1.4 Objectives and Approach	12
1.4.1 Statement of Problem	12
1.4.2 Organization of Investigation	13
2. THEORY	14
2.1 The Sound Field at the Tube Termination	14
2.2 The Standing Wave Ratio Method	19
2.3 The Two-Microphone Method	22
2.4 The Two-Hydrophone Method in the Pulse Tube	28
2.4.1 Signal Processing Procedures Using Pulses	29
3. TRANSDUCER DEVELOPMENT AND EVALUATION	37
3.1 Transducer Selection and Construction	37
3.1.1 Wall-Mounted Transducers	39

Page

3.1.2 PVDF Transducers 39

3.1.3 Composite PZT Transducers 46

3.2 Evaluation of Transducers 47

3.2.1 Measurement of the Mechanical and Acoustical Sensitivity 47

3.2.2 Measurement of the Insertion Loss . . 53

3.2.3 Measurement of the Transfer Function . 57

3.3 Effect of Pulse Length 63

3.4 Calibration of the Two-Hydrophone Probe . . . 63

3.4.1 Modified Switching Technique 66

3.4.2 Plane-Wave Technique 70

3.4.3 Comparison of Modified Switching Technique and Plane Wave Technique . . 73

4. EXPERIMENTAL PROCEDURES AND RESULTS 74

4.1 The Measuring Facility 75

4.2 Determination of the Phase Velocity 77

4.3 Experimental Technique 78

4.3.1 Standing Wave Ratio Measurements . . . 79

4.3.2 Two-Hydrophone Measurements 81

4.4 Presentation of Data 87

4.4.1 Pressure Release Termination 87

4.4.2 Steel Disk Termination 92

4.4.3 Absorbing Sample Termination 97

4.5 Precision of Measurement Results 101

4.5.1 Precision of Standing Wave Ratio Measurements 103

4.5.2 Precision of Two-Hydrophone Method . . 105

5. CONCLUSIONS AND RECOMMENDATIONS 110

Page

APPENDIX A: WAVE PROPAGATION IN CYLINDRICAL DUCTS . . 118

APPENDIX B: THE TUBE-FLUID INTERACTION 127

APPENDIX C: SIGNAL PROCESSSING PROCEDURES AND ERROR CONSIDERATIONS 131

APPENDIX D: PIEZOELECTRIC COEFFICIENTS AND TRANSDUCER SENSITIVITY 136

LIST OF FIGURES

Figure		Page
1.	Illustration of an incident $\bar{A}e^{-jkx}$ and reflected, $\bar{B}e^{+jkx}$, plane wave near the tube's termination	16
2.	Examples of how the normalized pressure magnitude varies as a function of kx for the case of: (a) varying the magnitude of the reflection factor, R, for $\phi = 0°$, and (b) varying the phase of the reflection factor, ϕ, for R = 1	18
3.	Location of the two hydrophones, x_1 and x_2, relative to sample surface at x = 0	23
4.	Magnitude and phase of the transfer function, $\bar{H}(f)$, computed for an ideal pressure release surface ($\bar{R}$ = -1) when the hydrophone separation, S = 1", and the two-hydrophone unit is at two different locations from the surface	27
5.	Illustration of how the sampling time T can be shown to depend on the pulse duration of the incident wave and the distance of the furthest hydrophone, x_2, from the sample surface. . . .	30
6.	Time history of the pressure field measured near the air surface of a water-filled acoustic tube for a 6 msec, 2 kHz incident pulse	32
7.	Theoretical sampling time, T, for various pulse durations and locations of the furthest hydrophone, x_2, as illustrated	33
8.	Upper frequency limit of two-hydrophone technique as a function of transducer separation distance $S = x_2 - x_1$	35
9.	Schematic of the two different types of wall mounted hydrophones investigated: the upper unit was a commercially procured Celesko LD-25; the lower unit was custom-made by the author	40
10.	Schematic of jig used to assemble the PVDF thin film material onto the stainless steel or lucite support rings	44
11.	Experimental set-up used to measure the mechanical sensitivity of the hydrophones in the water-filled pulse tube	49

Figure | Page

12. Measured mechanical sensitivities of the five different hydrophones investigated for possible use with the two-hydrophone technique in the water-filled pulse tube 52

13. Measured acceleration level of pulse tube wall normalized by the acoustic pressure inside the tube 54

14. Measured pressure level in tube showing insertion loss for stainless-steel, lucite and PZT-composite probes 56

15. Instrumentation set-up used to measure the transfer function between hydrophones 1 and 2 near the tube's termination 58

16. Measured coherence and transfer function for pressure release termination using the Lucite PVDF probes at x_1=1" and x_2=2" under pulsed excitation 60

17. Measured coherence and transfer function for pressure release termination using the PZT composite probes at x_1=1" and x_2=2" under pulsed excitation 61

18. Measured coherence and transfer function for pressure release termination using PZT probe at x_1=1" and x_2=2" under continuous excitation . . 64

19. Schematic of modified switching technique for calibrating the transfer function (a) initial configuration and (b) switched configuration . . 68

20. Transfer function calibrations for the PZT composite hydrophones measured using the plane-wave and the switching techniques 71

21. Schematic of plane-wave techniques for calibrating the transfer function 72

22. Relative phase response between two similar transducers measured at tube's termination showing propagation of higher order modes . . . 76

23. Experimental configuration for standing wave measurement in the water-filled pulse tube . . 80

24. Pressure level in standing wave field measured near tube's termination as a function of frequency for various locations away from pressure release surface (air) 82

Figure		Page
25.	Standing wave field measured for a pressure release termination (air) at frequencies of (a) 9.2 kHz and (b) 12 kHz. Wavelength tic marks where computed assuming a wave velocity of 1460 m/sec	83
26.	Standing wave field measured for pressure release termination (air) at frequencies of (a) 13.7 kHz and (b) 19.7 kHz. Wavelength tic marks where computed assuming a wave velocity of 1460 m/sec .	84
27.	Experimental set-up for two-hydrophone technique in a water-filled tube	86
28.	Measured coherence between the two PZT hydrophones at x_1=1" and x_2=2" for the case of air termination	88
29.	Measured transfer function between the two PZT hydrophones at x_1=1" and x_2=2" for the case of air termination	89
30.	Comparison of the reflection factors of an air termination using the standing wave technique (circles) and the two-hydrophone technique (solid lines)	91
31.	Measured coherence function between the two PZT hydrophones at x_1=1" and x_2=2" for the case of an air-backed 3/8" thick steel disk	93
32.	Measured transfer function between the two PZT hydrophones at x_1=1" and x_2=2" for the case of an air-backed 3/8" thick steel disk	94
33.	Theoretical calculation of the transfer function for an ideally rigid termination	95
34.	Comparison of the reflection factors for the air-backed 3/8" thick steel disk using the standing wave technique (circles) and the two-hydrophone technique (solid lines)	95
35.	Measured coherence function between the two PZT hydrophones at x_1=1" and x_2=2" for the case of an absorbing sample termination	98
36.	Measured transfer function between the two PZT hydrophones at x_1=1" and x_2=2" for the case of an absorbing sample	99

Figure		Page
37.	Comparison of the reflection factors for the absorbing sample using the standing wave techniques (circles) and the two-hydrophone technique (solid lines)	100
38.	Theoretical error in reflection factor phase as a function of phase velocity, c and location, x_1 and x_2, tolerances in the tube using the standing wave technique for an ideal pressure release surface	104
39.	Theoretical error in reflection factor phase as a function of phase velocity, c, and location, x_1 and x_2, tolerances using the two-hydrophone technique for an ideal pressure release surface .	108
40.	Cylindrical coordinate system used in computing the normal modes of wave propagation in a circular duct	121
41.	Tabulation of the value of the roots of the derivative of the Bessel Function of the first kind of order m	124
42.	Instantaneous pressure polarity (left) and corresponding pressure amplitude distribution (right) for four transverse modes of a circular duct with rigid walls	125
43.	Illustration of the piezoelectric effect associated with the transverse (upper) and the longitudinal (lower) deformations	138
44.	Low frequency equivalent circuit for a typical piezoelectric transducer, including the capacitance of the connecting cable.	140

NOMENCLATURE

$\bar{A}$	complex amplitude of incident pressure field
$\bar{B}$	complex amplitude of reflected pressure field
c	propagation velocity
c_{eff}	effective propagation velocity in tube with compliant walls
c_o	free-field propagation velocity in fluid
c_w	propagation velocity in tube material
C_{EM}	motional capacitance of piezoelectric transducer
C_o	electrical capacitance of piezoelectric transducer
d_{ij}	piezoelectric charge coefficient in ij direction
d_{3h}	hydrostatic piezoelectric charge coefficient
D	tube diameter
$E[\ ]$	expected value operator
E_i	electric charge per unit area
f	frequency
f_B	frequency band
f_c	center frequency of frequency band
f_{mn}	cut - off frequency for m,n mode in duct
F_j	force per unit area
g	acceleration
g_{ij}	piezoelectric voltage coefficient in ij direction
g_{3h}	hydrostatic piezoelectric voltage coefficient
G_{11}	auto-spectral density of pressure at location 1
G_{11}	estimated auto-spectral density of pressure at location 1

G_{12}	cross-spectral density between pressures at location 1 and 2
G_{12}	estimated cross-spectral density between pressures at locations 1 and 2
h	tube thickness
$\bar{H}$	complex transfer function between pressures at locations 1 and 2
$\bar{H}_{I1}$, $\bar{H}_{I2}$	frequency response of transducers, filters and amplifiers comprising channels 1 and 2, respectively
$\bar{H}^{Mi}$, $\bar{H}^{Ms}$	measured transfer function between channels 1 and 2 for initial and switched configuration, respectively
$H_m^{(1)}$, $H_m^{(2)}$	Hankel functions of the first and second kind, respectively, and order m
J_m	Bessel function of the first kind and order m
J'_m	first derivative of Bessel function
k^2	electro-mechanical coupling coefficient
k_z	wavenumber in z direction
k_r	wavenumber in radial direction
k_{mn}	value of k_r for m,n mode in duct
M_o	free-field voltage sensitivity
(m,n)	mode number, m denotes circumferential dependence, n denotes radial dependence
n_d	number of sample records
N_m	Neuman function of order m
p	pressure
$\bar{P}$	Fourier transform of pressure
P	magnitude of pressure
$\bar{P}_1$, $\bar{P}_2$	Fourier transform of total acoustic pressure at locations 1 and 2, respectively
Pa	Pascals

P_{1k}, P_{2k}	finite Fourier transform of pressure at locations 1 and 2, respectively, over the k^{th} record
r	radial coordinate
r_n	real component of normal specific acoustic impedance
R	magnitude of reflection factor or tube radius
$\bar{R}$	complex reflection factor
s	separation distance between locations x_1 and x_2
SWR	standing wave ratio
t	time coordinate or transducer thickness
T	sampling time
T_p	pulse duration
T_j	mechanical stress
u	velocity
V	voltage
x	distance coordinate
x_1, x_2	distance from tube termination to hydrophones 1 and 2, respectively
x_{min}	distance from tube termination to pressure minimum in standing wave field
X_n	reactive component of normal specific acoustic impedance
$\bar{Y}_1$, $\bar{Y}_2$	Fourier transform of pressure measured from channels 1 and 2, respectively
$\bar{Y}_1^i$, $\bar{Y}_2^i$	Fourier transform of pressure measured from channels 1 and 2, respectively, in initial configuration
$\bar{Y}_1^s$, $\bar{Y}_2^s$	Fourier transform of pressure measured from channels 1 and 2, respectively, in switched configuration
z	axial coordinate
Z_A	characteristic impedance of air

z_o	characteristic impedance of water
z_n	normal specific acoustic impedance
$\mathcal{Z}$	normalized specific acoustic impedance ($Z_n/\rho c$)
α_{mn}	roots of $J'_m(\alpha_{mn})=0$
γ_{12}^2	coherence function
Δ_f	frequency resolution
ε_o	permittivity constant
θ	circumferential coordinate
K_3	relative dielectric constant in 33 direction
λ	wavelength
λ_E	Young's modulus
ε	normalized random error
ρ	density
ρ_o	density of fluid
ρ_w	density of tube material
σ	normalized phase of reflection factor (ϕ/π)
ϕ	phase of reflection factor or phase of transfer function
ϕ_f	transformation factor
ω	angular frequency
$\omega_{m,n}$	angular frequency of m,n mode
$\lvert\ \rvert$	absolute value
*	complex conjugate or multiplication
~	stationary random variable
∇^2	Laplacian operator

ACKNOWLEDGEMENTS

This work was performed at the Applied Research Laboratory of The Pennsylvania State University under contract with the Naval Sea Systems Command.

The author would like to express his sincere appreciation and thanks to his adviser, Dr. Alan Stuart, who provided many hours of patient guidance and advice throughout the project. This project could not have been completed without the help of many staff members of the Applied Research Laboratory who rendered assistance in many forms. Special thanks goes to Dan Digiannantoni for his work on the transducer assembly jig, Lowell Stover for his help in machining the transducer parts and experimental equipment, and the staff of the Anechoic Tank Facility for their help in transducer calibration. The assistance of A. Safari and T.R. Gururaja at the Materials Research Lab is also gratefully acknowledged. Lastly, the author wishes to thank Dr. W. Jack Hughes and Dr. James Lawther for providing valuable input concerning the project and for serving on the defense committee.

CHAPTER 1

BACKGROUND

1.1 Introduction

The reflection and transmission of sound at a boundary is an important problem in both air and underwater acoustics. In architectural acoustics for example, the interaction of sound in a room with the surrounding walls is a primary consideration in describing the acoustic field within the room. A boundary can be considered as an abrupt discontinuity of the material properties between the acoustic fluid (air or water) and the bounding medium.

Two conditions must be satisfied at all times at the surface separating the two media: 1) the acoustic pressures on each side of the boundary must be equal, and 2) the normal particle velocities at the surface must be the same. Plane waves normally incident upon a flat boundary constitute the simplest form of boundary owing to the mathematical simplicity of formulating the above constraints. In the time harmonic case, the two continuity conditions at the interface can be satisfied by equating the ratio of acoustic pressure over the normal component of particle velocity on the incident side to the normal

specific acoustic impedance $\bar{Z}_n$ of the boundary. Since the pressure and particle velocity may not be in phase at the boundary, the normal specific acoustic impedance may be complex:

$$\bar{Z}_n = r_n + jx_n$$

where r_n is the resistive component and x_n the reactive component of the complex impedance.

The normal specific acoustic impedance of the boundary layer relative to the characteristic or wave impedance, ρc, of the acoustic fluid determines the reflection and transmission properties of the boundary. It is therefore an important parameter in predicting the performance of a material in a particular acoustic application and a great deal of effort has been expended since the turn of the century developing methods to accurately measure the specific acoustic impedance of surfaces.

This paper is concerned with the feasibility of adapting a specific measuring technique- the two-microphone method, developed for measuring the specific acoustic impedance of materials in air using tubes, for use in underwater applications. First however, it is instructive to briefly review the various techniques that have been developed to measure the specific acoustic impedance of a boundary.

1.2 Impedance Measuring Methods

The various schemes to measure the specific acoustic impedance can be roughly divided into three major groups including: [1]

1. Surface methods; where data such as volume velocity or pressure is measured at or very near the surface of a sample.
2. Comparison methods; where a known standard of acoustic impedance is compared to a measurement using an acoustic or electroacoustic bridge.
3. Transmission line methods, where data is taken somewhat removed from the surface, and where sound transmission is regarded as analogous with electromagnetic waves propagating through a transmission line, which treats one-dimensional propagation through a distributed system of series inductance and shunt capacitance.

Beranek [1] provides a comprehensive overview of the various surface, comparison and transmission line methods in common use up until 1948 to measure the acoustic impedance of materials in air. Bobber [2] gives a description of procedures used to measure the properties of materials including the acoustic impedance in underwater applications.

Transmission line methods are most commonly used today because of their experimental simplicity, accuracy and their realistic approximation to actual physical systems. Such techniques commonly involve the transmission of sound through pipes or ducts to insure that one-dimensional plane waves are normally incident on the sample material to be

measured. A review of various tube techniques developed for air and underwater measurements and their historical development follows in the next two sections.

1.3 Tube Techniques

As previously stated, tubes or ducts are commonly used in transmission line impedance measurements including the two-microphone technique under investigation in this thesis. It is therefore important to understand the limitations of treating sound transmission through ducts by simple transmission line theory.

The following is a brief description of sound propagation through infinitly long ducts; for a more detailed explanation see Appendix A. Such propagation can be treated by solving the wave equation for the specified tube geometry and boundary conditions. The wave equation is satisfied by an infinite series of solutions (modes) which define the acoustic field within the tube. The modes are designated by integer numbers (m,n). In a cylindrical duct, the m denotes the circumferential dependence of the pressure distribution (the number of circumferential nodes) and the n denotes the radial pressure distribution (the number of radial nodes between the center and the outside radius) for a particular mode. For finite length tubes, there would be another discrete set of wave numbers corresponding to resonances between the axial terminations. The (0,0) mode designates a plane wave transmitted in the axial direction

with uniform pressure distribution across the duct cross section (i.e. the case treated by transmission line theory) which propagates at a free-field sound velocity. All higher order modes have a non-uniform pressure distribution and a cutoff frequency. Below the cutoff, the mode will decay exponentially in the axial direction (i.e. will not propagate). Above the cutoff, the phase velocity of each mode will be faster than the free field phase velocity. Higher order modes in general are divided into two classifications, non-spinning modes, (0,n), in which the wave front travels in a purely axial direction, and spinning modes, (m,n), in which the wave front propagates in a spiral fashion. As long as the excitation frequency is below all higher order mode cutoff frequencies (i.e. the wavelength is long compared with the radial dimensions), then the wave propagation should be uniform across the duct cross-section, the one-dimensional case treated by transmission line theory.

1.3.1 In-Air Measurements

The first in-air measuring technique utilizing sound transmission through a duct was offered in 1913 by H.O. Taylor [3], who developed a method of measuring the sound absorption of a material by using a representative sample for the acoustic termination of a tube. By exciting a tube at one end with a pure tone and then measuring the maximum and minimum amplitude of the resultant standing wave created

by the superposition of the wave incident upon and the wave reflected from the end terminated by the sample, an expression for the absorption of the material was obtained. Taylor's work relied on the research of Helmholtz, Kundt, Kirchhoff, Rayleigh, Korteweg, Poisson and others, who examined the physical processes of sound propagation in pipes. As early as 1817, Poisson had developed a theoretical model of stationary waves for tubes of finite length which Helmholtz later expanded. In 1820, Poisson dealt with the case of an abrupt change in cross-section of a tube as well as the reflection and transmission of sound at normal incidence on the boundary between two different fluids [4]. In 1868, A. Kundt developed an experimental method for analyzing the sound field in tubes; specifically he measured the velocity of sound by using dust figures to view standing wave patterns. Tubes in which acoustic measurments are performed are frequently referred to as "Kundt tubes". The effects of fluid friction and viscosity on sound in tubes were investigated by Rayleigh [4].

Taylor's method was valid only for sound normally incident on the sample material. The tube (with a diameter much smaller than the smallest wavelength under consideration) provided a convenient means of ensuring perpendicular incidence upon the sample.

The successful use of the concept of electrical impedance precipitated the introduction of the term "acoustical impedance" by A.G. Webster in 1919 [1]. This complex quantity of pressure divided by the normal component of particle velocity at a given point accounted for all the quantities involved in the reaction of an acoustical system, and greatly simplified conceptual and notational problems. Wente and Bedell [5] in 1928 modified the measuring technique of Taylor by accounting for the phase shift in the nodes of the standing wave to include the calculation of acoustical impedance.

This technique was further developed and refined by a number of researchers [6-9]. The primary experimental problems involved accurately measuring the sound pressure within a tube, and thus defining the standing wave, without perturbing the sound field. Several approaches to the problem were offered. Taylor's original method was refined by Hall [6], who in 1939 developed an approach of imbedding a small microphone in one side of a square measuring tube, which could then be moved relative to the other sides. R.A. Scott [10], in 1946 used a small probe tube which was moved along inside the main tube. A third approach suggested by Bolt and Petrauskas [11] in 1943 but apparantly never implemented, used two fixed microphones of known separation to measure the pressure within the tube and thus resolve the standing wave.

The standing wave ratio method described above, in which the phase and amplitude of the standing wave inside a tube with a specific acoustic termination is determined, has proved to be the most popular technique to measure acoustic impedance. The technique has been refined to account for losses through dissipation at the tube walls, and is generally considered quite accurate if the proper precautions are taken [12]. There are, however, distinct disadvantages in using such an approach. The technique is very time consuming in that the standing wave is typically measured by manually traversing a microphone mechanism inside the tube while exciting the tube at discrete frequencies. It is suggested that the tube be at least one wavelength long, which can be a significant problem at low frequencies. The location of the first minimum must also be determined with a high degree of accuracy to avoid errors [13].

To circumvent these problems, Seybert and Ross in 1977 [14] and Chung and Blaser in 1980 [15] utilized modern signal processing hardware to implement the stationary two-microphone technique first introduced by Bolt and Petrauskas [11]. The cross-spectral density or the transfer function between two microphones, measured during excitation of the tube by broad band random noise, is used to resolve the incident and reflected fields. This decomposition then leads to the determination of the complex impedance. This

method has the advantage of avoiding discrete excitation of the tube and eliminates the need to manually transverse a microphone to resolve the standing wave in the tube. The result is that the two-microphone technique is not nearly as time consuming, however, it requires a dual-channel spectrum analyzer and complicated manipulation of data requiring computing facilities.

1.3.2 In-Water Measurements

The impedance measuring techniques thus described, have been developed principally for making measurements in air. Before and during the Second World War, considerable attention was devoted to developing anechoic materials for use underwater. The Germans were the first to develop refined techniques for measuring the underwater acoustic impedance of materials as part of their effort to silence submarines from sonar signals. The group of Walter Kuhl, Konrad Tamm, Hermann Oberst and Eugen Skudrzyk, under the direction of Ernst Meyer, systematically approached the problem of making underwater measurements and are responsible for much of our knowledge in this area [16,17].

The basic problem of applying the methods used in air to water involve the coupling of sound between the tube and the water contained within it [16]. The impedance of water

($\rho c = 1.48 * 10^6$ MKS Rayls) is much closer to steel ($\rho c = 39.0 * 10^6$ MKS Rayls) than is the impedance of air (c= 415 MKS Rayls). As a result, a significant amount of water-borne acoustical energy can be coupled into the tube itself. The resulting structure-borne energy can be reradiated into the water and interfere with measurements inside the tube. Some specific mechanisms involved in this coupling, and their effect upon measurements made in tubes are discussed in Appendix B.

Gmelin and Seiberth appear to be the first to introduce the Kundt tube into underwater sound techniques [16]. Whereas measurements in air are made on standing waves inside the tube during continuous excitation, the technique used with water involves sound pulses of short duration allowing the temporal separation of the incident and reflected fields. Tubes used in this manner are often referred to as "pulse" tubes. In underwater measurements, sound absorption is usually the most important quality characterizing a material so that a simple comparison between the amplitude of the wave reflected off a particular absorbing surface with the wave reflected off a completely reflective surface will suffice. If acoustic impedance is required, the phase as well as the amplitude differences between the two fields must be considered.

There are several advantages in using sound pulses. Less energy is coupled into the wall since the build-up time

of the tube wall oscillations is long compared to the short duration of the sound pulse. Typically one reciprocal transducer located at the bottom termination of the tube, can act as both transmitter and receiver, thus simplifying measurements. Samples can be tested under various pressures as no transversing mechanism is involved which would complicate sealing the tube. Finally, anomalous behavior at certain frequencies due to tube vibrations or other irregularities can be easily detected as extraneous or distorted pulses, so that measurements at these frequencies can be weighted less heavily [16].

The pulse technique has received almost universal acceptance as an accurate measurement of sound absorption for normally incident sound, where the phase change at the reflecting surface is not required. Various researchers have refined the technique and investigated in detail several aspects of the measuring scheme, including the tube wall-water interaction and the effects of higher order modes propagating inside the tube [17-21].

Impedance measurements using the pulse technique are problematic however, on account of the difficulty in measuring the phase change in the reflected wave. Various schemes have been developed to measure impedance using pulses, but they all suffer the common disadvantage of requiring a relative comparison with a reference reflector.

Such schemes also demand a significant amount of time as they involve making measurements at discrete frequency intervals. It appears however, that the transfer function technique developed by Seybert and Ross [14] and Blazer and Chung [15] for making impedance measurements in tubes containing air may also be appropriate for making measurements in tubes containing water [22].

1.4 Objectives and Approach

1.4.1 Statement of Problem

This thesis will investigate the feasibility of adapting the two-microphone technique to allow impedance measurements in water. This necessitates the development of suitable transducers which are insensitive to structure-borne noise in the tube wall, and which can be mounted inside the tube without perturbing the field. In addition, signal processing techniques which allow the transfer function to be performed on pulses captured at suitable moments of overlap between the incident and reflected fields in front of the tube's termination must be developed. We will refer to this technique as the two-hydrophone method. Such a technique combines the advantages of the two-microphone method (no reference required, very short measurement time), with the advantages of the pulsing technique (measurements possible at various pressures, small build up of tube wall vibrations).

1.4.2 Organization of Investigation

This study can be broadly categorized into three phases. The first phase was involved with the theoretical concerns in adapting the two-microphone method to the pulse tube, principally the signal processing procedures that had to be followed to allow the use of pulses in the tube. Next adaquate transducers had to be developed for the measuring scheme. This second phase entailed a considerable amount of time as a wide variety of transducers and testing procedures were developed before a suitable transducer was found. In the final phase, measurements were performed with the transducers to compare the traditional standing wave ratio method with the two-hydrophone technique.

Chapter 2 presents the theoretical development of both the standing wave ratio method and the two-microphone technique, and concludes with the specifics of how the two-microphone method can be adapted for use with pulse tubes. Chapter 3 describes the development and testing of the various transducers. The experimental procedure and a discussion of the experimental results including a comparison of measurements made on sample surfaces using both the standing wave ratio method and the two-hydrophone technique are presented in Chapter 4. Chapter 5 discusses the conclusions and presents recommendations for future work.

CHAPTER 2

THEORY

In this chapter we develop the theory of both the standing wave ratio method and the two-microphone or transfer-function technique for measuring the complex impedance of a surface. Adapting the two-microphone technique to making pulse measurements in water-filled tubes is then discussed. Both these methods are valid only for planar wave propagation, so that the tube in which the measurements are to be performed is assumed to be operating below its first cutoff frequency (i.e. the wavelengths are long compared with the tube diameter).

2.1 The Sound Field at the Tube Termination

Once a plane wave propagating inside a tube reaches the tube termination, it will reflect back and combine with the incident wave. The magnitude and phase of the returning wave will depend on the particular termination of the tube. Figure 1 shows the configuration at the termination. The incident plane wave $\bar{A}e^{j(wt-kx)}$ is partially reflected, represented by $\bar{B}e^{j(wt+kx)}$. The phase information is contained in the complex magnitudes $\bar{A}$ and $\bar{B}$. The total pressure on the incident side of the reflector is given by the sum of the incident and reflected fields (dropping the

time dependence):

$$\bar{P}(x) = \bar{A}e^{-jkx} + \bar{B}e^{jkx} \qquad (2.1)$$

$$= \bar{A}(e^{-jkx} + \bar{R}e^{jkx}) \qquad (2.2)$$

where $\bar{R}=\bar{B}/\bar{A}=Re^{j\emptyset}$, is called the reflection factor, and is the ratio of the complex amplitudes of the reflected and incident waves. The magnitude of $\bar{R}$ can vary between 0 and 1, and the phase can vary from 0 to $\pm 180^{o}$. The pressure can be rewritten as follows:

$$\bar{P}(x) = \bar{A}(e^{-jkx} + \bar{R}e^{jkx} + \bar{R}e^{-jkx} - \bar{R}e^{-jkx}) \qquad (2.3)$$

$$= \bar{A}[(1-\bar{R})e^{-jkx} + 2\bar{R}\cos kx] \qquad (2.4)$$

The first term in the above expression represents a travelling wave progressing toward the reflector, the second term represents a standing wave. For $\bar{R}=1$, i.e. $\bar{A}=\bar{B}$, the field consists entirely of the standing wave. The more energy transmitted through the termination the smaller R, and the greater the amplitude of the travelling wave component of 2.4, and the smaller the amplitude of the standing wave component. The magnitude of the pressure $P = [\bar{P} \cdot \bar{P}^{*}]^{1/2}$ at any location x, is given by:

$$P(x) = [\bar{A}(e^{jkx} + \bar{R}e^{-jkx})\bar{A}^{*}(e^{-jkx} + \bar{R}^{*}e^{jkx})]^{1/2} \qquad (2.5)$$

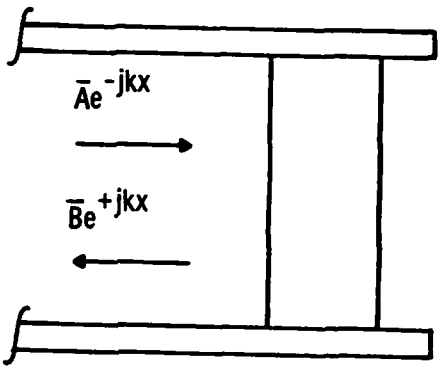

Figure 1. Illustration of an Incident $\bar{A}e^{-jkx}$ and Reflected, $\bar{B}e^{+jkx}$, Plane Wave Near the Tube's Termination

$$= A[1+Re^{-j(kx-\phi)}e^{-jkx} + e^{jkx}Re^{j(kx-\phi)} + R^2]^{1/2} \quad (2.6)$$

$$P(x) = A[1 + R^2 + 2R\cos(2kx-\phi)]^{1/2} \quad (2.7)$$

Figure 2a shows the effect on the pressure distribution P(x) of varying the magnitude of $\bar{R}=Re^{j\phi}$ for $\phi=0$. It can be seen that the location of the nodes and antinodes remains the same, but that the ratio of the maximum to the minimum decreases with decreasing R. The pressure magnitude at the nodes and antinodes is spaced equally above and below A the magnitude of the incident wave. The nodes are increasingly well defined for R approaching 1, until at R=1, the nodes go to zero, indicating no transport of energy in the standing wave.

Figure 2b shows the effect of three different phase terms $\phi = 0^\circ$ and $\pm 90^\circ$ of $\bar{R}=Re^{j\phi}$, for a constant magnitude of R=1. The ratio of the maximum to the minimum magnitude now stays the same, but the nodes and antinodes are shifted to the left or right depending on whether ϕ is positive or negative. For $\phi=0$, the magnitude is a maximum at the termination while for $\phi=\pm 90^\circ$, the magnitude of the standing wave pattern is shifted to the left or right by $kx= \pi/4$ ($x= \lambda/8$).

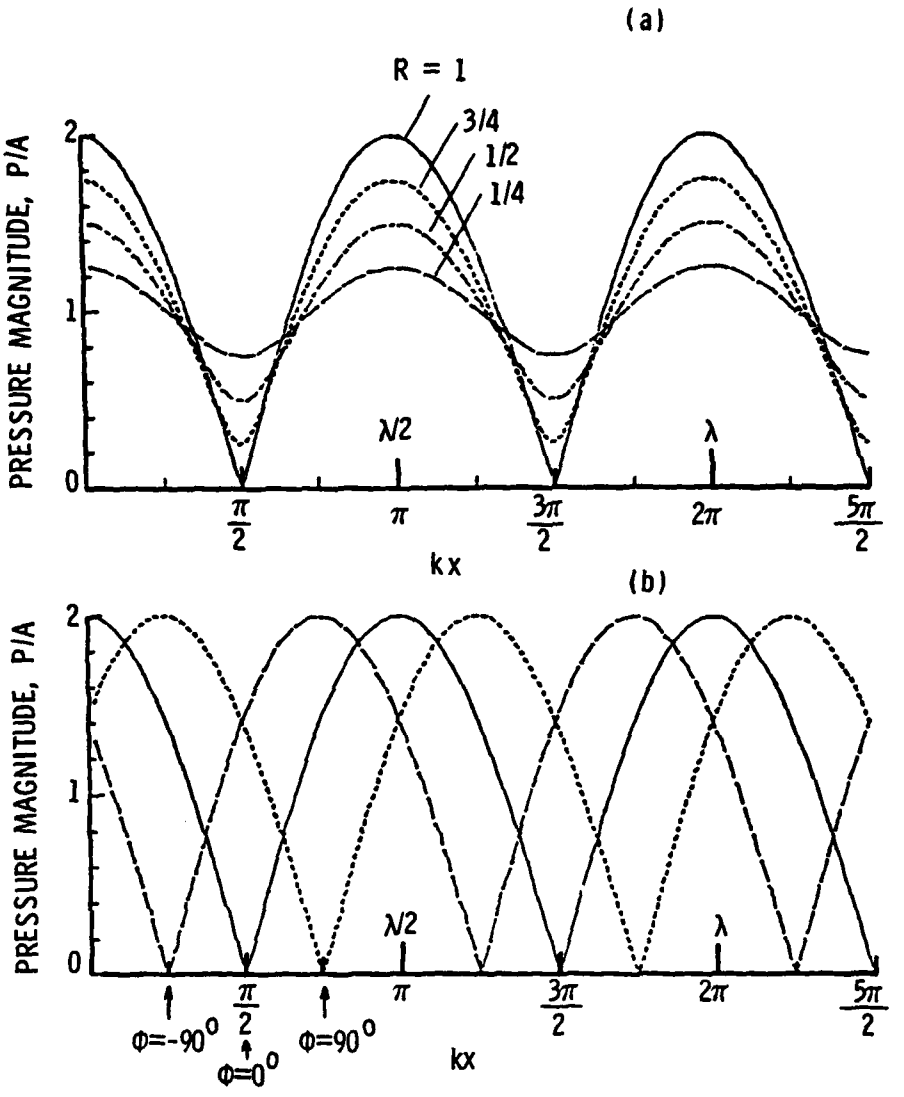

Figure 2. Examples of how the normalized pressure magnitude varies as a function of kx for the case of: (a) varying the magnitude of the reflection factor, R, for $\phi = 0°$, and (b) varying the phase of the reflection factor, ϕ, for R = 1.

2.2 The Standing Wave Ratio Method

To see how the complex reflection factor can be determined from the pressure magnitude, and thus the acoustic impedance of the sample surface, the reflection factor is rewritten as follows [2]:

$$\bar{R} = Re^{j\emptyset} = Re^{j\pi\sigma} \qquad (2.8)$$

with $\emptyset=\pi\sigma$ or $\sigma=\emptyset/\pi$. The pressure in the tube (Equation 2.7) becomes:

$$P(x) = A[1 + R^2 + 2R\cos 2(kx-\pi\sigma/2)]^{1/2} \qquad (2.9)$$

The phase term $\pi\sigma/2$ can be written as:

$$\pi\sigma/2 = [k/(2\pi/\lambda)]\pi\sigma/2 = k\lambda\sigma/4 \qquad (2.10)$$

so that 2.9 becomes:

$$P(x) = A[1 + R^2 + 2R\cos 2k(x-\lambda\sigma/4)]^{1/2} \qquad (2.11)$$

The minimum and maximum points of the pressure occur respectively when

$$\cos 2k(x-\lambda\sigma/4) = \pm 1 \qquad (2.12)$$

Substituting back into 2.9 and defining SWR as the ratio of the maximum pressure to the minimum pressure:

$$SWR = p_{max}/p_{min} = \frac{(1 + R^2 + 2R)^{1/2}}{(1 + R^2 + 2R)^{1/2}} = \frac{1+R}{1-R} \qquad (2.13)$$

or, by inverting 2.13, the amplitude of the reflection factor can be written in terms of the standing wave ratio as:

$$R = SWR-1/SWR+1 \qquad (2.14)$$

This formula can be used to find the magnitude of the reflection factor, given that the ratio of the pressure maximum (antinode) to the pressure minimum (node) is known.

The location of the pressure minimum or maximum relative to the absorber surface is used to find the phase ($\phi=\pi\sigma$) of the reflection factor. Since the minimums are more sharply defined than the maximums, especially for low values of absorption, the distance of the node from the sample surface is usually measured. For any termination condition, the magnitude of the standing wave is a minimum for the following condition:

$$\cos [\ 2k(x_{min} - \lambda\sigma/4)\ ] = -1 \qquad (2.15)$$

or:

$$2k(x_{min} - \lambda\sigma/4) = (2n + 1)\pi \quad n=0,1,2,3,... \qquad (2.16)$$

The first null occurs when n=0, and corresponds to:

$$x_{min} - \lambda\sigma/4 = \pi/2k = \lambda/4 \qquad (2.17)$$

and the location of the pressure minimum is:

$$x_{min} = (\lambda/4)(1 + \sigma) = (\lambda/4)(1+\phi/\pi) \qquad (2.18)$$

The reflection factor phase ϕ can be written in terms of x_{min} as follows:

$$\phi = \pi\sigma = \{\pi[x_{min}/(\lambda/4)] - 1\} = \pi(4fx_{min}/c - 1) \quad (2.19)$$

such that the complex reflection factor $\bar{R}$ in terms of the standing wave ratio (SWR) and the location of the first node (x_{min}) becomes:

$$\bar{R} = (SWR-1/SWR+1)e^{j\pi(4fx_{min}/c - 1)} \quad (2.20)$$

The impedance can be determined from the reflection factor as described below. The specific acoustic impedance of the surface is defined as the pressure divided by the normal component of the velocity of the sample surface:

$$\bar{Z}_n = p(x=0)/u(x=0) \quad (2.21)$$

where the velocity is related to the gradient of the pressure by Euler's equation:

$$u(x) = -j/k\rho c \frac{\partial p(x)}{\partial x} \quad (2.22)$$

Substituting the original expression for the pressure field (see Equation 2.2) into Equation 2.21, and using Equation 2.22, the surface impedance can be written in terms of the reflection factor as:

$$\bar{Z}_n = \frac{p_{x=0}}{u_{x=0}} = \frac{\bar{A}(e^{jkx} + \bar{R}e^{-jkx})_{x=0}}{\frac{-j\bar{A}}{k\rho c}(e^{jkx} - jk\bar{R}e^{-jkx})_{x=0}} = \frac{1+\bar{R}}{1-\bar{R}} \rho c \quad (2.23)$$

The surface impedance of the termination, relative to the characteristic impedance of the fluid medium, ρc, is then:

$$\bar{z} = \bar{Z}/\rho c = (1+\bar{R})/(1-\bar{R}) \qquad (2.24)$$

Conversely, the reflection factor can be written in terms of the surface impedance of the termination and the characteristic impedance of the fluid medium as:

$$\bar{R} = (\bar{Z}_n - \rho c)/(\bar{Z}_n + \rho c) \qquad (2.25)$$

In short, to measure the complex reflection factor or the surface impedance of the termination by the standing wave ratio method, one measures the maximum and minimum pressure in the acoustic pressure field, and the distance of the first minimum from the termination.

2.3 The Two-Microphone Method

The two-microphone or transfer function method of measuring the acoustic impedance is a variation of the SWR technique. It involves measuring the pressure field near the tube termination simultaneously at two separate locations of known distance from the sample surface, and then reconstructing the sound field assuming it consists of an incident and reflected plane wave. Figure 3 shows the configuration near the tube termination where the sound field is measured at points 1 and 2, at distances of x_1 and

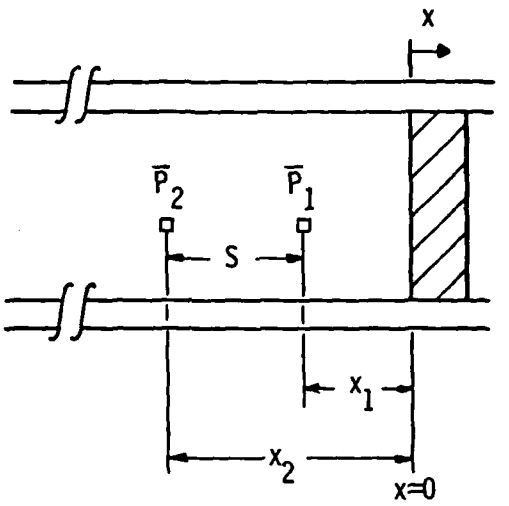

Figure 3. Location of the two hydrophones, x_1 and x_2, relative to sample surface at x = 0.

x_2 respectively from the sample surface. For pure tone excitation, the pressure consists of a standing wave field as in Equation 2.1. The pressure at each point can be written as:

$$p(x_1,t) = \bar{P}_1 e^{jwt} = (\bar{A}e^{-jkx_1} + \bar{B}e^{jkx_1})e^{jwt} \tag{2.26}$$

$$p(x_2,t) = \bar{P}_2 jwt = (\bar{A}e^{-jkx_2} + \bar{B}e^{jkx_2})e^{jwt}$$

where $\bar{A} = Ae^{j\phi}A$ and $\bar{B} = Be^{j\phi}B$ denote the amplitude and the phase, referenced at x=0, of the incident and reflected wave respectively. Dropping the time dependence of the pressure, $\bar{P}_1$ and $\bar{P}_2$ become:

$$\bar{P}_1 = \bar{A}e^{-jkx_1} + \bar{B}e^{jkx_1} \tag{2.27}$$

$$\bar{P}_2 = \bar{A}e^{-jkx_2} + \bar{B}e^{jkx_2}$$

By measuring the pressure $\bar{P}_1$ and $\bar{P}_2$ at points x_1 and x_2, the coefficients $\bar{A}$ and $\bar{B}$ can be written as follows, (using Cramer's rule):

$$\bar{A} = \frac{\begin{bmatrix} \bar{P}_1 & e^{jkx_1} \\ \bar{P}_2 & e^{jkx_2} \end{bmatrix}}{\begin{bmatrix} e^{-jkx_1} & e^{jkx_1} \\ e^{-jkx_2} & e^{jkx_2} \end{bmatrix}} \qquad \bar{B} = \frac{\begin{bmatrix} e^{-jkx_1} & \bar{P}_1 \\ d^{-jkx_2} & \bar{P}_2 \end{bmatrix}}{\begin{bmatrix} e^{-jkx_1} & e^{jkx_1} \\ e^{-jkx_2} & e^{jkx_2} \end{bmatrix}}$$

$$\bar{A} = \frac{\bar{P}_1 e^{jkx_2} - \bar{P}_2 e^{jkx_1}}{e^{jk(x_2-x_1)} - e^{-jk(x_1-x_2)}} \qquad \bar{B} = \frac{\bar{P}_2 e^{-jkx_1} - \bar{P}_2 e^{-jkx_2}}{e^{jk(x_2-x_1)} - e^{-jk(x_1-x_2)}}$$

The reflection factor $\bar{R}=\bar{B}/\bar{A}$, can then be written in terms of $\bar{P}_1$ and $\bar{P}_2$ as:

$$\bar{R} = \frac{\bar{B}}{\bar{A}} = \frac{\bar{P}_2 e^{-jkx_1} - \bar{P}_1 e^{-jkx_2}}{\bar{P} e^{jkx_2} - \bar{P}_2 e^{jkx_1}} \tag{2.28}$$

If the tube is excited by broad-band, stationary (ergodic) random noise, the pressure in each narrow frequency band of analysis can be considered as harmonic with a randomly varying amplitude [17]. The pressure at points 1 and 2 in a narrow frequency band, f_B, can then be written as:

$$\tilde{P}_1(x_1,t,f_B) = \tilde{A}(f_B,t)e^{j(\omega_c t - k_c x_1)} + \tilde{B}(f_B,t)e^{j(\omega_c t + k_c x_1)}$$
$$\tilde{P}_2(x_2,t,f_B) = \tilde{A}(f_B,t)e^{j(\omega_c t - k_c x_2)} + \tilde{B}(f_B,t)e^{j(\omega_c t + k_c x_2)} \tag{2.29}$$

where the tilda denotes a stationary random variable, and $k_c = \omega_c/c = 2\pi f_c/c$, where f_c is the center frequency of the frequency band f_B under consideration.

The same analysis as before can be carried out, except that the data must be frequency analyzed and statistically averaged to determine the mean or mean-squared value of the data. The average value of the ratio of the pressures as a function of frequency, $\bar{P}_2(f)/\bar{P}_1(f)$ is the transfer function, denoted by $\bar{H}(f) = H(f)e^{j\phi(f)}$, which denotes the gain and phase variation, as a function of frequency, between the points 1 and 2. The signal processing procedures for estimating the transfer function are described in Appendix C. The reflection factor $\bar{R}$, written in terms of the transfer function $\bar{H}(f)$ becomes:

$$\bar{R} = \frac{\bar{H}_{(f)}e^{-jkx_1} - e^{-jkx_2}}{e^{jkx_2} - \bar{H}_{(f)}e^{jkx_1}} \qquad (2.30)$$

For cases when $\bar{R}$ is independent of frequency, $\bar{H}(f)$ is a periodic function of frequency, repeating itself after an interval corresponding to a half wavelength separating x_1 and x_2. Computed examples of $\bar{H}(f)$ for $\bar{R} = -1$ (pressure release (water-air) boundary) are given in Figure 4 for two different receiver locations. Refering to the figure, the lowest frequency dip in $\bar{H}(f)$ occurs when x_2 is at a minimum in the pressure field. Next, a peak occurs at a frequency where x_1 is in a minimum and so forth. The periodicity of the transfer function in the two computed examples, does not change, even though the values of the receiver locations x_1

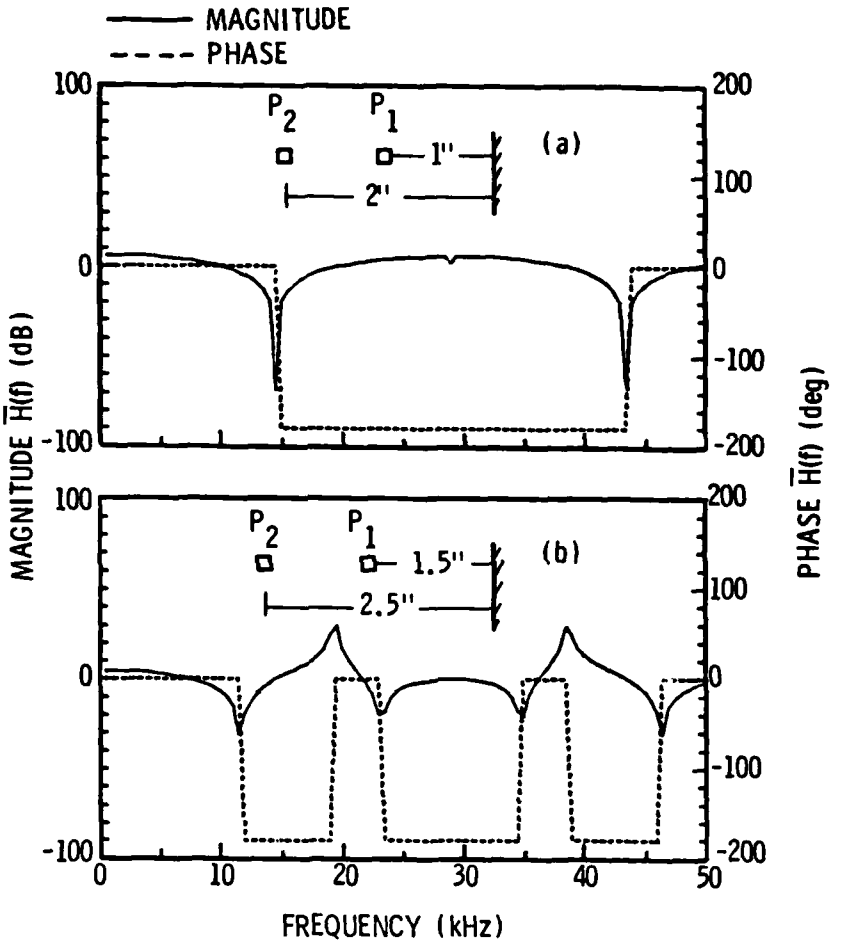

Figure 4. Magnitude and phase of the transfer function, $\bar{H}(f)$, computed for an ideal pressure release surface ($\bar{R} = -1$) when the hydrophone separation, S = 1", and the two-hydrophone unit is at two different locations from the surface.

and x_2 change, because the relative separation distance x_2-x_1 remains the same. The phase difference between $\bar{P}_1(f)$ and $\bar{P}_2(f)$ is 0^o or 180^o for R=1, and the dips or peaks of the magnitude ratio approach zero or large values.

When making measurements on highly reflective surfaces, data in the regions of the large dips or peaks are not valid. For separation distances between microphones equal to the half wavelength under analysis, the transfer function becomes indeterminant. For greater separations, the transfer function becomes indecipherable from separation distances of a half wavelength smaller. This "spatial aliasing" is analogous to frequency aliasing during digital analysis using time sampling, when the time signal is sampled slower than two times per period.

In summary, the two-hydrophone technique is valid for frequency ranges corresponding to a half wavelength of hydrophone spacing. In actual practice, $\bar{R}(f)$ will also vary as a function of frequency, which will result in more complicated patterns for $\bar{H}(f)$.

2.4 The Two-Hydrophone Method in the Pulse Tube

In adapting the two-microphone method to the pulse tube, the initial concern had been for the potential increase in coupling between the fluid-borne sound field and the structure-borne noise in the tube walls. For this reason it was felt that the tube should be ensonified with pulses rather than by a continuous source. Later analysis

indicated that the technique could also be performed using continuous excitation. Nevertheless, to allow comparison, the more involved signal processing procedures required for the pulse technique were developed and are presented in the next section.

2.4.1 Signal Processing Procedures using Pulses

For the transfer-function technique to be performed using pulses, the pressure field sampled by the two receivers must consist of both the incident and reflected fields, simutaneously. Figure 5 illustrates the sampling time available after a pulse is reflected off the sample surface and combines with the part of the pulse still incident upon the surface. No measurements can be taken until the leading edge of the reflected pulse passes the second receiver at x_2 , or a distance of $2x_2$, where x_2 is the distance from the top of the tube to the second receiver. Again, no measurements can be taken after the trailing edge of the incident pulse passes the receiver at x_2 When the pulse reflects off the bottom junction and returns to the top of the tube, it could interfere with measurements if the sampling takes place while the pulses combine. The maximum pulse length is therefore twice the length of the tube. For a pulse of this length the leading edge of the pulse reflected from the bottom termination would arrive at position x_2 just behind the trailing edge of the same pulse. These pulse lengths can be converted to

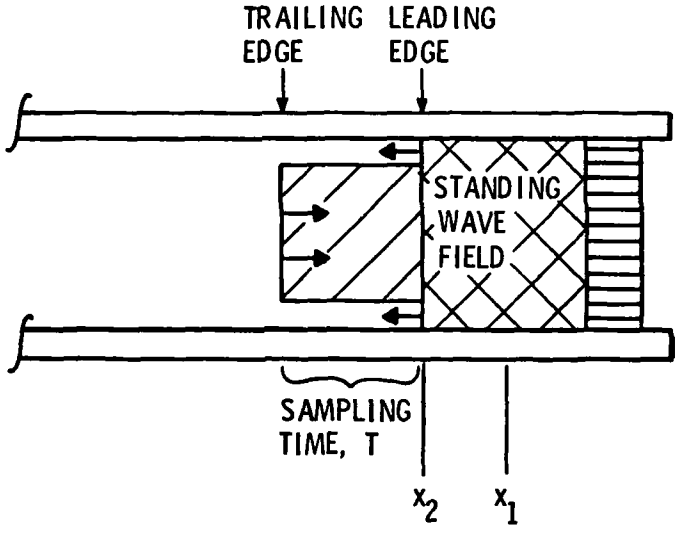

Figure 5. Illustration of how the sampling time T can be shown to depend on the pulse duration of the incident wave and the distance of the furthest hydrophone, x_2, from the sample surface.

pulse durations by dividing the propagation velocity by the pulse length.

Figure 6 shows an actual 6 msec, 2 Khz pulse received at the top of the water-filled measurement tube. The first pulse corresponds to the incident pulse superimposed with the reflected wave from the top surface. The two subsequent pulses are the initial pulse after reflecting off the bottom of the tube. Each subsequent pulse received is of lesser amplitude, indicating energy lost either at the top or bottom junctions. The propagation velocity in the tube was determined by measuring the exact distance travelled between successive pulses. The resulting value of c= 1,420 m/sec $\pm$50 m/sec (56,000 in/sec $\pm$2,000 in/sec) was then used to calculate the spatial length of various pulse durations. Figure 7 shows the overlap time available for sampling as a function of pulse duration (in milliseconds) for various values of x_2, the distance to the second transducer position Also indicated is the maximum pulse duration permissible, based on the length of the tube and the propagation velocity. It is clear that the closer the receivers are located to the surface, the longer the pulse can be sampled. However, by locating the probe too close to the sample surface, near-field effects resulting from the termination may effect the measurement results.

The sampling time T, places a limit on the frequency resolution of the spectrum analysis. Refering to Appendix

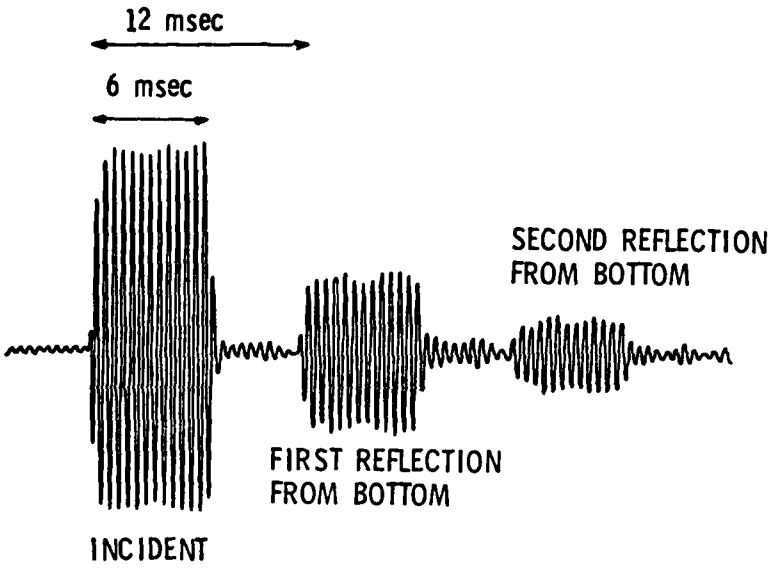

Figure 6. Time history of the pressure field measured near the air surface of a water-filled acoustic tube for a 6 msec, 2 kHz incident pulse.

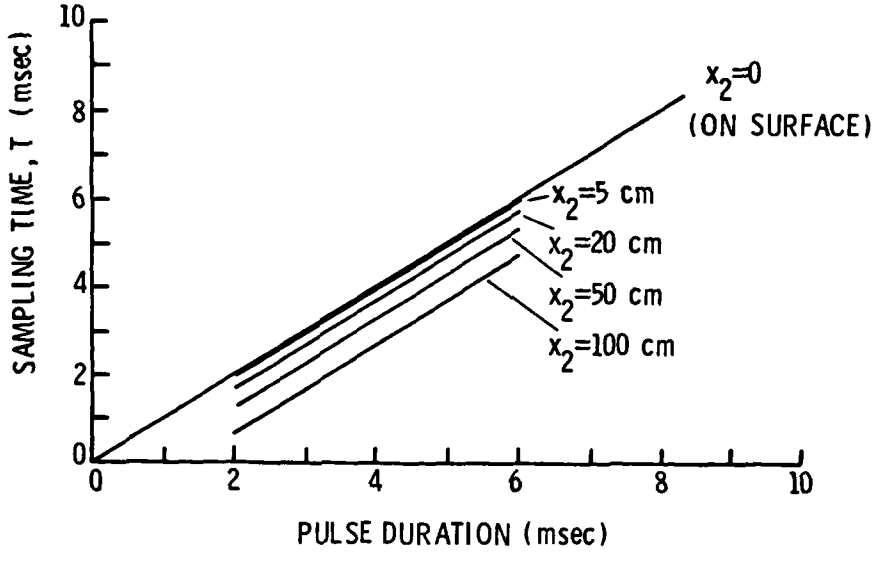

Figure 7. Theoretical sampling time, T, for Various pulse durations and locations of the furthest Hydrophone, x_2, as illustrated.

C, the transforms used in estimating the transfer function can only be evaluated over the period T, resulting in a frequency resolution of $\Delta f=1/T$. This could lead to bias errors if the data contains sharp spectral peaks.

Another significant factor is the separation distance $s=(x_2-x_1)$. A high value of coherence between the two transducers is desirable to keep the random errors small. This can be accomplished by keeping the units as close to each other as possible [13]. However, if the receivers are too close the accuracy of the low-frequency measurements will be reduced because the phase difference between the two receivers will become smaller, the longer the wavelengths propagating in the tube. The presence of the receivers in the tube may also create local disturbances or scattering effects in which the presence of one transducer affects the pressure measured at the location of the other unit. The receivers should therefore be separated far enough apart such that these local disturbances do not affect the measurement, although this is difficult to determine except empirically.

The separation distance s also determines the fundamental frequency of the periodic transfer function $\bar{H}(f)$, (See Figure 4). In base-band frequency analysis, the measurements can be performed up to a frequency for which the separation distance s is a half wavelength [15]. Figure 8 shows this upper frequency limit as a function of the separation distance s, between x_1 and x_2.

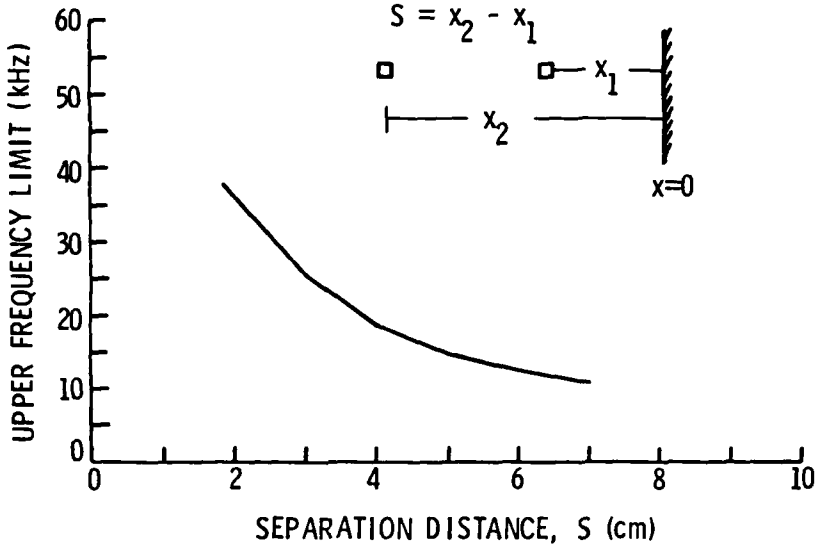

Figure 8. Upper frequency limit of two-hydrophone technique as a function of transducer separation distance $S = x_2 - x_1$.

In summary, certain tradeoffs must be considered when determining the pulse duration and the location of the transducers in the tube. The most important are as follows:

1. Pulse duration: Longer pulse durations allow greater sampling time and thereby increased frequency resolution and less bias error, but result in greater time for fluid-tube structure coupling to take place. Increasing this coupling could increase the level of the "reverberent field" in the tube which could reduce the signal-to-noise ratio and increase the random and bias errors.

2. Transducer separation: Closer transducer separations result in broader frequency ranges of analysis and high coherence, but also increased interference effects between receivers and reduced phase resolution, especially for longer wavelengths.

3. Termination distance: Locating the transducers close to the tube termination reduces the bias error and allows somewhat more sampling time, but may increase errors from near-field effects close to the sample surface.

These considerations are investigated in more detail in the experimental portion of the thesis (see Chapter 4).

CHAPTER 3

TRANSDUCER DEVELOPMENT AND EVALUATION

The most critical experimental constraint in adapting the two-microphone method to water-filled tubes, is the availability of suitable transducers to measure the pressure field inside the tube. This chapter describes the development of transducers units for use in the pulse tube, and the evaluation procedures to determine their suitability for use in the two-hydrophone technique.

3.1 Transducer Selection and Construction

Measurements that are made to determine the impedance of materials in air using tubes, are typically done using commerically available sensors. Generally these are wall-mounted pressure transducers or small diameter microphones that are inserted directly into the pressure field [14]. Likewise, hydrophones for measurements underwater have two possible designs that could be used with the pulse tube: 1) wall mounted or 2) internally mounted or suspended hydrophone transducers.

Wall mounted transducers are inserted in the tube wall, with the active area as nearly flush as possible with the inside diameter of the tube to avoid perturbing the internal acoustic pressure field. Although avoiding the problem of

disturbing the measured pressure distribution, such transducers may be susceptible to mechanical vibrations in the tube wall itself. In the water-filled tube, such structure-borne vibrations could significantly affect the measurement results. Internally suspended transducers should avoid the problem of wall vibrations in that they are suspended inside the tube with as little mechanical support as possible. Their presence inside the tube may, however, perturb the pressure field being measured.

A total of five different transducer designs were eventually tested for use in the measuring scheme. Initial efforts were focused on two different wall-mounted hydrophones since this configuration formed the closest analogy with the transducers used for air measurements. After it became apparant that the mechanical sensitivity of the wall-mounted hydrophones precluded their use in the water-filled tube, efforts were devoted to developing an internally suspended PVDF (Polyvinylideneflouride) thin film hydrophone. Two designs were developed, both of which proved unsatisfactory for reasons explained in this chapter. Finally, a small dimension PZT (lead zirconate titanate) composite transducer was designed. This suspended type hydrophone exhibited both a low mechanical sensitivity and a minimal perturbation effect on the acoustic pressure field inside the pulse tube, thus making it the most acceptable choice for use in the two-hydrophone technique.

3.1.1 Wall-Mounted Transducers

Two wall-mounted transducers were tested for use in the pulse tube: the commercially available Celesko LD-25 and a custom-made PZT wall-mounted hydrophone.

The Celesko LD-25 is a flush-mounted PZT transducer used for a variety of dynamic pressure and acoustical measurements in both air and water. It has a nominal acoustical sensitivity of -213 dB ref 1V/μPa and a mechanical sensitivity of 159 dB ref 1μPa/g as specified by the manufacturer.

The custom-made wall- mounted unit was modeled in part on the LD-25 with certain modifications, in an attempt to achieve a lower mechanical sensitivity. It consisted of a small cylindrical PZT crystal, surrounded by coroprene and encased with RTV silastic in a brass plug, which could be screwed into the tube wall. The mechanical and acoustical sensitivities are described in Section 3.2.1. A schematic of both transducers is given in Figure 9. Both wall-mounted units were rejected for use in the measurement scheme as will be discussed in Section 3.2.1.

3.1.2 PVDF Transducers

After ruling out the possibility of using wall-mounted transducers for the impulse tube, a novel, internally suspended transducer was developed and tested which utilized PVDF piezoelectric film. This transducer will be described

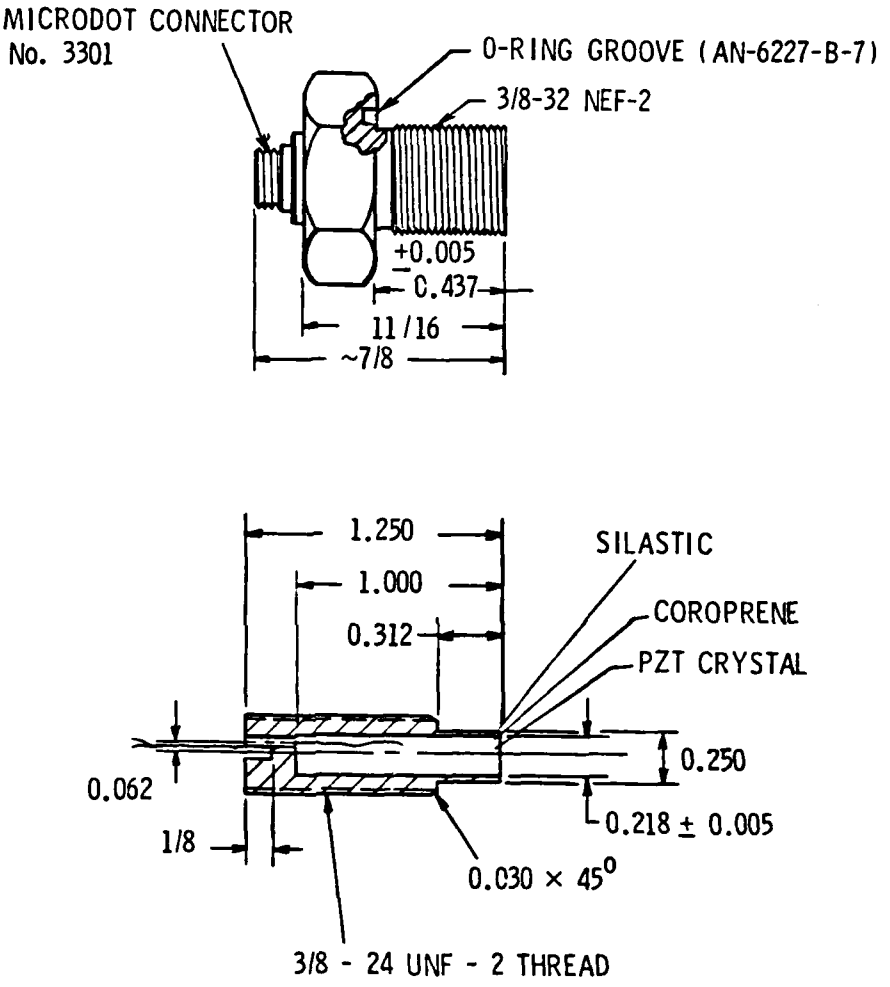

Figure 9. Schematic of the two different types of wall-mounted hydrophones investigated: the upper unit was a commercial procured Celesko LD-25; the lower unit was custom-made by the author.

in some detail, since it was a strong contender for use in the two-hydrophone technique for much of the period of the thesis research.

Much research has been done on the piezoelectric properties of thin film polymers in the last decade, especially after the discovery in 1969 by Kawai of the strong piezoelectric effect in polyvinylideneflouride (PVDF) [23]. PVDF is a semicrystalline polymer, which, when permanently polarized exhibits significantly higher piezoelectric activity than other polymers. Its piezoelectric and mechanical properites, including its flexibility, ruggedness and low acoustic impedance, have led to its increased application in audio frequency, ultrasonic and underwater transducers. The piezoelectric activity in PVDF is descibed briefly in Appendix D. PVDF sheets are commercially available in a variety of thicknesses and sizes.

Sessler [23] gives a good review of PVDF's physical properties as well as some current applications. Sullivan and Powers [24] describe a PVDF flexural disk hydrophone with a sensitivity of -200 dB ref 1V/μPa. DeReggi et al. [25], developed a piezoelectric polymer probe for ultrasonic applications with the principal advantage of minimally perturbing the acoustic field. The transducer probe developed for this thesis is modeled in part on this latter

design. Similar pobes are described by Shotten et al. [26] and Bacon [27]. PVDF film was choosen specifically because its characteristic impedance is closely matched to that of water.

It was felt that PVDF thin film hydrophones would have two advantages over conventional hydrophones in the pulse tube. The very thin sensing area should provide a good resolution of the standing wave field in the tube. Also the large cross-sectional area could possibly average out some of the local disturbances over the cross-section of the tube (including higher-order modes).

Two different PVDF probes were developed for testing in the tube. The original was made from piezoelectric material obtained from the Kreha Corporation of America, consisting of pre-poled and stretched 30 micron thick sheets metalized on each surface with aluminum. The probe itself consisted of a sheet of PVDF film stretched between two stainless steel rings of 1 15/16" outside diameter, 1 9/16" inside diameter and 1/8" thickness. The aluminized surfaces of the film were etched using conventional photolithographic techniques so that an active circular area of 1 7/16" was left inside the rings. A jig was built to maintain the tension of the film inside the rings while they were glued

together. The rings and Piezofilm were positioned in the jig by three small pins. The jig itself is shown in Figure 10. The film was placed between the two rings, stretched tight by hand and then secured in the jig by several wing nuts holding the bottom and top together. The rings were cemented using room-curing epoxy, and held together with a weight placed on top of the fixture. After drying, the excess film was trimmed from the circular rings to yield a circular, taut membrane probe which could be inserted inside the impulse tube. Fine wires were attached with conductive paint to the aluminized surface and soldered to an intermediate pad attached to the surface of one ring for mechanical stress relief. A shielded twisted pair of wires encased in teflon was then soldered to the pad to form the leads. The metal ring of this unit was found to significantly perturb the acoustic field in the tube and was replaced by a second-generation PVDF probe described below.

The second-generation PVDF probe was of a similar design, but differed in the construction materials. More sensitive, nickel coated PVDF sheets of 110 micron thickness were obtained through the Pennwalt Corporation. The rings were formed of more acoustically transparant Lucite which was annealed at 158° F for twelve hours prior to transducer assembly. The inside diameter of the Lucite rings was 1/16" greater than for the metal rings of the first-generation unit.

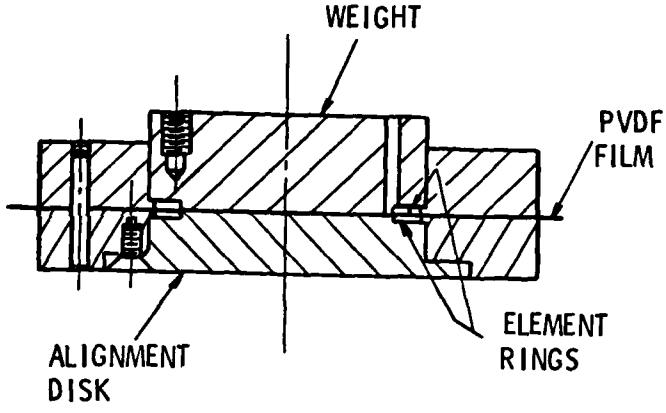

Figure 10. Schematic of jig used to assemble the PVDF thin film material onto the stainless steel or lucite support rings.

Two of these newer units were constructed in a similar fashion as for the stainless steel units using the jig for assembly. Fine wires were again attached with conductive paint to the metallized surface and terminated on the Lucite rings on small metal sockets glued into the rings into which fine wire leads could be inserted. Each unit had 3 evenly spaced holes on the same radius, into which small Lucite pins could be inserted to separate the two units a fixed distance apart. Smaller holes were drilled between the 3 pin holes to enable passing the lead wires from the bottom transducer through the top transducer to make insertion into the pulse tube easier.

The final assembled unit or "probe" consisted then of two transducers, held apart at a known separation which could be varied by using different pin lengths. The location of the two units in the tube could also be reversed quite easily by detaching the wire leads, reversing the units, reinserting the connecting pins and finally reattaching the wire leads. A bakelite rod was attached to the uppermost unit so it could be screwed in and out of the unit to facilitate positioning the probe into the tube.

Although significantly less perturbing of the acoustic field than the first-generation design, this transducer was also rejected for reasons to be explained in Section 3.2.3.

3.1.3 Composite PZT Transducers

PZT-polymer composites are a fairly recent innovation to improve the hydrostatic sensitivity of PZT ceramics. Basically, drilling holes in a sintered PZT block and back-filling the holes with epoxy, decouples the d_{33} and d_{31} piezoelectric coefficients, thus enhancing the d_{3h} hydrostatic charge coefficient. See Appendix D for more details. Using PZT-composites, relatively high sensitivities can be obtained from fairly small sample sizes.

Two sample composites fabricated at the Material Research Laboratory at The Pennsylvania State University, were obtained from A. Safari. The construction of the sample composites is detailed in reference [28]. The samples were between 2 and 3 mm in thickness with a square surface area of approximately 0.4 cm^2. Fine wire leads were attached to the poled surfaces using conducting epoxy, and the entire unit was then potted in butyl rubber. The resulting transducers exhibited sensitivities of between -210 to -215 dB ref 1V/μPa (see Section 3.2.1).

To maintain a constant separation spacing between the two PZT composite transducers and to allow insertion into the tube, two transducers were affixed to a 1/8 inch diameter bakelite rod with small rubber O-rings. This rod could then be inserted through the upper termination and attached to the top of the tube.

3.2 Evaluation of Transducers

The primary criterion for accepting or rejecting any particular transducer was its ability to accurately measure the acoustic pressure near the tube termination without significantly perturbing the pressure field. Four tests were devised during the course of experimentation to evaluate the performance of the individual transducers or the two-hydrophone probes as follows:

1. Measurement of the mechanical sensitivity of the individual transducers.
2. Measurement of the acoutical sensitivity of the individual transducers.
3. Measurement of the insertion loss to determine the effect of the probe on the pressure field.
4. Measurement of the transfer-function $\bar{H}(f)$ at the tube's termination using the transducer probe to evaluate the performance of the probe in an actual measurement configuration.

Each test, its significance and the performance of the individual transducers or probes will be discussed separately in the following sections.

3.2.1 Measurement of the Mechanical and Acoustical Sensitivity

Due to the increased tube-water coupling in the pulse tube, the mechanical pick-up of the transducers could alter the measured pressure response. This was investigated in the following tests.

Figure 11 shows a schematic diagram of the experimental set-up to measure the mechanical sensitivities of the various transducers. For the wall-mounted transducers, a sample tube of short length was fashioned with the same diameter and thickness of the pulse tube into which the units could be inserted. This was to avoid drilling holes in the existing facility before it was known whether such transducers were appropriate. The mechanical sensitivity of the internally suspended transducers was measured in the actual pulse tube. A complete description of the pulse tube is given in Section 4.1.

Pure tones generated by a Rockland Frequency Synthesizer were amplified with a McIntosh 75 watt power amplifier and fed to an LC-32 hydrophone projector mounted on the bottom end of the tube. A flat spot was machined on the top side of the tube wall, on which a BBN 501 accelerometer was mounted with Super glue to monitor the radial wall acceleration.

The transducer under evaluation was mounted either internally or in the tube wall, close to the location of the accelerometer. The water level was kept well below the position of the unit so that the transducer output could be attributed solely to the tube wall acceleration. The outputs of the transducer and the accelerometer were amplified and filtered with Ithaco model 257A preamplifiers.

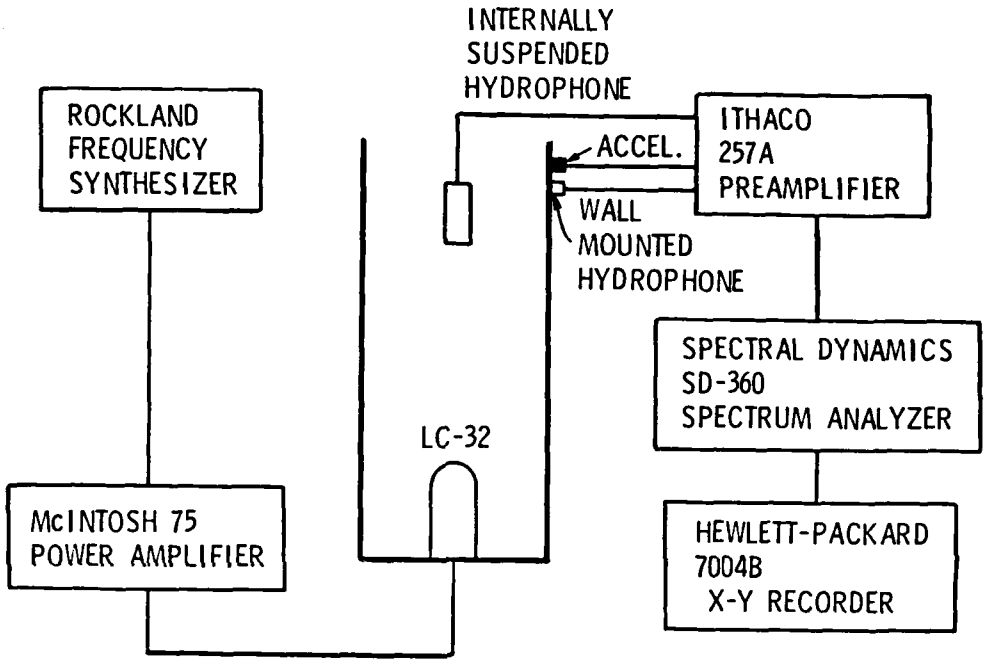

Figure 11. Experimental set-up used to measure the mechanical sensitivity of the hydrophones in the water-filled pulse tube.

Spectral analysis was performed by a Spectral Dynamics SD-375 or SD-360 dual-channel digital spectrum analyzer, and the output was recorded on a Hewlett-Packard 7004B X-Y recorder.

The accelerometer was calibrated by the manufacturer and has a flat frequency response ($\pm$3dB) up to 40,000 Hz and a mounted resonance frequency of 65,000 Hz.

The acoustical sensitivity of each of the transducers was determined by lowering the unit down inside the tube along with a small calibrated PZT transducer, and making relative comparisons in response for incident pure tone pulses. The theoretical sensitivity of the two PVDF hydrophones designs and the PZT composite transducers was also calculated as follows (see Appendix D):

Stainless steel PVDF transducer:

$$M_o = g_{3h}t = (90 * 10^{-3}\ \text{V-m/N})\ (30 * 10^{-6}\ \text{m}) \qquad (3.1)$$

$$= -231\ \text{dB ref 1V/}\mu\text{Pa}$$

Lucite PVDF transducer:

$$M_o = g_{3h}t = (90 * 10^{-3}\ \text{V-m/N})\ (110 * 10^{-6}\ \text{m}) \qquad (3.2)$$

$$= -220\ \text{dB ref 1V/}\mu\text{Pa}$$

PZT Composite Transducer:

$$M_o = g_{3h} t = (15 * 10^{-3} \text{ V-m/N}) (2.3 * 10^{-3} \text{ m}) \quad (3.3)$$

$$= -209 \text{ dB ref } 1\text{V}/\mu\text{Pa}$$

where g_{3h} is the hydrostatic piezoelectric voltage coefficient, provided by the manufacturer, and t is the thickness of the transducer in the 33 direction. These values agreed reasonably well with those measured, with the exception of the sensitivity of the PZT composite transducer, which had a 3-4 dB sensitivity drop across the transducer leads (see Appendix D).

With the above values for the mechanical and acoustical sensitivities, the equivilent acoustical output resulting from the mechanical vibration was determined. Figure 12 summarizes the response (dB ref 1 μPa/g) of all the transducers tested. The mechanical response of the PVDF transducers was almost 30 dB lower than that for the wall mounted hydrophones. The response of the PZT composite transducers was 20 dB lower than the response of the PVDF transducers.

To determine the significance of the mechanical pick-up, a measurement was performed on the pulse tube wall to determine the acceleration levels for typical acoustical signals. The measurement was performed as before, except that the acceleration of the tube wall, as measured by the

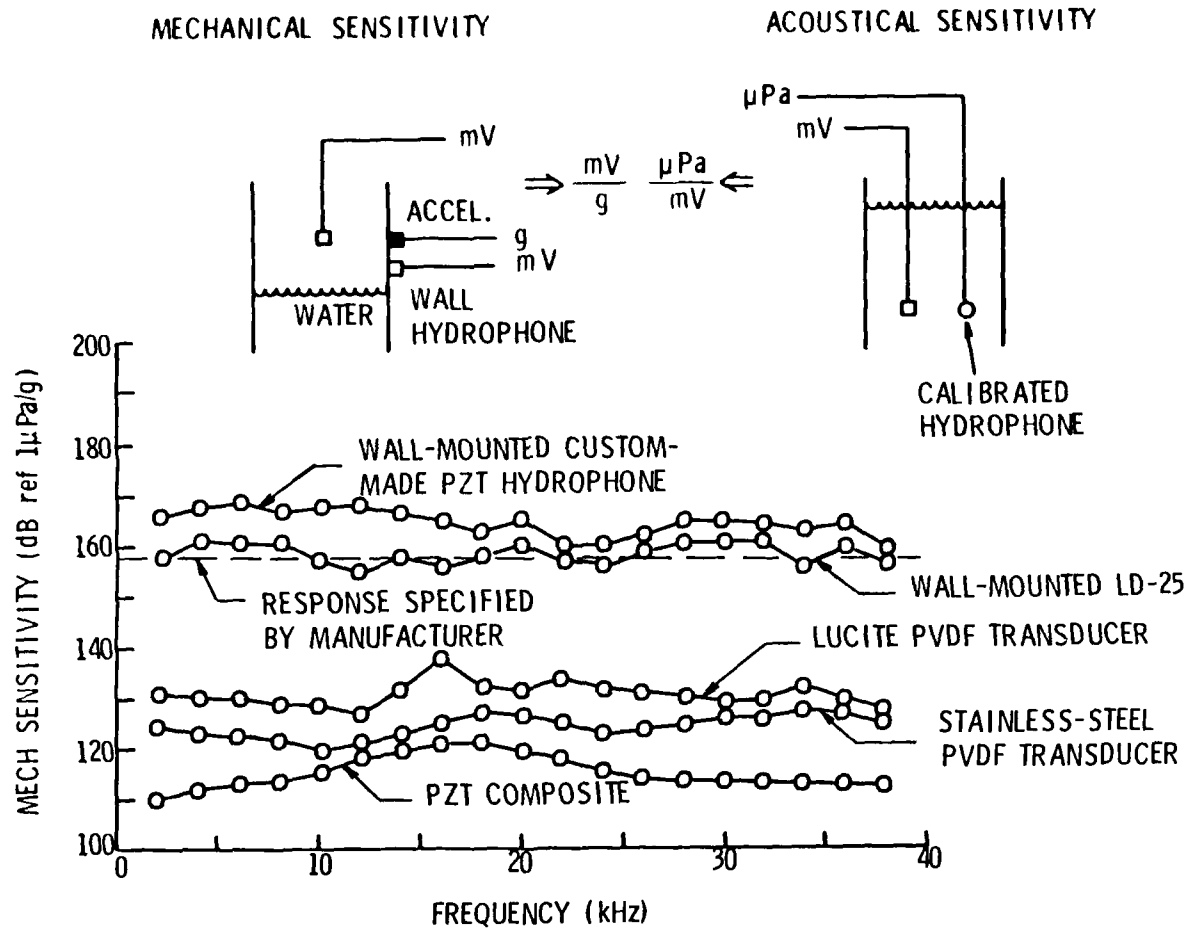

Figure 12. Measured mechanical sensitivities of the five different hydrophones investigated for possible use with the two-hydrophone technique in the water-filled pulse tube.

BBN accelerometer, was normalized by the measured pressure response of a calibrated LC-10 hydrophone inserted in the water at the top of the tube. Great care was taken to isolate the LC-10 from the tube wall itself.

Figure 13 shows the acceleration level of the tube wall relative to the measured sound pressure level in the water at the top of the tube. It can be seen that there are relatively higher acceleration levels around the 20-30 kHz region. Picking this region as the worst case tube wall acceleration level, the percentage of the acoustical signal that would result from the mechanical acceleration was determined for each transducer. Over 30 percent of the signal output would result from the wall acceleration, using the wall-mounted transducers. The PVDF and PZT units fared much better in that less than 1% of the signal output level resulted from the tube wall acceleration for the worst case frequency region. For this reason, the wall mounted units were rejected as candidate transducers for the impedance measuring scheme, and the remaining tests were performed only on the internally suspended transducers.

3.2.2 Measurement of the Insertion Loss

The perturbation effect of the internally suspended transducers was more difficult to analyze. To get an initial impression of the effect of the transducers on the sound field inside the tube, an insertion loss measurement was performed as described below.

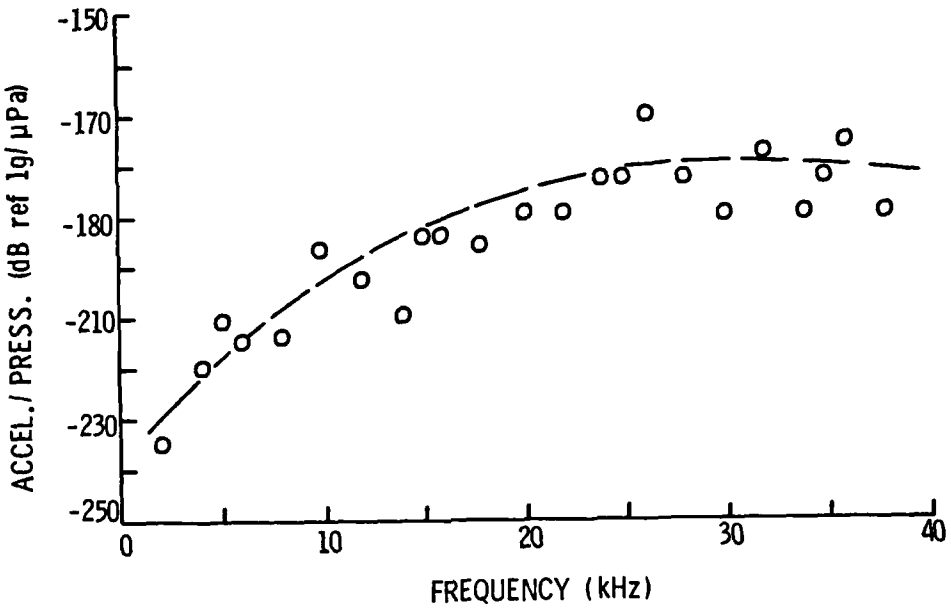

Figure 13. Measured acceleration level of pulse tube wall normalized by the acoustic pressure inside the tube.

The insertion loss was determined by comparing the levels of pure tone pulses transmitted and received by the LC-32 hydrophone, located at the bottom termination of the tube. A sweeping oscillator swept through a frequency range from 3-35 kHz and the magnitude of the return pulse was measured and recorded using a Hewlet-Packard Network Analyzer interfaced with a HP-9825B computer. The magnitude of the return pulse with and without the two-hydrophone probes inserted at the top of the tube (10 cm below the water-air surface) was then recorded as shown in Figure 14.

The insertion loss can be determined from the level difference of the return pulses as compared with the no-insert case. The stainless-steel PVDF probe has a significant effect, especially above 25 kHz. The Lucite PVDF probe has a minimal effect, and no level difference whatsoever could be detected with the composite PZT probe inserted into the tube.

The perturbation effect of the stainless-steel probe was also corroborated by other measurements made using the transducer, including distorted standing wave ratio measurements. For this reason it was also rejected as a candidate transducer.

Referring back to Figure 14, the frequency dependent pressure level in the tube can be seen. There is a

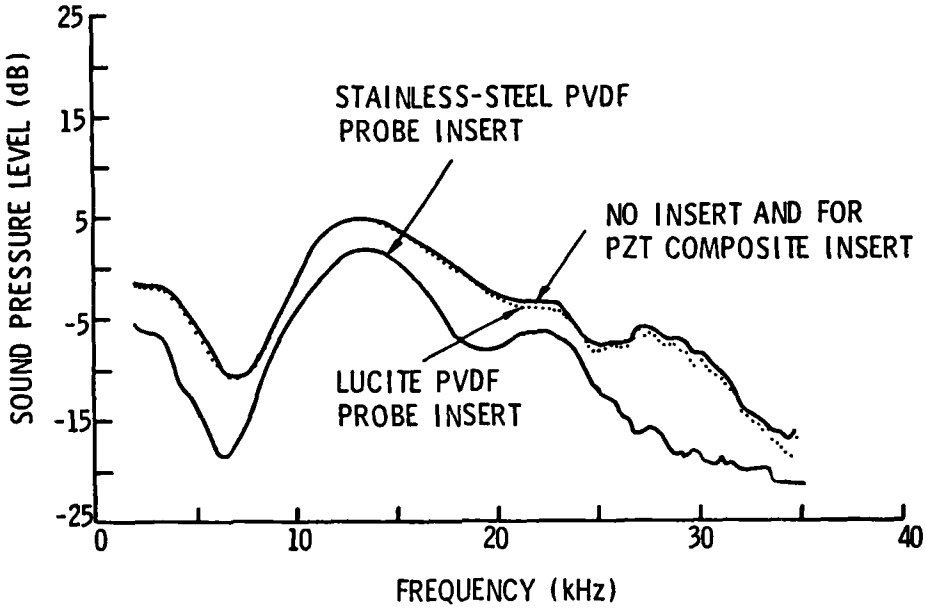

Figure 14. Measured pressure level in tube showing insertion loss for stainless-steel, lucite and PZT-composite probes.

significant dip below 10 kHz and a gradual decline in pressure level toward the higher frequencies, the significance of which will be discussed in the next section.

3.2.3 Measurement of the Transfer Function

The final test performed on the Lucite PVDF probe and the PZT composite probe was a measurement of the transfer function $\bar{H}(f)$ between transducers 1 and 2 near the tube termination. This test was to simulate the use of the probe in an actual measurement configuration. The coherence function (see Appendix C) was also recorded.

Figure 15 shows a schematic diagram of the experimental set-up. The output of a General Radio type 1390-B random noise generator was filtered with an Ithaco 4112 bandpass filter, gated to a 10 msec pulse with a Dranetz series 206 digital tone burst timing generator and amplified with a McIntosh 75 watt power amplifier. The amplified, gated signal was fed to the LC-32 mounted on the bottom end of the tube. The outputs of the two transducers in the probe were amplified and high-pass filtered with Ithaco model 257A preamplifiers. The output of the preamplifiers was then gated with a Scientific Atlanta receive gate according to a receiver "delay" and receiver "on" pulse command sent from the Dranetz pulse generator. Spectral analysis was performed by a Spectral Dynamics SD-360 or SD-375 dual-channel digital spectrum analyzer by ensemble averaging.

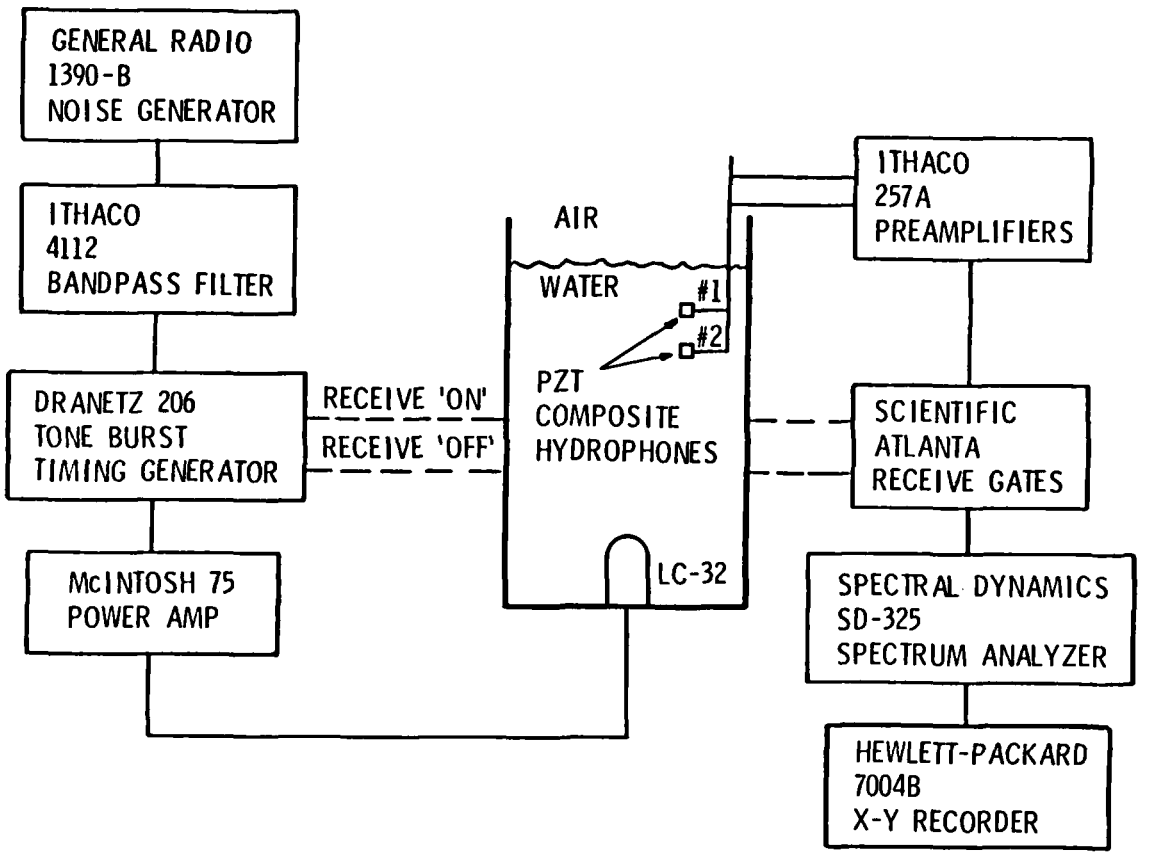

Figure 15. Instrumentation set-up used to measure the transfer function between hydrophones 1 and 2 near the tube's termination.

The output was recorded on a Hewlett-Packard 7004B X-Y recorder.

Figure 16 shows the coherence function and the magnitude and phase of $\bar{H}(f)$ for a pressure release surface (air), using the PVDF lucite probe. The transducer separation, 's', was 2.54 cm (1 inch) and the uppermost transducer was approximately 2.54 cm (1 inch) below the termination. Pulses of 10 msec duration were used for the measurement, which corresponds to the sampling time T for the analysis range selected (0-40 kHz).

Figure 17 shows the same measurements using the PZT composite probe. Both these figures can be compared with the theoretical transfer function for the same configuration, as given in Figure 4.

Both similarities and differences are apparent between the two measurements. There is a large dip in the coherence function in both measurements corresponding to the frequency where the second transducer is in a node in the standing wave field. A high value of coherence extends down to around 3 kHz with the PZT composite prove, while the coherence drops significantly below 10 kHz for the PVDF lucite probe. The coherence seems to vary considerably above 26 kHz in both measurements.

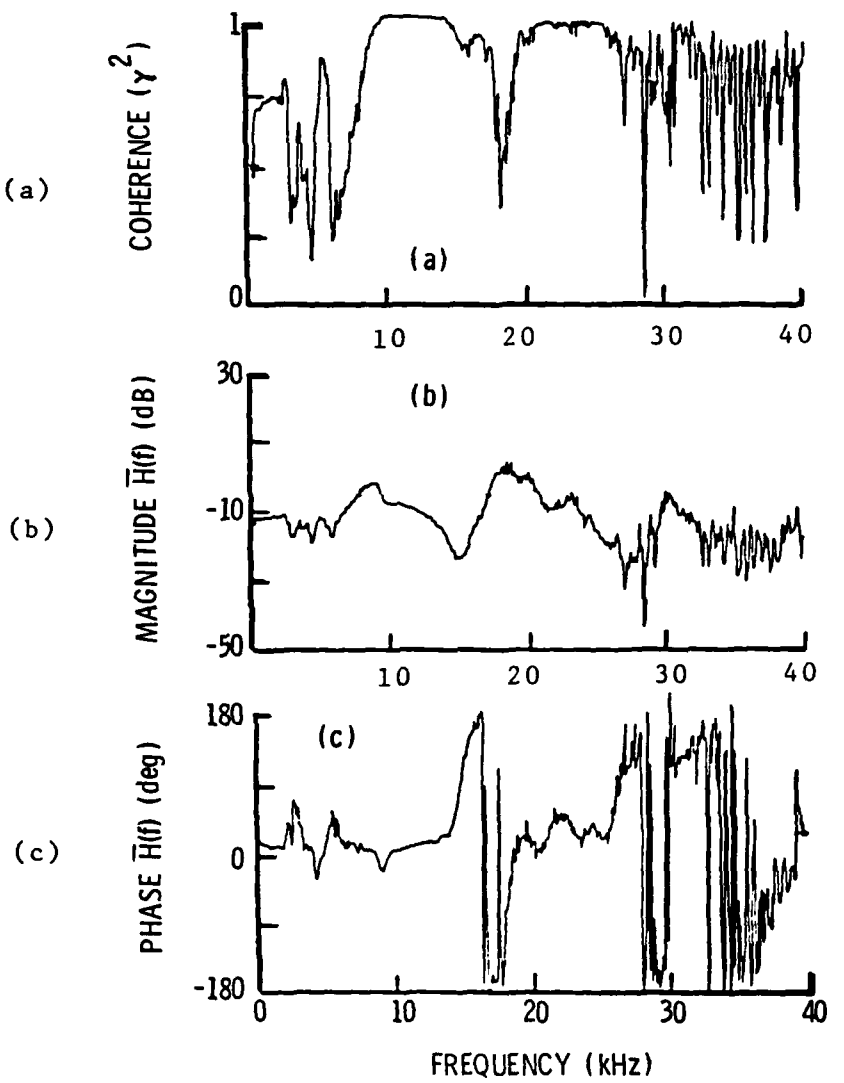

Figure 16. Measured coherence and transfer function for pressure release termination using the Lucite PVDF probes at x_1=1" and x_2=2" under pulsed excitation.

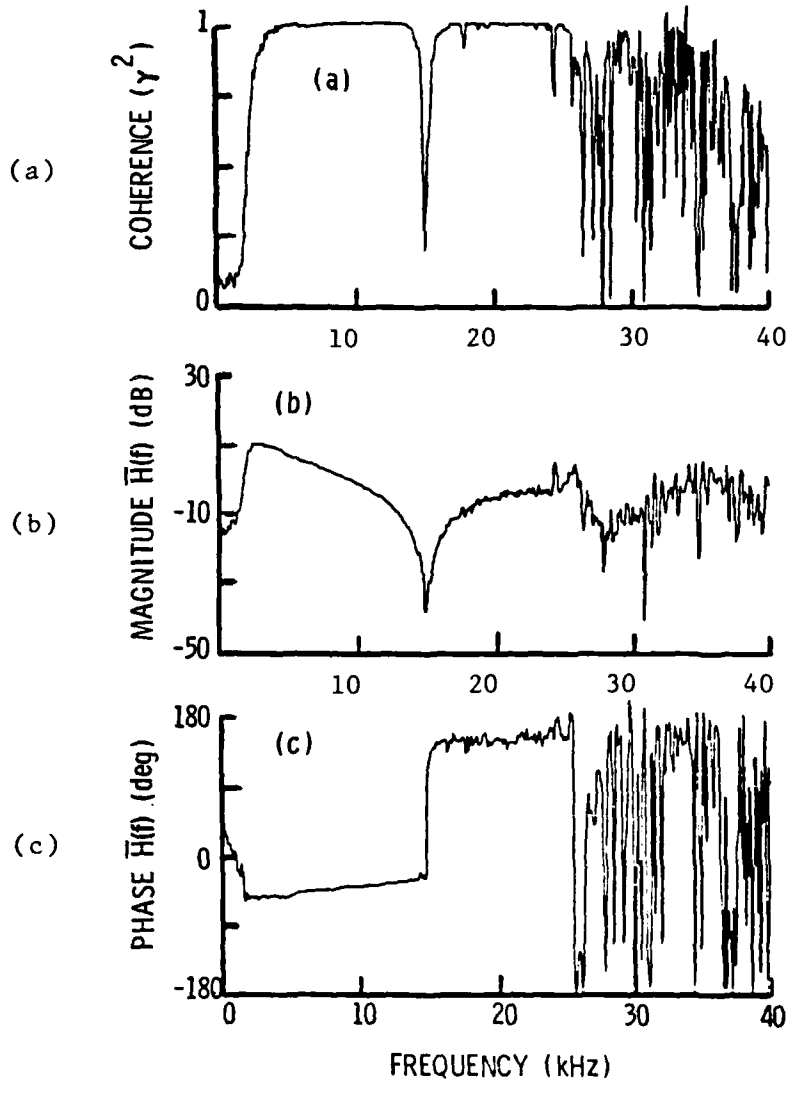

Figure 17. Measured coherence and transfer function for pressure release termination using the PZT composite probes at x_1=1" and x_2=2" under pulsed excitation.

Generally, the magnitude and phase of the transfer function measured using the PZT composite transducers closely resemble that of the theoretical transfer function as given in Figure 4, in the range from 3 to 26 kHz. The ratio of the maximum to minimum magnitude of $\bar{H}(f)$ is limited to around 48 dB. There is a phase discrepancy due to the fact that the transducers were not calibrated in the above measurement.

The Lucite PVDF probe does not appear to perform as well. There are large phase shifts over the measurement range which could be due to diffraction effects. The magnitude of the transfer function also appears to be distorted, with a maximum to minimum ratio limited to around 28 dB. The coherence dips significantly below 10 kHz and again in the range from 15 to 20 kHz, as well as above 26 kHz. The large drop in coherence below 10 kHz may be due to the fact that the sound pressure level in the tube drops significantly in this region, as can be seen in Figure 14. The higher sensitivity of the PZT composite transducers extends the measurement range to almost 3 kHz at the lower end of the spectrum.

Based on this relative comparison of the transfer function and coherence measurement near the tube termination, the PZT composite probe was chosen for use in the two-hydrophone impedance measuring technique. It offers

a broader frequency range of analysis, with a phase and magnitude estimate of the transfer function much closer to that of the theoretical.

3.3 Effect of Pulse Length

To ascertain the effect of the pulse duration on the measured transfer function, the previous measurement was repeated for varying pulse durations, using the PZT composite probe for the measurement. No significant differences were found for pulse durations larger than 10 msec, the approximate sampling time for the analysis range employed. The tube was also ensonified continuously and the measurement repeated, as shown in Figure 18. Again no significant difference was detected in the measured transfer function for the pressure release termination. This somewhat surprising result indicated that the more elaborate signal processing procedures described in section 2.4.1, to allow the use of pulses in the tube, are unnecessary when applying the two-microphone method to water-filled tubes. All subsequent measurements were performed by continuously exciting the tube, to simplify the signal processing procedures.

3.4 Calibration of the Two-Hydrophone Probe

Referring to Figures 4 and 18, showing the theoretical and measured transfer functions for a pressure release termination, there is a consistant phase discrepancy

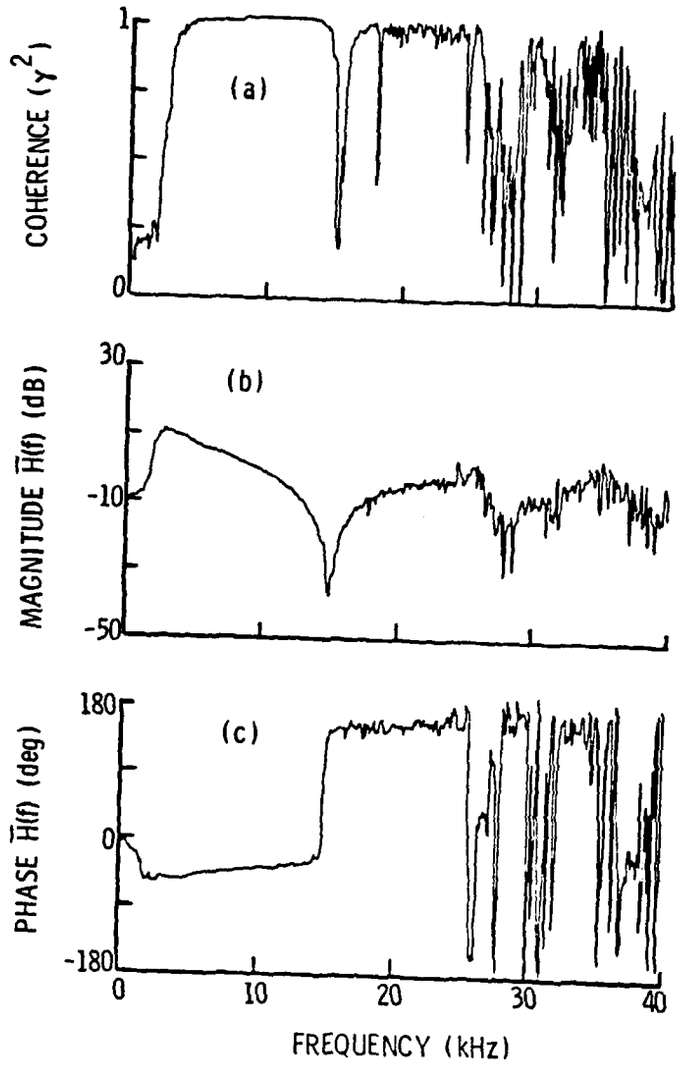

Figure 18. Measured coherence and transfer function for pressure release termination using PZT probe at x_1=1" and x_2=2" under continuous excitation.

apparant. This is due to a relative difference in the phase response of the two individual transducers in the measuring probe. A relative difference in the magnitude response would also effect the measured magnitude of the transfer function. This section explores calibration procedures to correct for such relative differences in response between the individual transducers used in the two-hydrophone probe.

As can be seen from Equation 2.30, only the complex pressure ratio $\bar{P}_2(f)/\bar{P}_1(f)$ is needed to calculate the complex impedance or the reflection factor of a particular termination. Since the absolute pressure at points 1 and 2 is not needed, it is not necessary to calibrate either transducer individually, but only the magnitude and phase response of one relative to the other.

Two different calibration techniques are discussed in the literature. Blaser [15] describes a switching technique in which the two microphone sensors are interchanged for each measurement. Seybert [14] discusses a plane-wave technique, in which the two microphones are exposed to the same plane-wave field at the termination of a tube and the transfer function between the two units measured.

The switching technique is not as convenient in the water filled tube because it is time consuming to switch the transducers for each measurement performed and the transducers must be allowed to stabilize in the tube after

being inserted. For this reason an alternative technique was investigated which the author will call the modified switching technique. Seybert's plane-wave technique was also investigated and a comparison made between the two calibration results as described below.

3.4.1 Modified Switching Technique

The switching technique as described by Blaser [15] involves switching the transducers for each measurement performed. In the modified switching technique, the transducers are only interchanged once, to obtain a relative calibration valid for all subsequent measurements.

The measurement scheme for both techniques can be represented by Figure 19, where $\bar{H}_{I1}$ and $\bar{H}_{I2}$ represent the complex transfer functions between the pressures in the tube at points 1 and 2, and the measured response after being received by the transducers, amplified, filtered and transmitted to the spectrum analyzer. The desired transfer function $\bar{H}(f)$, is equal to $\bar{P}_2(f)/\bar{P}_1(f)$ where $\bar{P}_1(f)$ and $\bar{P}_2(f)$ are the complex Fourier transforms of the pressures measured at locations 1 and 2. The initial measured transfer function $\bar{H}^{Mi}(f)$ is equal to $\bar{Y}^i{}_2/\bar{Y}^i{}_1$, where $\bar{Y}^i{}_1$ and $\bar{Y}^i{}_2$ are the Fourier transforms of the measured pressure from channels 1 and 2. Here 'channel' refers to the entire

transduction chain, including the transducer and all subsequent amplifiers, filters and cables. The measured transfer function can be written as follows:

$$\bar{H}^{Mi}(f) = \bar{Y}_2^i/\bar{Y}_1^i = (\bar{H}_{I2}\ \bar{P}_2)/(\bar{H}_{I1}\ \bar{P}_1)$$

$$= (\bar{H}_{I2}/\bar{H}_{I1})\bar{H}(f) \qquad (3.4)$$

where $\bar{H}(f)$ is the desired complex transfer function.

If the transducers and channels are now switched, (see Figure 19) the measured transfer function can be written as:

$$\bar{H}^{Ms}(f) = \bar{Y}_2^s/\bar{Y}_1^s = (\bar{H}_{I1}\ \bar{P}_2)/(H_{I2}\ \bar{P}_1)$$

$$= (\bar{H}_{I1}/\bar{H}_{I2})\ \bar{H}(f) \qquad (3.5)$$

By taking the geometric mean of $\bar{H}^{Mi}(f)$ and $\bar{H}^{Ms}(f)$ as follows:

$$[\bar{H}^{Mi}(f)\quad \bar{H}^{Ms}(f)]^{1/2} = [(\bar{H}_{I2}/\bar{H}_{I1})\ \bar{H}(f) * (\bar{H}_{I1}/\bar{H}_{I2})\ \bar{H}(f)]^{1/2}$$

$$= \bar{H}(f) \qquad (3.6)$$

the relative phase and amplitude differences between the two channels cancel, and the desired transfer function can be measured. This is the microphone switching technique described by Blaser. As discussed however, it is difficult

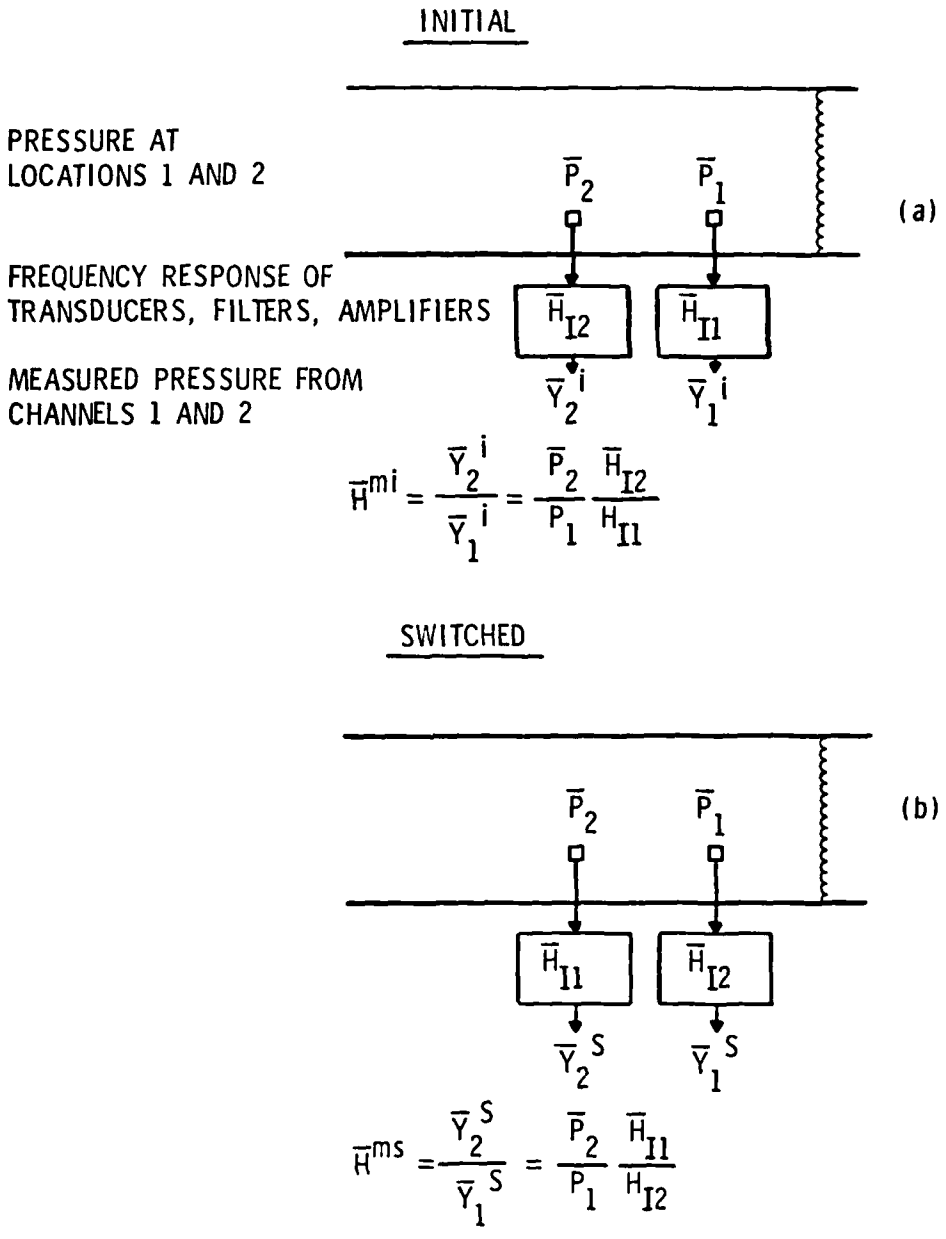

Figure 19. Schematic of modified switching technique for calibrating the transfer function (a) initial configuration and (b) switched configuration.

and time consuming to switch the transducers for each measurement. To arrive at a relative calibration, Equations 3.4 and 3.5 are equated as follows:

$$\bar{H}(f) = \bar{H}^{Mi}(f)\ (\bar{H}_{I1}/\bar{H}_{I2}) = \bar{H}^{Ms}(f)\ (\bar{H}_{I2}/\bar{H}_{I1}) \qquad (3.7)$$

The relative frequency response of the two channels is then:

$$\bar{H}_{I1}(f)/\bar{H}_{I2}(f) = [\bar{H}^{Ms}(f)/\bar{H}^{Mi}(f)]^{1/2} \qquad (3.8)$$

This quantity is independent of the pressures being measured. It is dependent only on the transducers, filters and amplifiers used in each channel. It can be measured once and stored in the computer such that only $\bar{H}^{Mi}(f)$ or $\bar{H}^{Ms}(f)$ in Equation 3.7 is necessary to compute the desired transfer function for each measurement taken.

Theoretically, this calibration should work regardless of the location of the units in the tube, as long as the pressure field does not change in the course of switching the transducers. Changes could occur if, 1) the units are not reinserted in exactly the same position relative to the termination of the tube, 2) the presence of one unit effects the other in an unsymmetrical fashion, or 3) the acoustical system changes during the course of the measurements.

The modified switching technique was performed as described above, using the PZT composite transducer probe with a 2.54 cm (1 inch) transducer separation, on a pressure release termination with the uppermost unit 2.54 cm below

the air surface termination. The tube was continuously excited by broad-band random noise (1-35 kHz) and spectral analysis was performed, as in Section 3.2.3, with the output of the spectrum analyzer interfaced with a PDP-11 computer. The relative frequency response $\bar{H}_{I1}/\bar{H}_{I2}$, calculated using Equation 3.8, is shown in Figure 20.

3.4.2 Plane-Wave Technique

The plane-wave calibration technique is less involved than the modified switching technique, in that only one measurement is performed with the transducers inserted to the same depth relative to the top of the tube.

The measurement configuration is detailed in Figure 21. In this case the relative frequency response $\bar{H}_{I1}/\bar{H}_{I2}$ can be obtained by measuring the transfer function $\bar{Y}_1/\bar{Y}_2$ between the outputs of the transduction chain.

This calibration was performed by inserting the transducers side-by-side, just below the water-air interface at the tube termination. The measured ratio, $\bar{H}_{I1}/\bar{H}_{I2}$, is given in Figure 20.

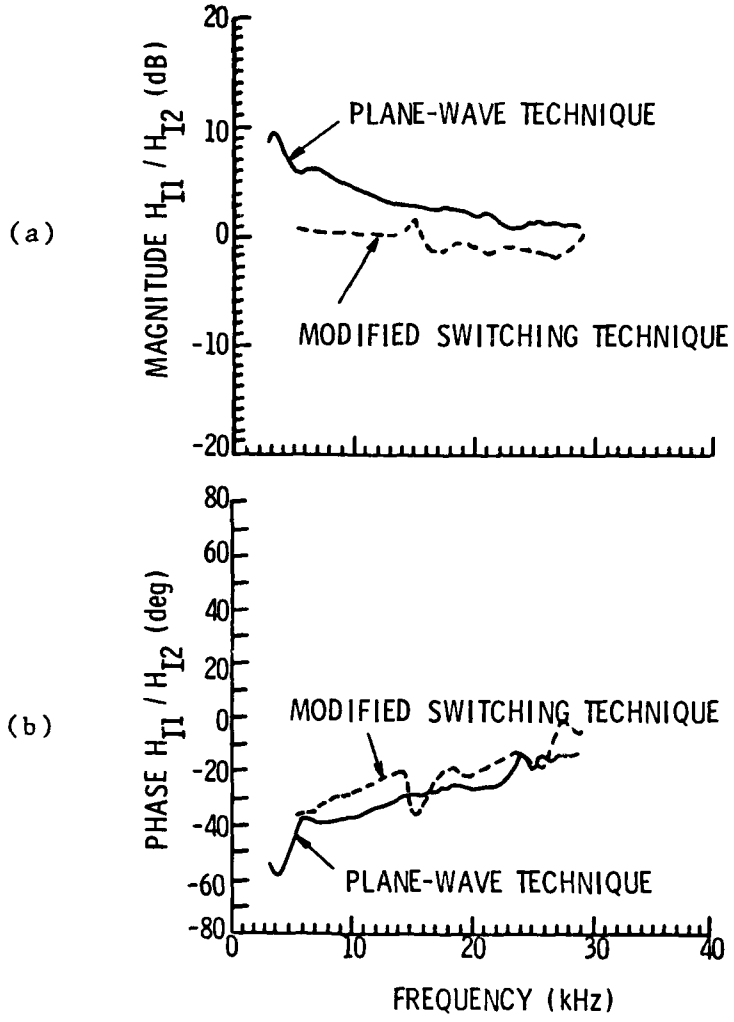

Figure 20. Transfer function calibrations for the PZT composite hydrophones measured using the plane-wave and the switching techniques.

$$\frac{\bar{Y}_1}{\bar{Y}_2} = \frac{\bar{P}_1 \bar{H}_{I1}}{\bar{P}_1 \bar{H}_{I2}} = \frac{\bar{H}_{I1}}{\bar{H}_{I2}}$$

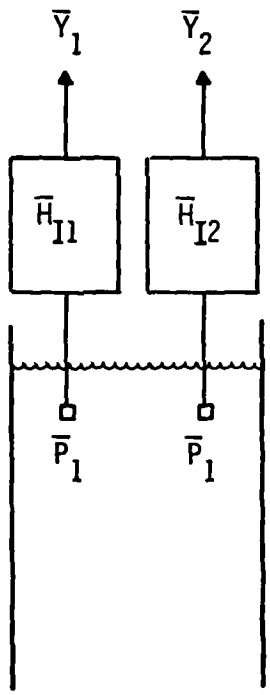

Figure 21. Schematic of plane-wave technique for calibrating the transfer function.

3.4.3 Comparison of Modified Switching Technique and Plane-Wave Technique

There are some differences in the relative calibration using the two techniques as can be seen in Figure 20. The dip in phase or the corresponding amplitude peak around 15 kHz in the switching technique calibration is due to the fact that the transducer at location x_2 was in a node. Generally, the magnitude response from one technique is within 3 dB of the other in the frequency range from 12 to 30 kHz. The phase response is within 10 degrees throughout the frequency range.

The measurements were repeated to get some idea of the variability of the results. The plane-wave calibration was consistently repeatable to within ± 1 dB and to within a few degrees throughout the frequency range. The modified switching calibration was more variable, possibly because of the difficulty in exactly relocating the probe in the tube after the transducers had been interchanged. As a result, the plane-wave calibration was choosen as the more reliable technique. It also avoids the problem that either one of the transducers could be located at a pressure node at certain frequencies.

CHAPTER 4

EXPERIMENTAL PROCEDURES AND RESULTS

The two-hydrophone technique was implemented in the existing pulse tube facility at the Applied Research Laboratory using the PZT composite transducers described in the previous chapter. In this chapter we present a comparison of experimental data collected from complex reflectivity measurements on three simple terminations using both the standing wave ratio method and the two-hydrophone method. The experimental procedure is described in detail, including a preliminary measurement to determine the precise sound velocity in the tube.

The three terminations consisted of the following: 1) pressure release (air), 2) 1/2 inch thick steel disk, and 3) sample rubber absorbing material mounted on 1/2 inch thick steel disk.

The first termination was a simple system for which the theoretical reflectivity could be easily calculated. The second termination consisted of a cylindrical stainless-steel disk, 49.2 mm in diameter (1 15/16 inch) and 12.7 mm (1/2 inch) in thickness. For the absorbing termination, a 6.4 mm (1/4 inch) thick sample of rubber material was mounted on the rigid steel disk. Both the latter samples were backed by 1 inch of water for the measurement.

4.1 The Measuring Facility

All measurements were performed on the existing pulse tube at the Applied Research Laboratory at The Pennsylvania State University. The facility consists of a 8.53 meter (28 foot) stainless steel tapered pulse tube mounted vertically and supported by a flange at the top. The upper part of the tube has an inside diameter of 5.08 cm (2 inches) and a wall thickness of 1.27 cm (1/2 inch). The tube is filled with distilled water and kept at a constant temperature of 20° C. The bottom of the tube is terminated by a LC-32 hydrophone which can act to ensonify the tube and to receive signals.

To determine the range of planar propagation in the tube, the two wall-mounted transducers were flush-mounted in a 1/2 inch thick cylindrical steel disk, which was then inserted at the top of the tube to form the upper termination. Figure 22 shows the relative phase response between these two transducers, using the LC-32 for broadband excitation (0-100 kHz) of the tube. The gradual changes in phase response between the two units up to a frequency of 40 kHz can be attributed to the phase variations in the frequency response of the individual transducers. Above 40 kHz, the large fluctuations are due to higher order modes propagating in the tube, or from disturbances from the tube wall structural vibration. All subsequent measurements were restricted to frequencies at least below 40 kHz to insure that only planar waves would be propagating in the tube.

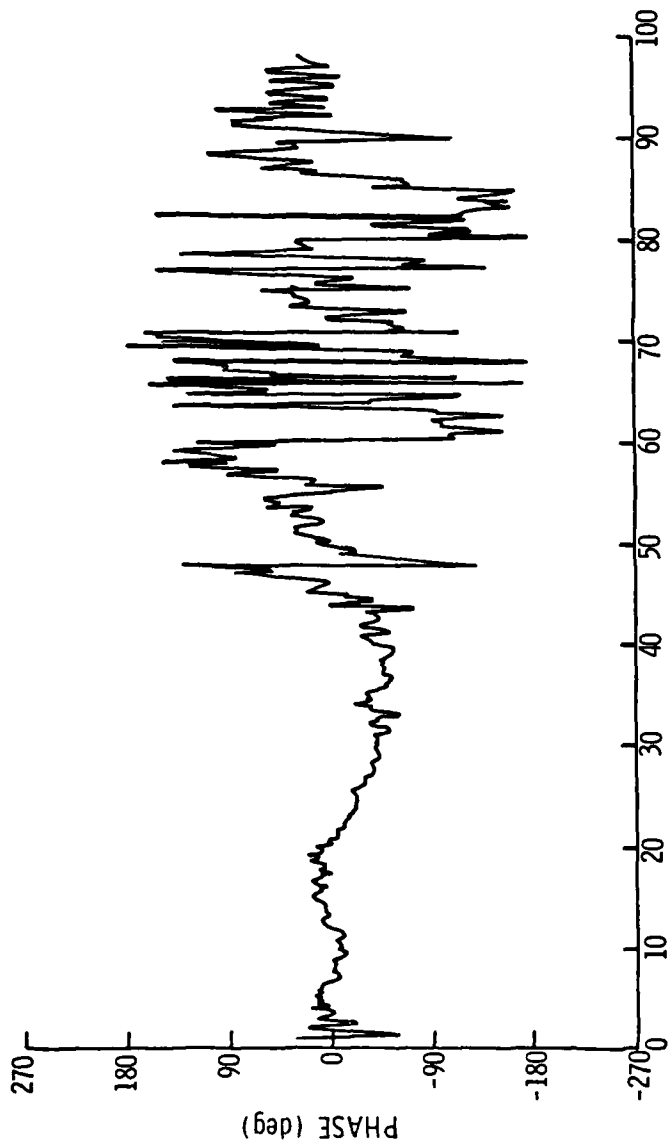

Figure 22. Relative phase response between two similar transducers measured at tube's termination showing propagation of higher order modes.

4.2 Determination of the Phase Velocity

An accurate determination of the phase velocity in the tube is necessary for precision measurements using the standing wave ratio technique or the two-hydrophone method. This velocity may differ from the free-field sound velocity due to the compliance of the tube wall as explained in Appendix B. A simple measurement was described in Section 2.4, in which the sound velocity was determined by measuring the propagation delay time between successive pulses. A value of c=1420 m/sec $\pm$50 m/sec was obtained. By referring to Equation 2.19, the relative error for the phase of the complex reflection factor can be determined as a function of frequency. An error of $\pm$50 m/sec in the determination of the propagation velocity would result in an error of $\pm$12 degrees for the value of the phase of the complex reflection factor at a velocity of 1420 m/sec at 15,000 Hz.

A more precise measurement can be performed by determining the distance between successive nodes in the standing wave for a particular frequency [16]. The frequency can be accurately determined to within $\pm$50 Hz using the spectrum analyzer with a bandwidth of 20 kHz, and the distance between nodes can be determined to within $\pm$.5 mm by measuring the volume of water added to the tube.

The measurement was performed by inserting one PZT composite hydrophone in the tube approximately 2.54 cm (1

inch) below the water-air interface. The tube was ensonified with broad-band white noise (3-30 kHz) and the magnitude of the acoustic pressure at the hydrophone location was measured by ensemble averaging using the SD-360 spectrum analyzer. At this location, the node occured at 15050 Hz (±50 Hz). Without changing the hydrophone position, water was added in milliliter increments until the second node at 15,050 Hz was measured at the hydrophone position with the new water level.

In this fashion, the value of $\lambda/2$ (the distance between nodes) at 15,050 Hz was measured to within ±.5 mm. The resulting propagation velocity was determined to be c=1440 m/sec ±20 m/sec (56,700 ±800 in/sec). This velocity was within 1.5% of the value determined form the Korteweg formula (see Appendix B), for a steel tube of 2 inches inside diameter and 1/2 inches in thickness. The resulting error in the phase of the reflection factor would then be reduced to ±5 degrees at 15,050 Hz.

4.3 Experimental Technique

This section details the experimental technique employed to measure the complex reflectivity using both the standing wave ratio method and the two-hydrophone method.

4.3.1 Standing Wave Ratio Measurements

In the standing wave ratio method, the magnitude of the complex reflection factor is determined from the ratio of the maximum to minimum acoustic pressure level in the standing wave. The phase is determined from the location of the first null relative to the sample termination (see Equation 2.19). The following experimental procedure was implimented to measure the profile of the standing wave field as a function of distance from the tube termination.

A schematic of the experimental set-up is given in Figure 23. The tube was ensonified continuously with broad-band white noise (1-30 kHz) and spectral analysis was performed using the Nicholet single channel spectrum analyzer and ensemble averaging. The position of the hydrophone was moved relative to the sample termination by using the bakelite rod, with the postion marked against a reference ruler attached to the top of the tube. A small slot was formed on the outside edge of the two sample disks to allow insertion of the rod between the edge of the sample and the inside edge of the tube wall. The hydrophone was moved at 1/4 inch increments, starting at 1/4 inch away from the sample, over a distance of 3 inches. The magnitude of the acoustic pressure as a function of frequency was recorded for each location.

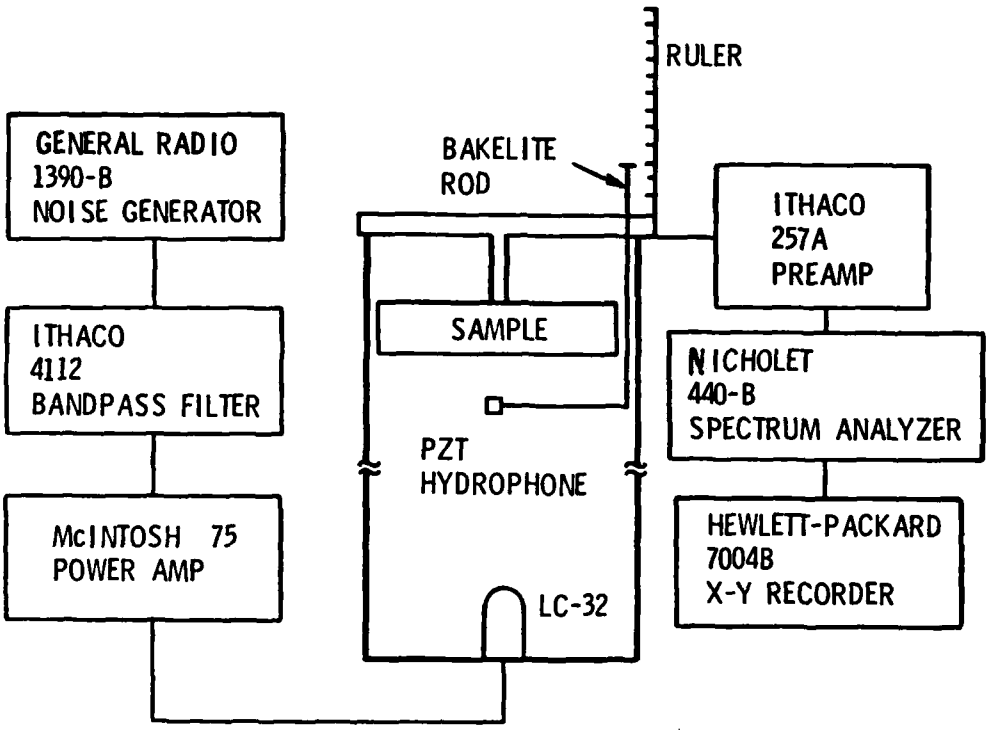

Figure 23. Experimental configuration for standing wave measurements in the water-filled pulse tube.

The resulting series of graphs, such as in Figure 24, were manually transposed to yield a series of plots of pressure magnitude versus location (i.e. the standing wave) in the tube at a particular frequency (see Figures 25 and 26). Referring to Figure 24, it can be seen that the pressure fields measured at the various locations cannot be differentiated below 7 kHz and again above 25 kHz. Therefore, the analysis range was restricted to intermediate frequencies.

As the accuracy of the technique is highly dependent on precisely locating the position of the node, only frequencies were chosen for which the hydrophone position was in a node in one of the original pressure versus frequency curves. In some cases, the position of the hydrophone corresponded to the second node (see Figure 26b).

The magnitude of the reflection factor was then determined from the standing wave ratio and the phase from the position of the node relative to the termination as in Equation 2.19.

4.3.2 Two-Hydrophone Measurements

The two-hydrophone technique requires the measurement of the complex transfer function between the acoustic pressures at two locations of known distance near the sample termination under evaluation. The complex reflectivity or impedance can then be determined from Equation 2.30. The

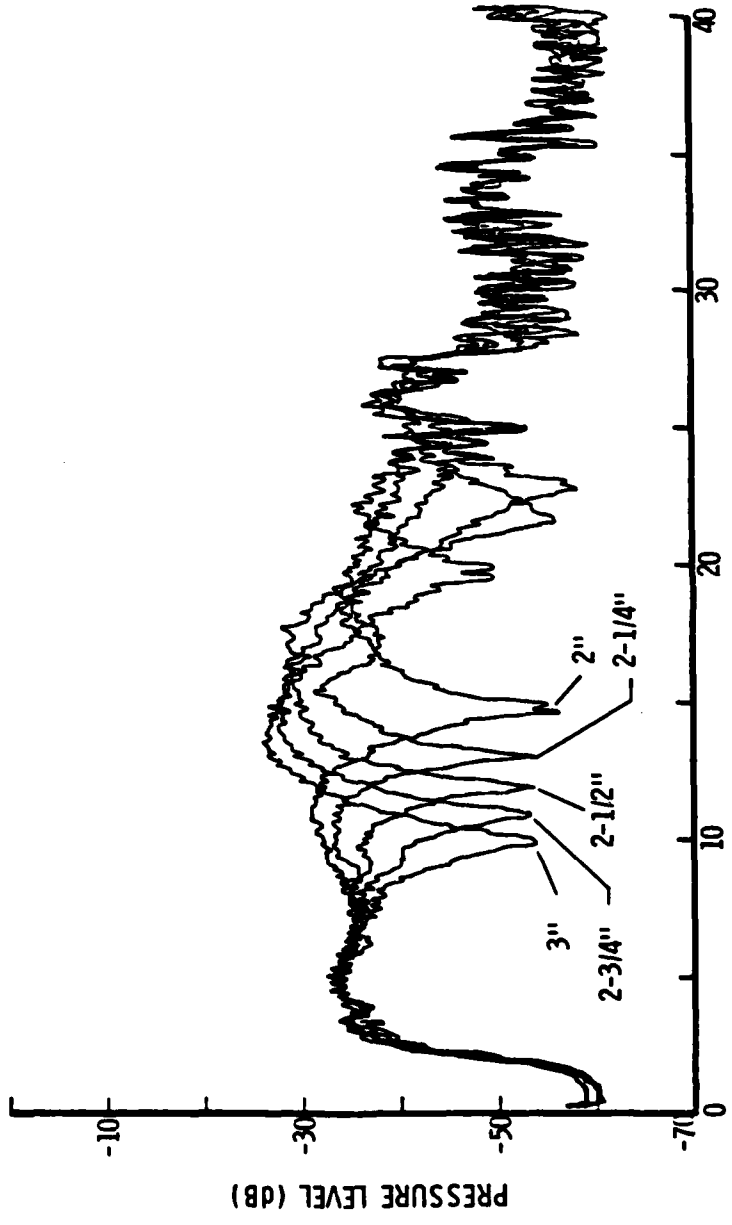

Figure 24. Pressure level in standing wave field measured near tube's termination as a function of frequency for various locations away from pressure release surface (air).

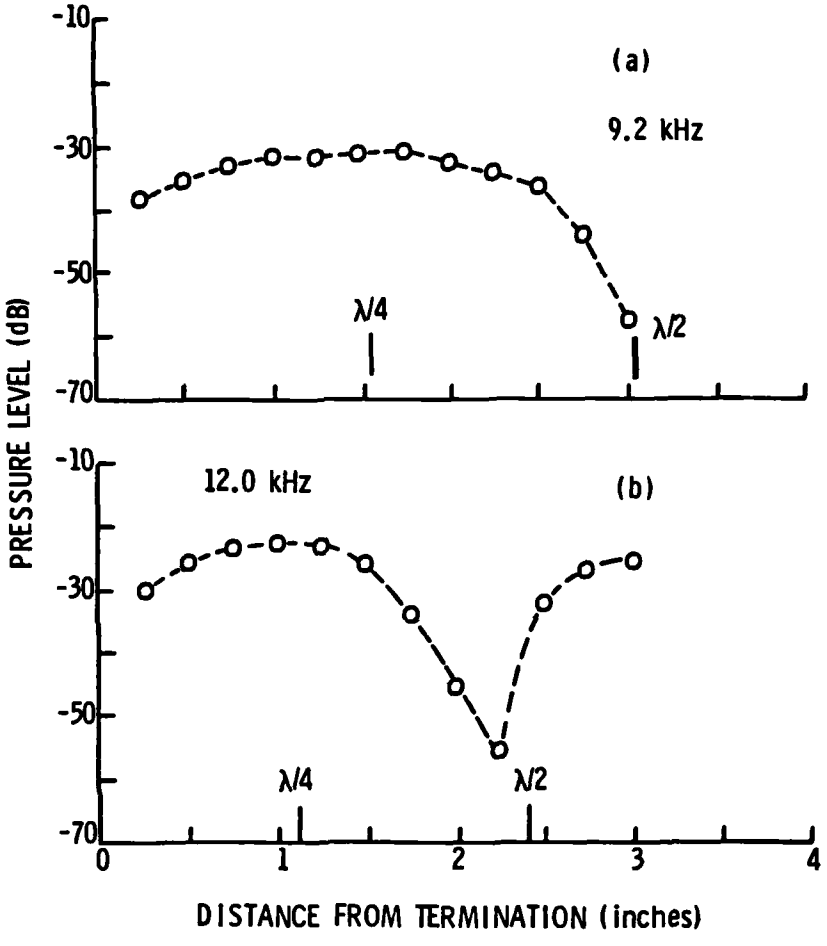

Figure 25. Standing wave field measured for a pressure release termination (air) at frequencies of (a) 9.2 kHz and (b) 12 kHz. Wavelength tic marks were computed assuming a wave velocity of 1460 m/sec.

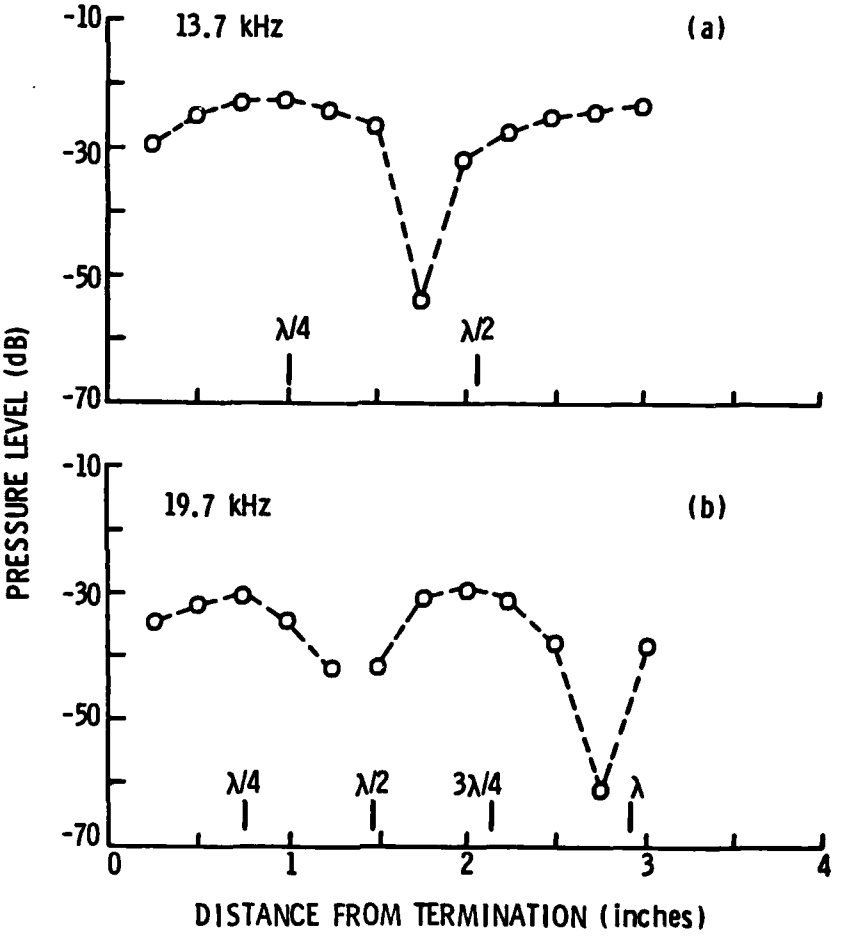

Figure 26. Standing wave field measured for pressure release termination (air) at frequencies of (a) 13.7 kHz and (b) 19.7 kHz. Wavelength tic marks were computed assuming a wave velocity of 1460 m/sec.

experimental set-up to measure the complex transfer function $\bar{H}(f)$ is described below.

Figure 27 details the experimental configuration. The two PZT composite hydrophones were attached to the bakelite rod as described in Section 3.1.3, with a separation distance of 2.54 cm (1 inch). This allowed analysis over a 30 kHz bandwidth as described in Section 2.4.1. The rod was inserted into the tube so that the uppermost unit was 2.54 cm (1 inch) away from the sample surface under evaluation. The tube was continuously excited by an LC-32 projector with broad-band noise (1-30 kHz), and the complex transfer function between the two hydrophones measured with a dual-channel Spectral Dynamics SD-360 FFT signal analyzer. A total of 512 ensemble averages were taken and the real and imaginary parts of the transfer function transmitted to a PDP-11 computer.

The data was corrected by the relative calibration obtained using the plane-wave technique as described in Section 3.4.2 using Equation 3.7. The complex reflection was them computed using Equation 2.30. The output was printed on a Tektronics digital plotter by employing software written by the author along with Tektronics' Plot-10 graphics software package.

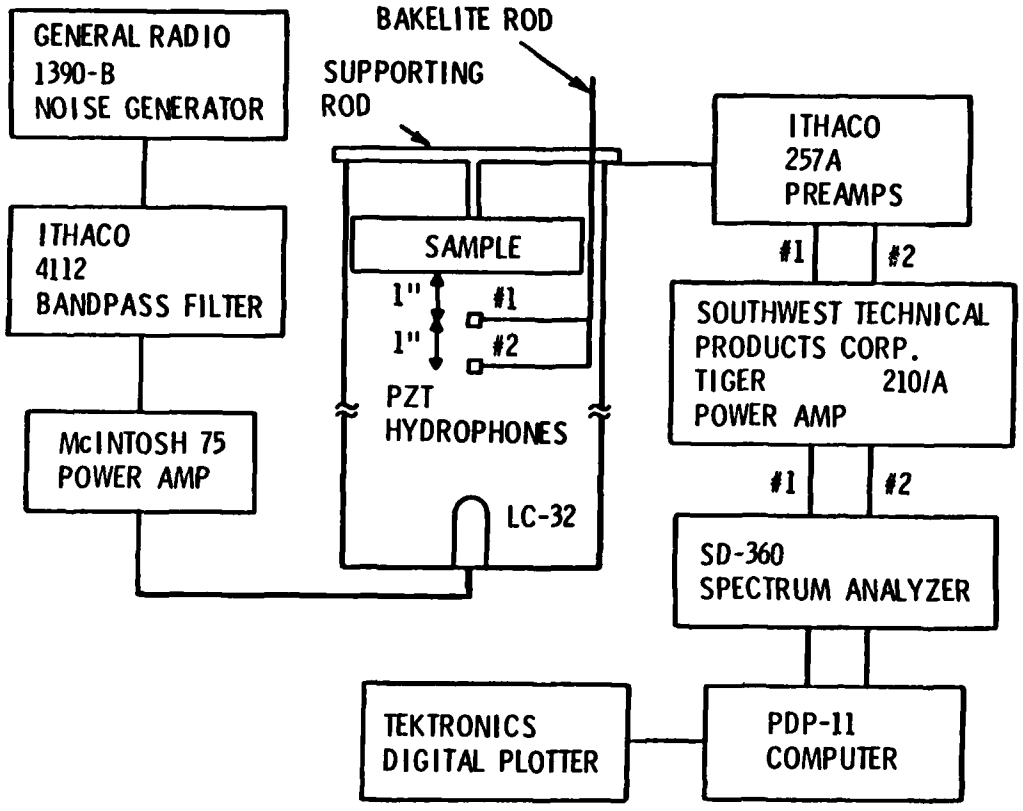

Figure 27. Experimental set-up for two-hydrophone technique in a water-filled tube.

4.4 Presentation of Data

The complex reflection factor measured using the standing wave ratio technique described in Section 4.3.1 and the two-hydrophone technique described in Section 4.3.2 is presented in the next three sections, each section dealing with the specific termination under evaluation.

4.4.1 Pressure Release Termination

As the characteristic impedance of air (ρc=428 MKS Rayls) is much smaller than that of water (ρc=1.48 * 10^6 MKS Rayls), air forms an effective pressure release termination for water-filled tubes. The theoretical complex reflection factor can be determined using Equation 2.25 as follows:

$$\bar{R} = \frac{Z_A - Z_O}{Z_A + A_O} \tag{4.1}$$

where Z_A is the characteristic impedance of air and Z_o is the characteristic impedance of water. The theoretical value for the reflection factor is then:

$$\bar{R} = (428 - 1.48 * 10^6)/(428 + 1.48 * 10^6)$$

$$= -1.00 = 1e^{j\pi}$$

The measured coherence function and the magnitude and phase of the transfer function for the two-hydrophone measurement is given in Figures 28 and 29 respectively. The

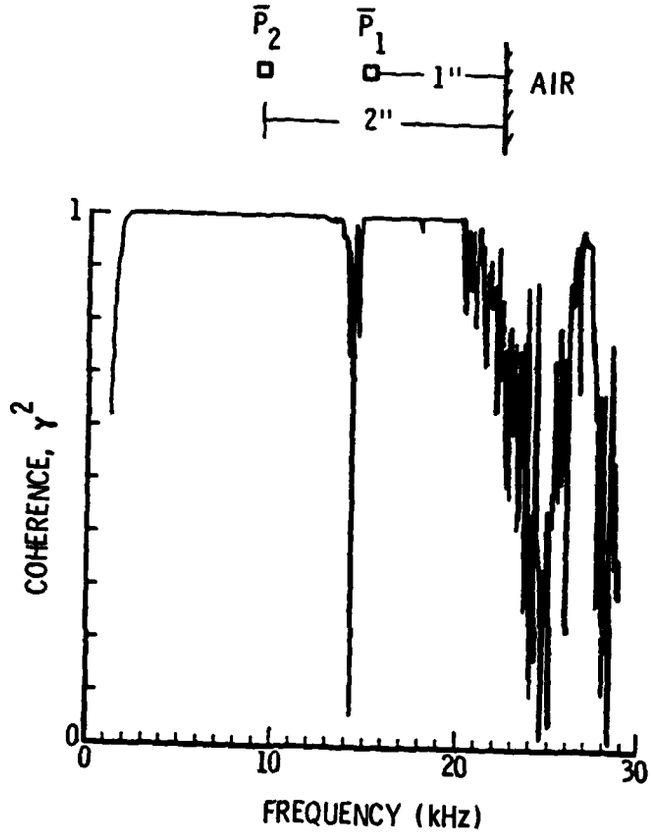

Figure 28. Measured coherence between the two PZT hydrophones at x_1=1" and x_2=2" for the case of air termination.

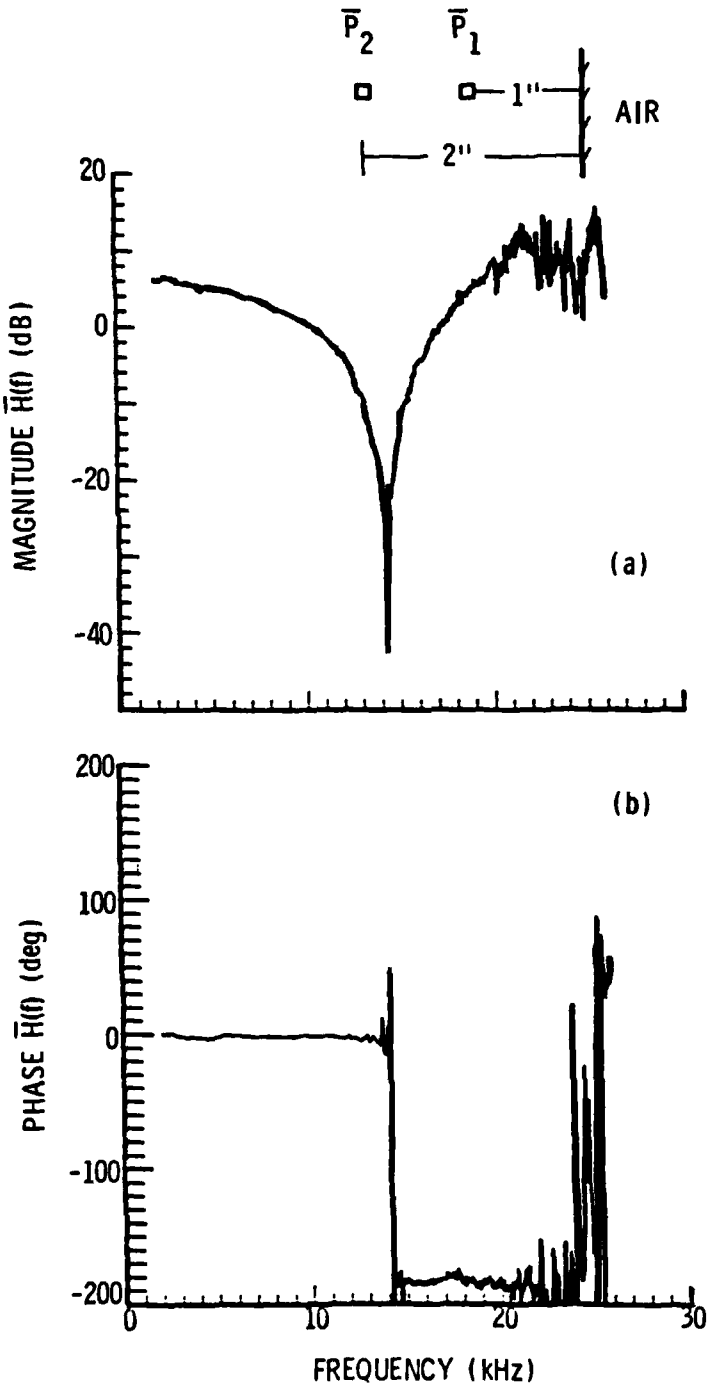

Figure 29. Measured transfer function between the two PZT hydrophones at x_1=1" and x_2=2" for the case of air termination.

coherence is unity in the range from 3-21 kHz except in the frequency region for which the second hydrophone was in a node. All subsequent analysis was restricted to this region of high coherence to insure repeatability of the results.

The measured transfer function for the air termination can be compared to the theoretical transfer function computed for a pressure release termination shown in Figure 4. There is excellent agreement for both the magnitude and phase values in the range for which the coherence is approximately unity.

The complex reflection factor, computed from the measured transfer function is shown in Figure 30. The two-hydrophone data has been smoothed somewhat. Also indicated are the values measured from the standing wave ratio technique at the discrete frequencies for which data was available.

The magnitude of the reflection factor from both measurement techniques is very close to the theoretical value of unity. The standing wave ratio data differed from the two-hydrophone data by at most 10%.

The measured reflection factor phase varied within ± 30 degrees from the theoretical value of -180 degrees. The measurement results from the two methods are consistant to within 20 degrees except at the high frequencies. The phase

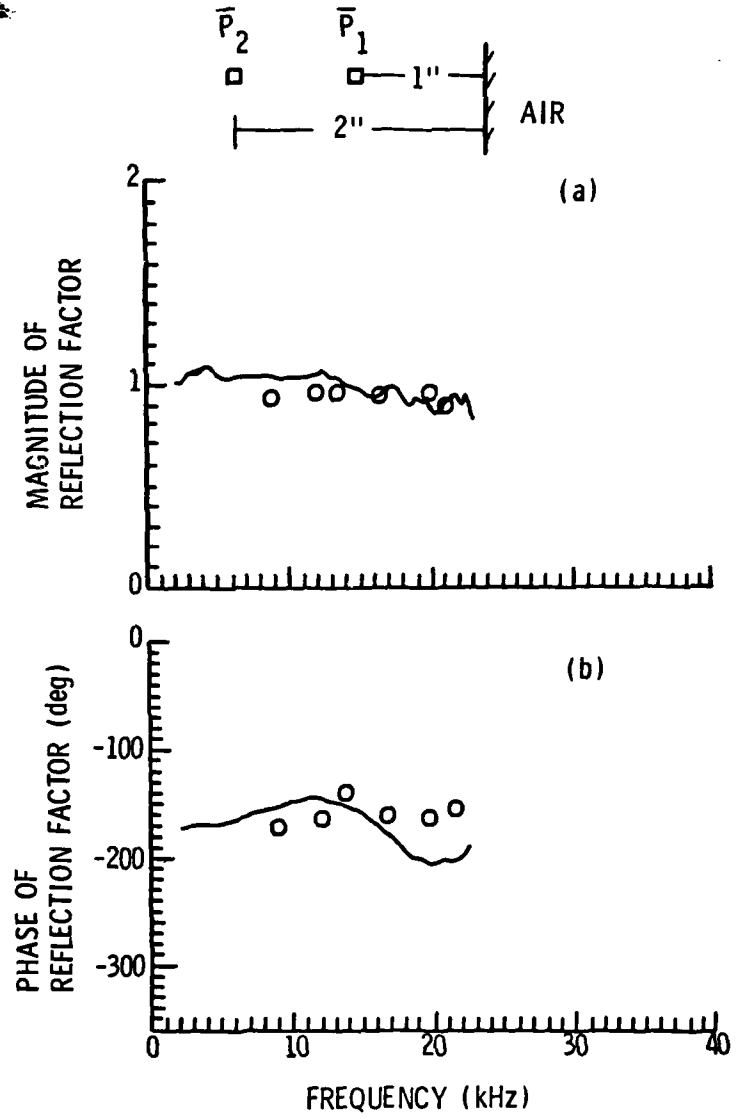

Figure 30. Comparison of the reflection factors of an air termination using the standing wave technique (circles) and the two-hydrophone technique (solid lines).

values from the two-hydrophone technique appear to be consistently biased as a function of frequency either above or below the theoretical value of -180 degrees. This could be due to an inaccurate placement of the hydrophones in the tube as will be explored further in Section 4.5.2.

4.4.2 Steel Disk Termination

The measured coherence function from the two-hydrophone technique measurement of the 1/2 inch thick steel disk is shown in Figure 31. There are sharp drops in coherence corresponding to frequencies for which the hydrophone positions were in a node. In addition, there is a broader dip in coherence in the frequency region from 16 to 19 kHz. The coherence also deteriorates above 21 kHz.

The measured transfer function $\bar{H}(f)$ is given in Figure 32. This can be compared with the theoretical $\bar{H}(f)$ computed for a rigid termination presented in Figure 33. There appears to be good agreement except in the region from 16-19 kHz. The drop in coherence in this region corresponds to an extra peak in the magnitude, and widely fluctuating values in the phase of the measured transfer function.

The complex reflection factor is shown in Figure 34. The magnitude estimates from the standing wave ratio method are consistantly lower than the values from the two-hydrophone measurement. The extra peak in the transfer function in the region from 16-18 kHz corresponds to a large

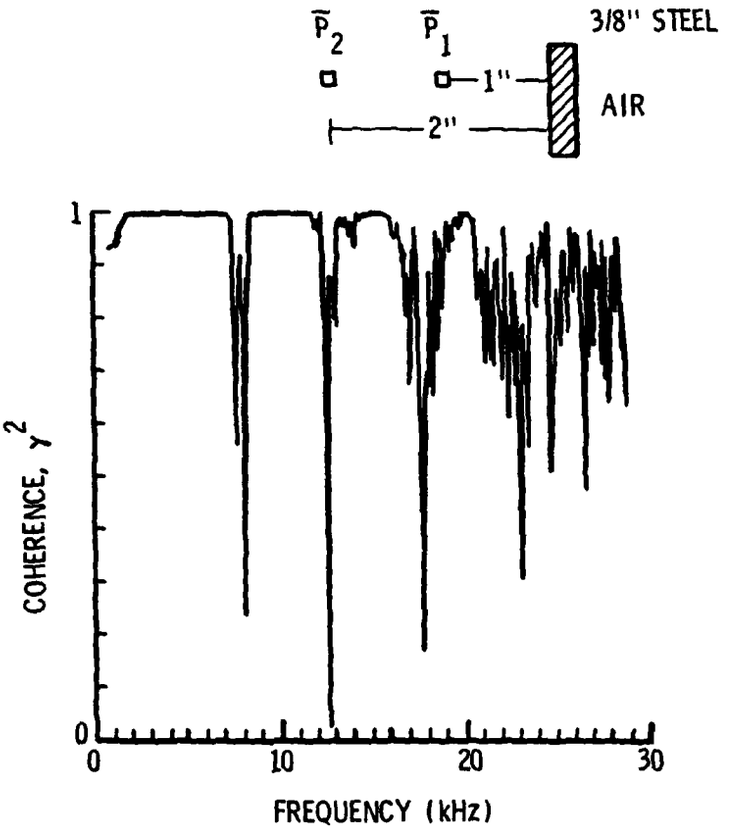

Figure 31. Measured coherence function between the two PZT hydrophones at x_1=1" and x_2=2" for the case of an air-backed 3/8" thick steel disk.

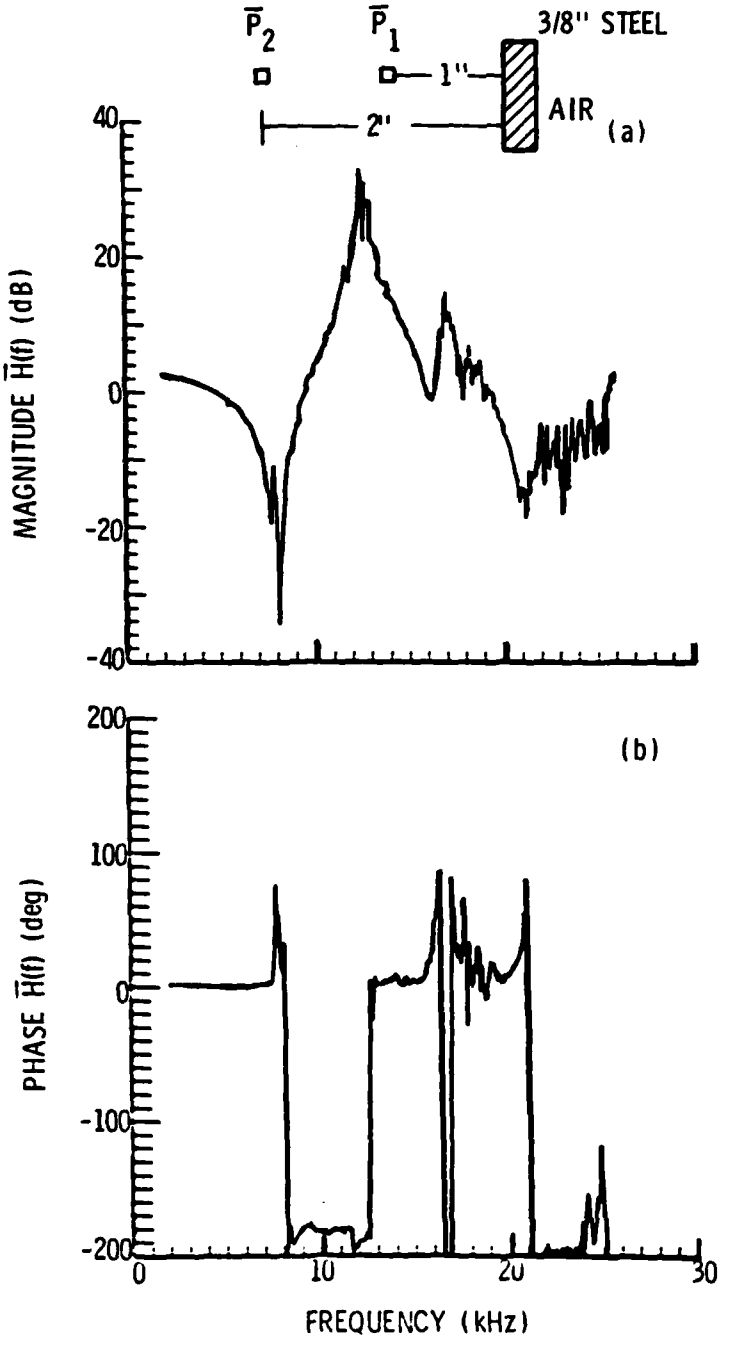

Figure 32. Measured transfer function between the two PZT hydrophones at x_1=1" and x_2=2" for the case of an air-backed 3/8" thick steel disk.

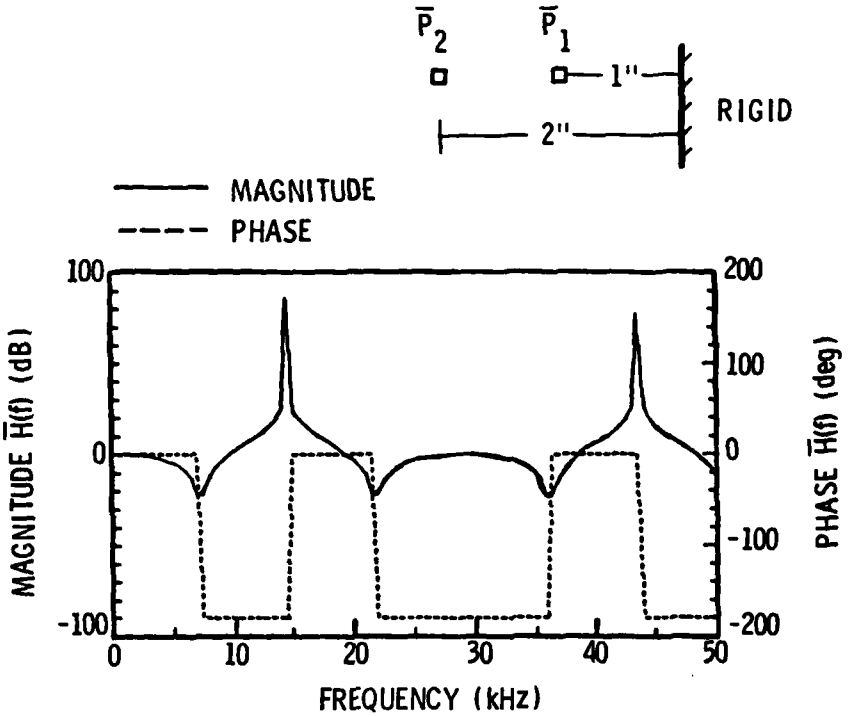

Figure 33. Theoretical calculation of the transfer function for an ideally rigid termination.

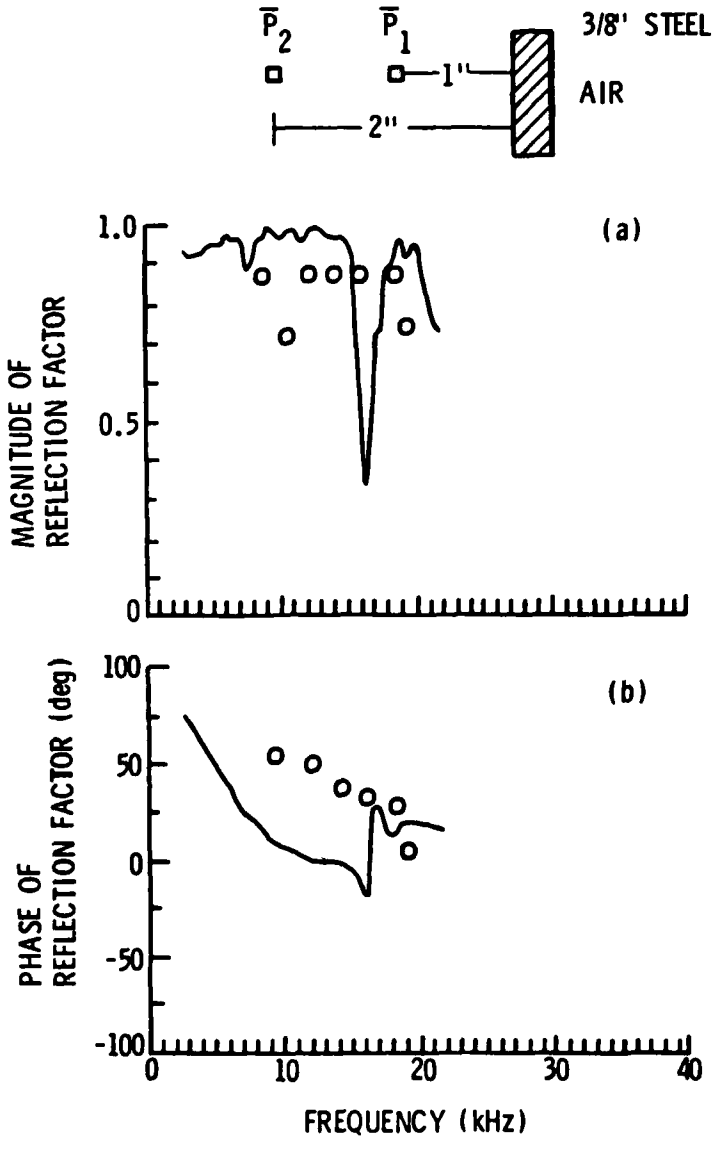

Figure 34. Comparison of the reflection factors for the air-backed 3/8" thick steel disk using the standing wave technique (circles) and the two-hydrophone technique (solid lines).

dip in the measured reflection factor magnitude. Data in this region should be discounted. The smaller dip around 8 kHz also corresponds to a region of low coherence.

The phase estimate of the reflection factor differs significantly between the two techniques. The standing wave ratio data is consistently almost 90 degrees greater than the two-hydrophone data below 16 kHz. The consistency of the phase error suggests an additional bias error perhaps due to an initial displacement error in locating the hydrophone for the standing wave ratio measurements. There is also a discontinuity in the phase estimate around 16-18 kHz, in the region of low coherence. The reflection factor phase estimate from the two-hydrophone measurement is consistent with data reported by Meyer et al [16] for a 12 mm thick iron disk measured in a similar tube, as shown by the "x's" in Figure 34b.

4.4.3 Absorbing Sample Termination

The coherence, transfer function and reflection factor data for the absorbing sample is presented in Figures 35, 36 and 37, respectively. There are no sharp drops in the coherence function below 20 kHz, indicating that the surface was not reflective enough to generate sharp nodes in the standing wave field. There is again a hump in the magnitude estimate in the range from 16-18 kHz, which is the same region of erratic data as for the steel disk, although the

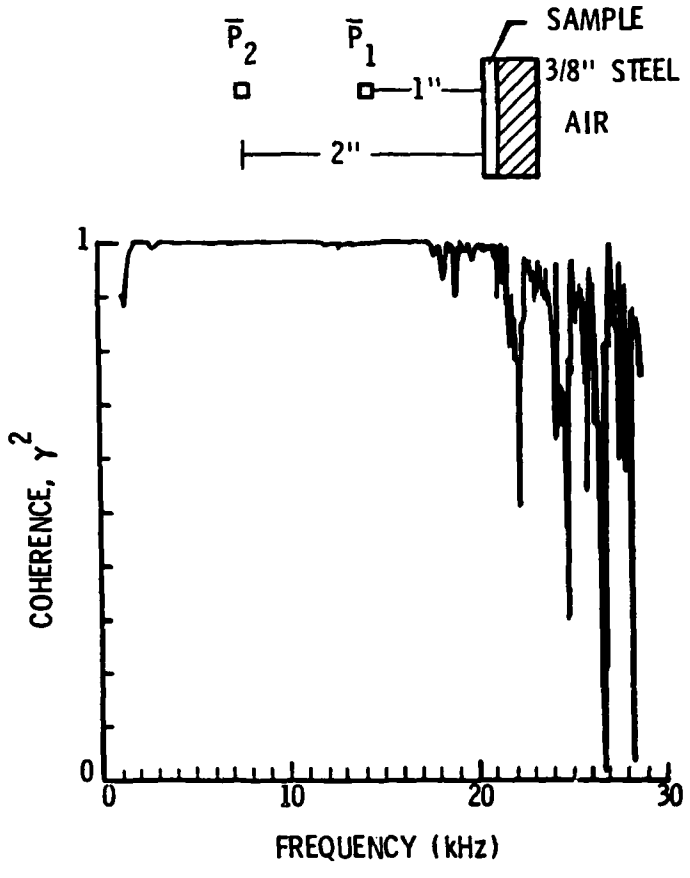

Figure 35. Measured coherence function between the two PZT hydrophones at x_1=1" and x_2=2" for the case of an absorbing sample termination.

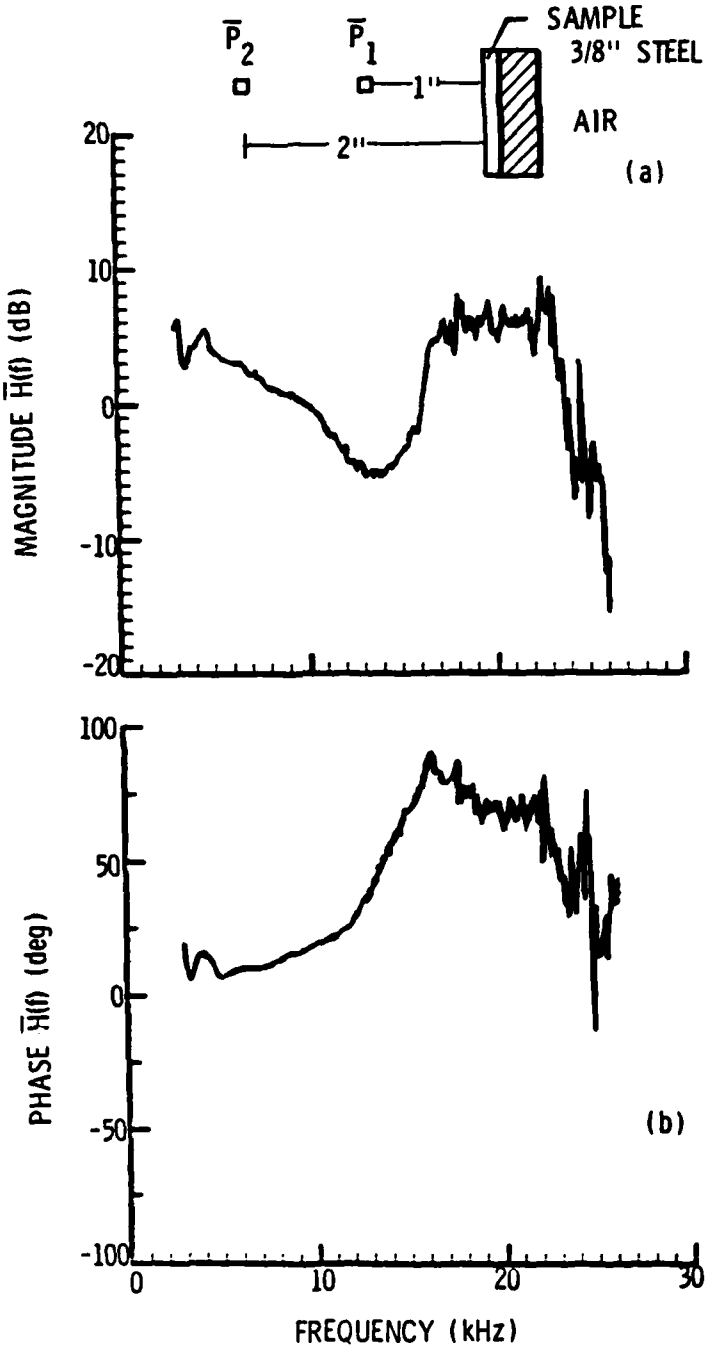

Figure 36. Measured transfer function between the two PZT hydrophones at x_1=1" and x_2=2" for the case of an absorbing sample.

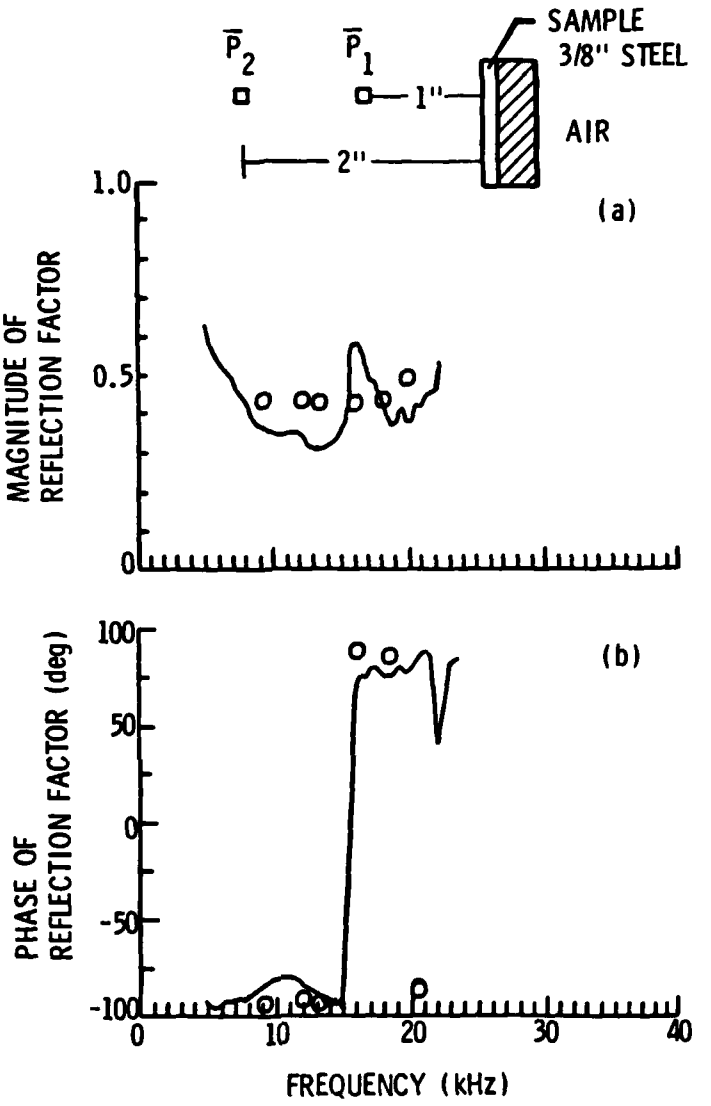

Figure 37. Comparison of the reflection factors for the absorbing sample using the standing wave technique (circles) and the two-hydrophone technique (solid lines).

coherence in this region does not drop. The standing wave ratio data and the two-hydrophone data are generally consistent to within 20% of one another.

The phase estimates for the reflection factor are within 20 degrees of one another except for the one standing wave ratio data point at 20 kHz. The phase of the reflection factor exhibits a transition around 15 kHz, which was measured using both techniques.

It was not immediately apparent why the coherence consistantly dropped above 20 kHz for all the terminations tested. The region from 20-30 kHz however, does correspond to higher tube wall acceleration levels (see Figure 13), which may introduce noise into the measurement. The pressure level in the tube is also decreasing in this region (see Figure 14), which may lower the signal-to-noise level and decrease the coherence. Finally, the finite size of the transducers themselves may produce scattering at the higher frequencies.

4.5 Precision of Measurement Results

To accurately measure the complex reflection factor using either the standing wave ratio method or the two-hydrophone technique, great care must be taken in the experimental procedure. Significant errors can result, especially in the measured value for the phase of the reflection factor, by inaccurate estimates of the location

of the transducer(s) in the tube relative to the termination under evaluation. Errors in the measured phase velocity in the tube will also affect the value of the phase of the reflection factor.

From an experimental viewpoint, the standing wave ratio method places greater demands on both the experimenter and the experimental hardware, in that the location of the transducer in the tube must be precisely determined for a number of measurements over a range of locations in the tube. In the two-hydrophone technique, modern signal processing considerably reduces the time involved in the measurements, because the transducers are positioned in the tube only once. However, once positioned, any inaccuracies in placement will affect the entire measurement. This could lead to considerable bias errors in the measurement of the reflection factor phase. Such errors are especially difficult to detect for measurements on surfaces of unknown impedance. Random and bias errors also occur from the signal processing procedures in the two-hydrophone technique, which are discussed in Appendix C.

This section will investigate the extent of the errors resulting from the tolerance of hydrophone placement in both the standing wave ratio method and the two-hydrophone method in an attempt to explain some of the inconsistencies in the measurement results as presented in the preceding section.

In addition, the effect of the tolerance in the measured phase velocity will be discussed.

4.5.1 Precision of Standing Wave Ratio Measurements

Equation 2.19 which is repeated here, can be used to find the error as a function of frequency, of the reflection factor phase:

$$\phi = \pi[(4fx_{min}/c) - 1] \qquad (4.2)$$

The location of the node (x_{min}) could be resolved to within $\pm$1/8 inch ($\pm$3mm) using the PZT composite probes for the measurement. Assuming a velocity of 1440 m/sec in the tube, the absolute value of the phase measurement was determined for each extreme (+3mm, -3mm) at each frequency, and is plotted in Figure 38, for a theoretical reflection factor of $\bar{R}$=-1 (pressure release).

The absolute range of the error is the span along the y axis, between the two lines at any particular frequency. As can be seen in the figure, the error at 20 kHz is approximately $\pm$15 degrees around the correct value of -180 degrees.

The phase velocity, measured as described in Section 4.2, had a value of 1440 m/sec $\pm$20 m/sec. Using Equation 4.2, the absolute error in the reflection factor phase was determined for a pressure release termination as a function of frequency, for the given phase velocity tolerance, $\pm$20 m/sec, and is also plotted in Figure 38.

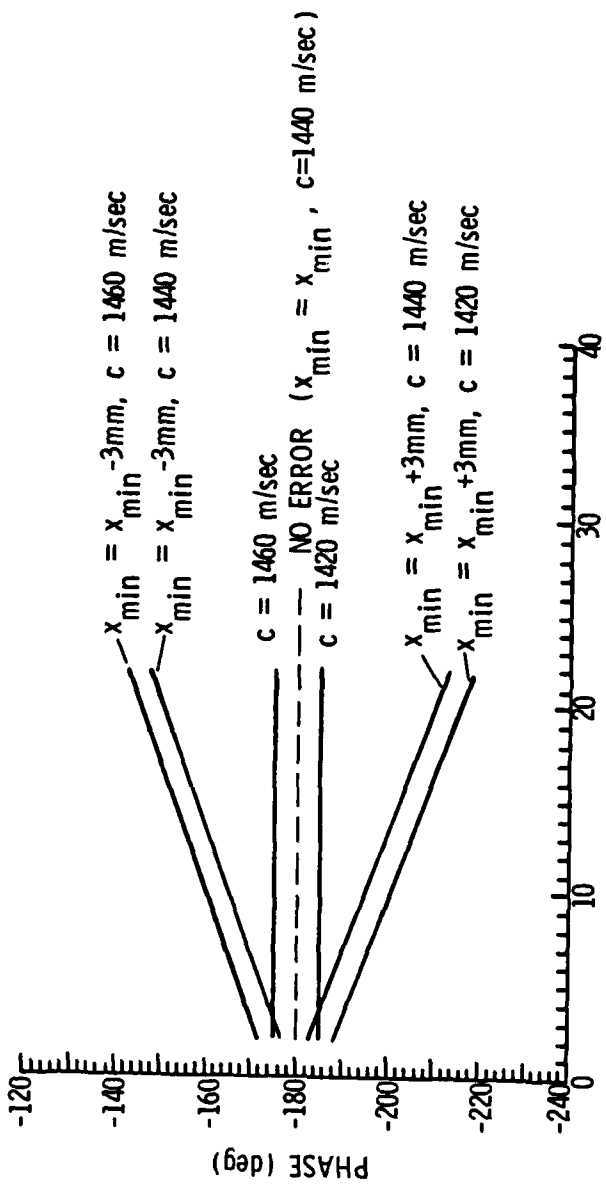

Figure 38. Theoretical error in reflection factor phase as a function of phase velocity, c and location, x_1 and x_2, tolerances in the tube using the standing wave technique for an ideal pressure release surface.

These errors in velocity determination and hydrophone placement are additive. Assuming both errors are present, the absolute value of the reflection factor phase error at the two extreme ranges of velocity and location tolerance is again plotted in Figure 38. As can be seen in the figure, at 20 kHz, the error is as high as $\pm$36 degrees at c=1440 m/sec.

There is also an error introduced from the tolerance of the frequency measurement ($\pm$50 Hz), but this is insignificant in comparison to the above errors.

The effect of the hydrophone placement tolerance on the magnitude of the reflection factor is more difficult to determine. The error is a function of the amplitude of the standing wave ratio as well as the frequency. The technique employed for the standing wave ratio measurement, in which only frequencies which corresponded to nodes at the various hydrophone locations were chosen, should minimize any potential errors in the magnitude estimate.

4.5.2 Precision of Two-Hydrophone Method

The effects of inaccuracies in hydrophone position and phase velocity on the reflection factor phase, using the two-hydrophone technique, were determined for a pressure release termination as described below.

The theoretical pressure field at location x_1 and x_2 for an ideal reflection factor of $\bar{R}=-1$, was determined using Equation 2.2, and used for the input data of the two-hydrophone technique. The data was then reconstructed to yield the reflection factor. When the same parameters (x_1, x_2, c), specified for the input data, were used for the reconstruction formula, the reflection factor came out exactly as specified, which was to be expected. However, by varying the input parameters used to construct the artificial data, around their tolerances, and then reconstructing the data assuming no changes had been made, bias errors appeared in the phase of the reconstructed reflection factor. These theoretical induced errors can be viewed as typical of the measurement errors resulting from inaccurate hydrophone placements in the tube, or in uncertainty in the phase velocity.

The PZT hydrophones were approximately 1/8 inch thick. They were located in the tube so that the center of the unit was within $\pm$1/16 inch ($\pm$1.5 mm) of the specified location (X_1= 1 inch, x_2= 2 inch) from the sample termination. It was then estimated that the acoustic center of the hydrophones could be located to within $\pm$1/8 inch ($\pm$3 mm) of the specified value.

A series of theoretical plots were generated, showing how the reflection factor phase deviates, for various

permutations of microphone location around their specified values, in the frequency range from 2 to 22 kHz. Deviation curves were also generated using the two extreme velocity values, where the correct hydrophone placement was assumed.

All of these plots are superimposed on the same graph in Figure 39. The maximum error can be determined from the "envelope" of the outermost lines in the figure. The error resulting from the phase velocity inaccuracy (the innermost lines in the figure) should be added to this. As can be seen, an error of almost $\pm$35 degrees can result at 20 kHz for the estimate of the reflection factor phase, based on the location and velocity tolerances in the experimental procedure.

The magnitude of the reconstructed reflection factor was not affected for this special case of R constant. It is to be expected that for cases where R varied as a function of frequency, some bias errors would result in the magnitude estimate from variations in hydrophone placement around their tolerances.

Additional errors can result from an inaccurate relative calibration, although the measured transfer function for the pressure release termination indicates that the hydrophone calibration errors were relatively small.

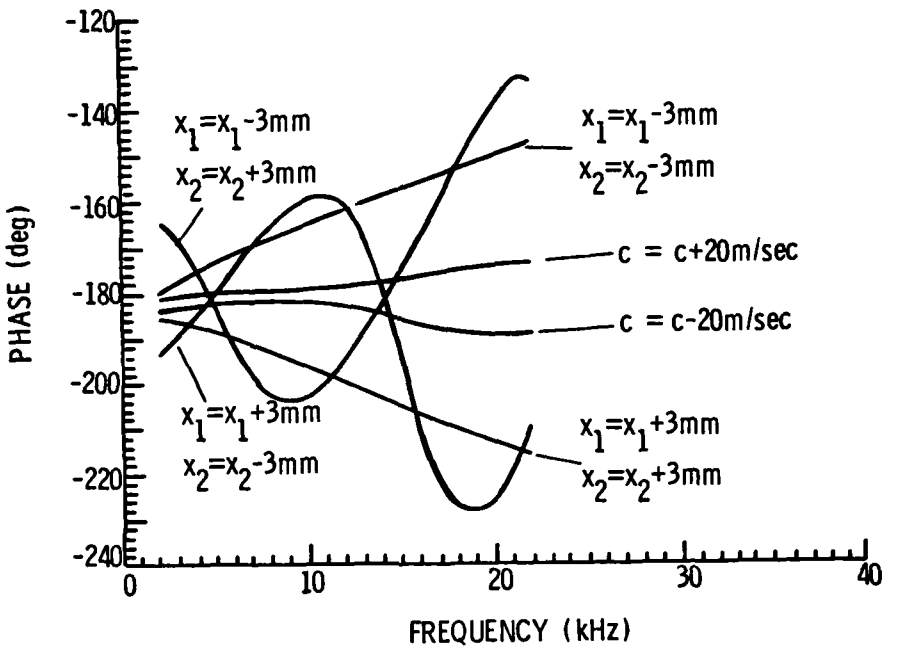

Figure 39. Theoretical error in reflection factor phase as a function of phase velocity, c, and location, x_1 and x_2, tolerances using the two-hydrophone technique for an ideal pressure release surface.

In summary, both the two-hydrophone technique and the standing wave ratio technique are extremely sensitive to errors in the location of the hydrophones relative to the termination under evaluation, especially in the determination of the phase of the complex reflection factor. The relative effect is similar for each measurement technique, and of approximately the same magnitude.

Referring back to the data for the three sample terminations, the phase estimates of the complex reflection factor are generally within the above tolerances, with the possible exception of the the rigid termination measurement.

Although no error tolerances were determined for the measurement of the reflection factor magnitude, the results from both techniques were generally consistent to within 20% of one another.

CHAPTER 5

CONCLUSIONS AND RECOMMENDATIONS

The following conclusions can be made concerning the use of the two-hydrophone technique to measure the complex reflection factor in water-filled tubes:

1. The technique is feasible if careful consideration is given to transducer selection and design. Wall-mounted hydrophones are not appropriate because of their mechanical sensitivity and the relatively high value of the tube wall acceleration level. Insertion type hydrophones must be small enough so as not to perturb the acoustic pressure field. PZT composite transducers are well suited in this respect for the measurement scheme.

2. The tube can be continuously ensonified to perform the measurement. The technique can also be performed using pulses, if proper signal processing procedures are adopted. Although pulsed signals did not provide any significant improvements using tubes, such methods could prove valuable in other measurement configurations (such as in anechoic tanks).

3. The measured complex reflection factor appears to be valid only in frequency regions for which the coherence is approximately unity. For the transducers and tube configuration in the present study, the range of high coherence was limited to a range between 3 and 20 kHz.

4. The accuracy of the two-hydrophone technique, especially in the determination of the reflection factor phase, is highly dependent on the precision with which the hydrophones can be located in the tube, relative to the surface of the sample under evaluation. This constraint is neither more nor less severe than in other transmission line methods in which the standing wave field in the tube is measured near the tube termination.

5. The two-hydrophone technique provides a considerable savings in experimental effort and time over the traditional standing wave ratio method.

The following recommendations can be made concerning the use of the two-hydrophone technique in water-filled tubes:

1. It is highly desirable to develop a transducer and mounting configuration in which the acoustic center of the transducers could be located with greater precision in the tube. The following recommendations are made in this regard:

   A) A more permanent probe could be devised which could be left inserted in the tube. The acoustic center of the hydrophones could be accurately determined by measuring the frequencies for which nodes occured at the two hydrophone locations, for a water-air termination above the probe, which could be precisely repeated.

   B) Thin film PVDF hydrophones may be well suited for this task if the transducer and mounting configuration could be devised so as not to perturb the pressure field. In this regard the author recommends the use of thinner, smaller diameter rings of acoustically transparant material to suspend the PVDF film. The smaller diameter rings should also minimize the pick-up of structure-borne noise.

C) A means should be devised in which the sample under evaluation could be more precisely located above the hydrophone probe. A small groove on the inside diameter of the tube wall on which the bottom of the sample could rest may be feasible.

2. The use of a piston-type hydrophone projector to ensonify the tube may provide higher signal levels in the tube, especially at higher frequencies, which could improve the signal-to-noise level of the measurements, and increase the range of good coherence to higher frequencies.

BIBLIOGRAPHY

1. Beranek, Leo L. Acoustic Measurements. New York: John Wiley & Sons Inc., 1949.

2. Bobber, Robert J. Underwater Electroacoustic Measurements. Naval Research Laboratory, Washington D.C. July 1970.

3. Taylor, H. O. "A Direct Method of Finding the Value of Materials as Sound Absorbers," Physical Review. Vol. 2, pp. 270-287, 1913.

4. Lord Rayleigh. The Theory of Sound. New York: Dover Publications Inc., 1945.

5. Wente, E. C. and Bedell, E. H. "Measurement of Acoustic Impedance and the Absorption Coefficient of Porous Materials," Bell System Technical Journal. Vol. 7, pp.1-10, 1928.

6. Hall, W. M. "An Acoustic Transmission Line for Impedance Measurement," J. Acoustical Soc. of Amer. Vol. 11, pp. 140-146, 1939.

7. Beranek, L. L. "Precision Measurements of Acoustic Impedance," J. Acoustical Soc. Amer. Vol. 12, p. 3-13 , 1940.

8. Sabine H. J. "Notes on Acoustic Impedance Measurements," J. Acoustical Soc. Amer. Vol. 14, pp.143-150, 1942.

9. Beranek, L. L. "Some Notes on the Measurement of Acoustic Impedance," J. Acoustical Soc. Amer. Vol. 19, pp.420-427, 1947.

10. Scott, R. A. "An Apparatus for Accurate Measurement of the Acoustic Impedance of Sound-Absorbing Materials," Proc. Phys. Soc. Vol 58, pp. 253-264, 1946.

11. Bolt, R. and Petrauskas. "An Acoustic Impedance Meter for Rapid Field Measurements," (Abstract) J. Acoustical Soc. Amer. Vol. 15, p.79, 1943.

12. ASTM C384-558, 1972, Standard Method of Test for Impedance and Absorption of Acoustic Material by the Tube Method.

13. Seybert, A.F. and Soenarko, B. "Error Analysis of Spectral Estimates with Applications to the Measurement of Acoustic Parameters using Random Sound Fields in Ducts," J. Acoustical Soc. Amer. Vol 69(4), pp. 1190-1199, 1981.

14. Seybert, A. F. and Ross, D. F. "Experimental Determination of Acoustic Properties using a Two-Microphone Random-Excitation Technique," J. Acoustical Soc. Amer. Vol 61, No. 5, pp.1362-1370, 1977.

15. Chung, J. Y. and Blaser, D. A. "Transfer Function Method of Measuring In-Duct Acoustic Impedance, I. Theory, II. Experiment," J. Acoustical Soc. Amer. Vol 68(3), pp. 907-921, 1980.

16. Meyer, E. et al. "Sound Absorption and Sound Absorbers in Water," NAVSHIPS 900,166 U.S. Dept. of the Navy, Washington D.C., 1950.

17. Kuhl, Walter, Oberst, Hermann and Skudrzyk, Eugen. "Impulsverfahren der Reflexion von Wasserschall-absorbern in Rohren," Acustica. Vol. 3, pp.421-433, 1953.

18. Sabine, Gerald A. "Acoustic-Impedance Measurements of High Hydrostatic Pressure," J. Acoustical Soc. Amer. Vol 40(6), pp. 1345-1353, 1966.

19. Cremer, L. "Theorie der Luftschall-Daemmung Zylindrischen Schalen," Acustica. Vol. 5, p.245-256, 1955.

20. Heckl, M. "Experimentelle Untersuchungen zur Schalldaemmung von Zylindern," Acustica. Vol. 8, p.259-256, 1958.

21. Shaw, E. A. G. "The Acoustic Wave Guide. I. An Apparatus for the Measurement of Acoustic IMpedance using Plane Waves and Higher Order Mode Waves in Tubes," J. Acoustical Soc. Amer. Vol 25(2), pp.224-230, 1953.

22. Waterhouse, Richard. "Comments on Impedance Tube Measurements," J. Acoustical Society of America. Vol. 69(5), pp. 1516-1517, 1981.

23. Sessler, G.M. "Piezoelectricity in Polyvinylidene-flouride," J. Acoustical Soc. Amer. Vol 70(6), pp. 1596-1608, 1981.

24. Sullivan, T.D. and Powers, J.M. "Piezoelectric Polymer Flexural Disk Hydrophone," J. Acoustical Soc. Amer. Vol 63(5), pp. 1396-1401, 1978.

25. DeReggi, A.S. et al., "Piezoelectric Polymer Probe for Ultrasonic Applications," J. Acoustical Soc. Amer. Vol 69(3), pp. 853-859, 1981.

26. Shotton, K.C., Bacon, D.R. and Quillam, R.M. "A PVDF Membrane Hydrophone for Operation in the Range 0.5 mHz to 15 mHz," Ultrasonics May, 1980, pp.123-126.

27. Bacon, D.R. "Characteristics of a PVDF Membrane Hydrophone for use in the Range 1-100 mHz," IEEE Transactions on Sonics and Ultrasonics. Vol SU-29, No. 1, Jan. 1982, pp. 18-25.

28. Safari, A. et al. "Perforated PZT Polymer Composites for Piezoelectric Transducer Applications," Ferroelectrics. Vol. 41, pp. 197-205, 1982.

29. Skudrzyk, Eugen. The Foundations of Acoustics. Wein: Springer-Verlag, 1971.

30. Walter, J.L. "Coincidence of Higher-Order Modes- A Mechanism of the Excitation of Cylindrical Shell Vibrations via Internal Sound," Ph.D. Thesis in Mechanical Engineering, The Pennsylvania State University, 1979.

31. Skudrzyk, E.J. Personal communication.

32. Bendat, J.S. and Piersol, A.G. Engineering Applications of Correlation and Spectral Analysis. New York: John Wiley and Sons, 1980.

33. Oppenheim, Alan V. and Schafer, Ronald W. Digital Signal Processing New Jersy: Prentice-Hall, Inc. 1975.

34. Bendat, J.S. and Piersol, A.G. Measurement and Analysis of Random Data. New York: John Wiley and Sons, 1966.

35. Woodward, B. "The Suitability of Polyvinylidene Flouride as an Underwater Transducer Material," Acustica. Vol 38, pp. 264-268, 1977.

36. Chrisler, V.L. "Acoustical Work of the National Bureau of Standards." J. Acoustical Soc. Amer. Vol. 7(2), pp.79-87, 1935.

37. Johnson, Walter C. Transmission Lines and Networks. New York: McGraw-Hill Book Company, Inc. 1950.

38. Morse, P. M. Vibration and Sound. New York: McGraw-Hill Book Company, Inc. 1948.

39. Sabine, Wallace Clement. Collected Papers on Acoustics. New York: Dover Publications Inc. 1964.

40. Morse, Philip M. and Ingard, K. Uno. Theoretical Acoustics. New York: McGraw-Hill Book Company, Inc. 1968.

APPENDIX A

WAVE PROPAGATION IN CYLINDRICAL DUCTS

In this appendix we develop an expression for the sound field inside a cylindrical tube by making certain simplifications regarding the fluid-shell interface.

The sound field inside the cylinder can be described in terms of a modal summation of solutions of the wave equation which satisfy the given boundary conditions [29]. The solution of the wave equation is straightforward in cylindrical coordinates as outlined below. It is difficult however, to obtain an analytic expression for the cutoff frequencies of the higher-order modes because of the complicated boundary condition between the fluid-shell interface, especially when the fluid considered is water.

We are concerned with the higher-order modes only to the extent of avoiding their excitation as the measuring techniques described in this thesis assume planar propagation. However, they are important not only in describing the behavior of the acoustical field within the tube, but also in considering the interaction of the sound field with the tube walls.

By making simplifications regarding the tube fluid boundary- such as considering the tube to be rigid and the

fluid inside to exert no loading effects on the tube wall, general remarks which are illustrative of the physical system can be made.

The cylindrical coordinate system is given in Figure 40. Starting with the general form of the wave equation:

$$\bar{\nabla}^2 p(r,\theta,Z,t) = \frac{1}{C^2}\frac{\partial^2 p}{\partial t^2} \qquad (A.1)$$

and assuming a time-harmonic solution of the form:

$$p(r,\theta,z,t) = P(r,\theta,z)e^{j\omega t} \qquad (A.2)$$

the wave equation becomes:

$$\frac{\partial^2 p}{\partial r^2} + \frac{1}{r}\frac{\partial p}{\partial r} + \frac{1}{r^2}\frac{\partial^2 p}{\partial \theta^2} + \frac{\partial^2 p}{\partial Z^2} + k^2 p = 0 \qquad (A.3)$$

with $k^2 = \omega^2/c^2$, using the cylindrical form of the Laplacian operator. Assuming the spatial function can be separated into three independent terms,

$$P(r,\theta,z) = R(r)\,\chi(\theta)Z(z) \qquad (A.4)$$

by using the method of separation of variables, the differential equation (A.3), reduces to three ordinary

differential equations:

$$\frac{\partial^2 R}{\partial r^2} + \frac{1}{r}\frac{\partial R}{\partial r} + R\left(k_r^2 - \frac{m^2}{r^2}\right) = 0 \qquad (A.5)$$

$$\frac{\partial^2 \chi}{\partial \theta^2} + m^2 \chi = 0 \qquad (A.6)$$

$$\frac{\partial^2 Z}{\partial Z^2} + k_Z^2 Z = 0 \qquad (A.7)$$

with $k_r^2 = k^2 - k_z^2$. By imposing spherical symmetry on the θ coordinate, single valuedness requires that m be an integer. Equation (A.5) represents Bessel's equation, with a progressive wave solution of the form:

$$R(r) = \bar{A} H_m^{(1)}(k_r r) + \bar{B} H_m^{(2)}(k_r r) \qquad (A.8)$$

where $H_m^{(1)}$ and $H_m^{(2)}$ are Hankel functions of the first and second kind, respectively, and order m. The standing wave solution is in the form of cylindrical Bessel and Neuman functions of order m:

$$R(r) = \bar{A} J_m(k_r r) + \bar{B} N_m(k_r r) \qquad (A.9)$$

Equation (A.6) and (A.7) have as solutions the familiar harmonic waves:

$$\chi(\theta) = \bar{C} e^{jm\theta} + \bar{D} e^{-jm\theta} \qquad (A.10)$$

$$Z(z) = \bar{E} e^{jk_z z} + \bar{F} e^{-jk_z z} \qquad (A.11)$$

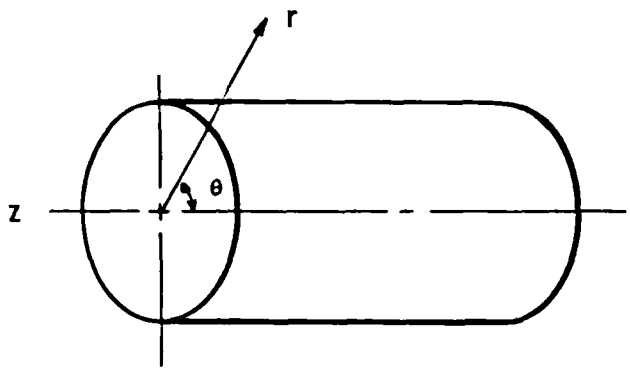

Figure 40. Cylindrical coordinate system used in computing the normal modes of wave propagation in a circular duct.

By substituting back into (A.4) and reinserting the time dependence, the complete solution takes the following form:

$$\begin{Bmatrix} \bar{A}H_m^{(1)}(k_r r) \\ \bar{B}H_m^{(2)}(k_r r) \end{Bmatrix} \begin{Bmatrix} \bar{C}e^{jm\theta} \\ \bar{D}e^{-jm\theta} \end{Bmatrix} \begin{Bmatrix} \bar{E}e^{jk_z z} \\ \bar{F}e^{-jk_z z} \end{Bmatrix} \tag{A.12}$$

Any particular solution will be some combination of the three groups of functions, depending on the physical system and boundary conditions. For finite radius tubes it is more advantageous to use the standing wave forms for the solution:

$$\begin{Bmatrix} \bar{A}J_m(k_r r) \\ \bar{B}N_m(k_r r) \end{Bmatrix} \begin{Bmatrix} \bar{C}\cos m\theta \\ \bar{D}\sin m\theta \end{Bmatrix} \begin{Bmatrix} \bar{E}\cos k_z z \\ \bar{F}\sin k_z z \end{Bmatrix} \tag{A.13}$$

or some combination of the two.

For wave motion inside an infinitly long cylinder, where the solution must be finite everywhere inside the tube, the solution takes the form:

$$p = \bar{A}_m e^{j(\omega t - k_z z + m\theta)} J_m(k_r r) \tag{A.14}$$

where the values of k_r are determined by specifying the boundary condition at the tube wall (r=R).

For a rigid tube, the radial component of the velocity is considered to be zero at the tube wall, resulting in the following boundary condition:

$$\frac{\partial}{\partial r} J_m(k_r r)_{r=R} = k_r J_m'(k_r R) = 0 \tag{A.15}$$

or $k_r R = \alpha_{mn}$, where α_{mn} are the roots of $J_m'(\alpha_{mn}) = 0$. m denotes the order of the Bessel function and n denotes the root number. Figure 41 shows a chart for the values of $J_m'(\alpha_{mn})=0$. [29]

Any particular mode can then be described as:

$$p_{mn} = A_{mn} J_m(k_{mn} r) e^{j(\omega t - k_z z + m\theta)} \qquad (A.16)$$

where $k_{mn}=\frac{\alpha_{mn}}{R}=k_r$ and $k_z^2=k^2-k_{mn}^2$. This is a progressive wave solution for waves propagating down an infinitely long duct. It can be seen that the wavenumber $k_z = \sqrt{k^2-k_{mn}^2}$ will be imaginary for $k^2<k_{mn}^2$ (i.e. below cutoff). Any particular higher-order mode with cutoff frequency:

$$f_{mn} = \frac{\omega_{mn}}{2\pi} = \frac{k_{mn} c}{2\pi} = \frac{\alpha_{mn} c}{2\pi R} \qquad (A.17)$$

will not propagate as long as $f<f_{mn}$, as the exponential involving the z coordinate will be entirely real, signifying an exponential decay of the sound field in the z direction. The plane wave mode is given by:

$$p_{oo} = A e^{j(\omega t - k_z z)} \qquad (A.18)$$

where $k_z = k = \omega/c$. (i.e. the axial wave number is equal to the free-field wavenumber.)

Figure 42 illustrates the nature of the first few higher order modes, where the radial pressure amplitude is given by the magnitude of the Bessel function. The values

THE FIRST ROOTS OF $J_m'(\alpha_{mn}) = 0$

m	n=0	n=1	n=2	n=3
0	0	3.83	7.02	10.17
1	1.84	5.33	8.54	11.71
2	3.05	6.71	9.97	13.17
3	4.20	8.02	11.35	14.59

Figure 41. Tabulation of the value of the roots of the derivative of the Bessel Function of the first kind of order m.

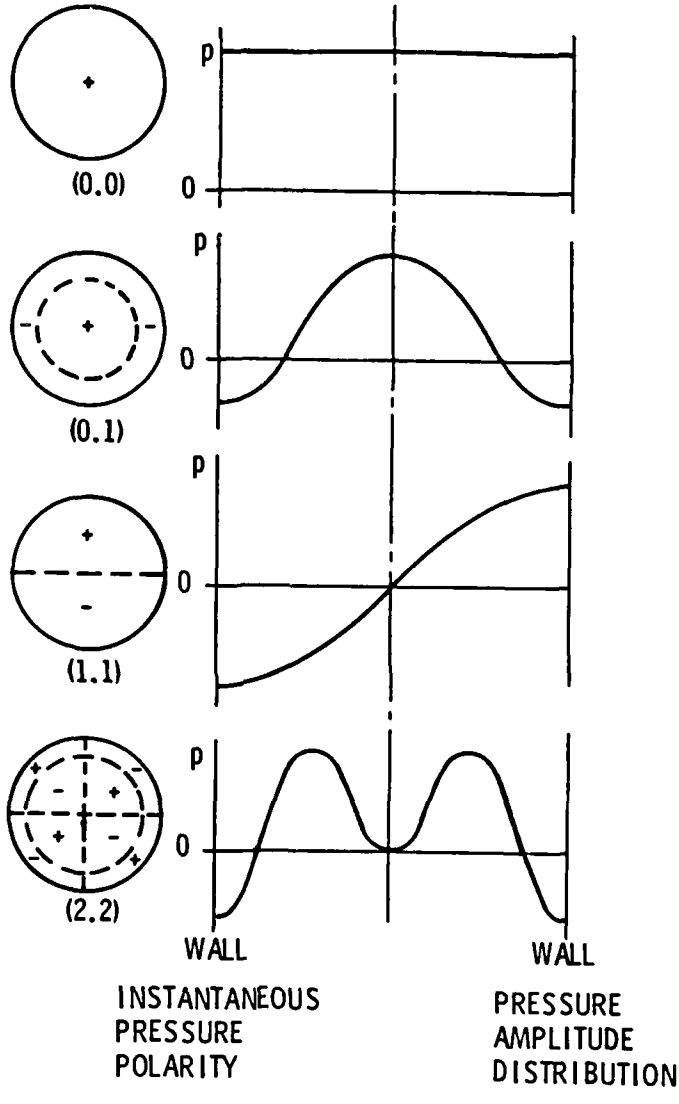

Figure 42. Instantaneous pressure polarity (left) and corresponding pressure amplitude distribution (right) for four transverse modes of a circular duct with rigid walls.

for the cutoff frequency of any particular mode can be determined from Equation A.17, where the values for α_{mn} are given in Figure 41. By referring to the figure, the lowest cutoff mode for the rigid tube is given by $\alpha_{10}=1.84$, corresponding to a frequency of

$$f_{10} = \frac{.293c}{R} \quad \text{or} \quad \lambda = \frac{R}{.243} = \frac{2R}{.586} \simeq 2D \qquad (A.19)$$

i.e. only planar waves will propagate as long as the wavelength is longer than twice the tube's diameter.

The plane wave mode can be excited at all frequencies, and the presence of higher-order modes when the tube is excited above their respective cutoff frequencies is dependent on the manner in which the tube is excited. If the excitation is from an ideal plane piston it should be possible to concentrate most of the energy in the plane-wave mode, even though the tube is excited above the cutoff frequencies of various higher-order modes [22].

APPENDIX B

THE TUBE-FLUID INTERACTION

This appendix outlines some of the more significant mechanisms of the tube-fluid coupling, and the possible effects on the measuring scheme in question.

Walter [30] demonstrated experimentally for air-filled tubes that the primary interaction between the tube-fluid system takes place at the so called "coincidence" frequencies, where the circumferential order m and phase velocity of the acoustic mode matches that of the bending mode of the shell. (See [30] for an excellent description of coincidence). He also developed an analytical expression based on a decoupled tube-fluid model which accurately predicted the coincidence frequencies of air-filled tubes. Coincidence occurs close to the cutoff frequency of the acoustic mode. Unlike a plate (from which the analogy is taken and which has only one coincidence frequency), the shell-fluid system can have many different frequencies on account of the dispersive nature of the two systems.

Difficulties can develop from using the decoupled model to predict the coincidence frequencies or behavior of water-filled tubes, because the systems cannot be considered independent [30]. The dispersion relationships predicted by

using the uncoupled model will no longer be valid and a complicated system in which the shell and fluid are coupled must be considered.

The problem encountered in this thesis is of a simplier nature in that the tube will be operating below the first cutoff frequency where only the plane-wave acoustic mode is considered to be propagating in the tube. There should be no problem of severe coupling through coincidence type phenomenon with higher-order bending modes in the tube wall, because the circumferential orders would not match that of an acoustic plane wave inside the tube.

The axial boundary conditions are not considered, as coincidence is not associated with a resonance determined by the axial terminations. The coupling takes place, rather, as the waves are propagating in the axial direction. There may however, be coupling near the axial boundaries of the tube, similar to the coupling causing the edge radiation of a plate below coincidence [31]. The great difference between wavelengths in the tube wall and fluid will generally cause cancellation due to the incoherency of the two fields, except near the boundaries, where the volume flow may not completely cancel. The wave equation would have many higher order terms needed to satisfy the axial boundary conditions, and these "evanescent" waves cause distortions near the boundaries that may increase the coupling.

The effect of the compliance of the tube wall on the plane-wave acoustic mode should also be considered. By ignoring the bending stiffness of the tube (which he shows to be a reasonable approximation below the "ring" frequency) and treating the tube-fluid interaction as a "local" effect, confined to an immediate ring area of tube-fluid interface, Skudrzyk [29] has derived the so called Korteweg formula. This formula relates the effective propagation velocity of sound in tubes with compliant walls, with the free-field propagation velocity, by accounting for the apparent change in compressibility of the fluid caused by the expanding tube wall. The ratio of effective velocity to free-field velocity is as follows:

$$\frac{C_{eff}}{C_o} = \frac{1}{\sqrt{1 + \frac{\rho_1 C_1^2 R}{\lambda_{Eh}}}} = \frac{1}{\sqrt{1 + \frac{\rho_o C_1^2 R}{\rho_\omega C_\omega^2 h}}} \qquad (B.1)$$

where ρ_o is the density of the fluid, c_0 the free-field sound velocity in the fluid, R is the tube radius, h the tube thickness, and λ_E is Young's modulus for the tube material. In the second equation, λ_E has been replaced by $\rho_w c_w^2$, where ρ_w is the density and c_w is the velocity of sound for the material of which the tube is comprised. It can be seen that the effect of the compliance is to slow down the propagation velocity of the plane wave, with the effect becoming more pronounced for thin-walled or large diameter tubes.

For the most part, these added complications can be overcome be ensonifying the tube with pulses at frequencies below the first cutoff [31]. The pulse incident upon the termination of the tube should then resemble a plane wave in a free-field environment, with the possible exception of the propagation velocity being slower due to the increased compliance of the tube walls.

APPENDIX C

SIGNAL PROCESSING PROCEDURES AND ERROR CONSIDERATIONS

This appendix describes in more detail the signal processing procedures and error consideration in estimating the transfer function $\bar{H}(f) = \bar{P}_2(f)/\bar{P}_1(f)$ of the pressure in the tube between points x_1 and x_2.

The transfer function is estimated by feeding the output of the transducers at locations x_1 and x_2 into a dual channel FFT processor, in this case a Spectral Dynamics SD-360, which then performs the required signal processing. This analyzer takes sample blocks of data for each channel consisting of 1024 samples. The estimated transfer function is then sent to a PDP-11 computer as 512 real and 512 imaginary numbers for further processing. To better understand the errors involved, the mathematical details of the signal processing are given below.

The transfer function $\bar{H}(f)$ is equivilent to the ratio of the cross-spectral density between the pressures measured at locations 1 and 2, normalized by the autospectral density of the pressure at location 1 [32]:

$$\bar{H}(f) = \frac{G_{12}(f)}{G_{11}(f)} \qquad (C.1)$$

The cross-spectral density or cross-spectrum and the auto-spectral density or auto-spectrum are defined as follows:

$$G_{12}(f) = \lim_{T\to\infty} \frac{2}{T} E\left[P^{*}_{1k}(f_1 T)\, P_{2k}(f_1 T)\right]$$
$$G_{11}(f) = \lim_{T} \frac{2}{T} E\left[P^{*}_{1k}(f_1 T)\, P_{1k}(f_1 T)\right] \qquad (C.2)$$

where

$$P_{12}(f_1 T) = \int_o^T P_{1k}(t) e^{-j\omega t} dt$$
$$P_{2k}(_1 T) = \int_o^T P_{2k}(t) e^{-j\omega t} dt \qquad (C.3)$$

are the finite Fourier transforms over the k_{th} record of length T. The expected value operator E denotes an averaging operation over the index k.

The integrals are evaluated by taking a collection of sample records, n_d, each of length T, performing the finite Fourier transforms by an FFT algorithm, and then performing the expected value operation by averaging the results. In the case of the fixed point processor, the sampling time T is determined by dividing the number of block samples by twice the bandwidth selected (i.e. T = 1024/2B) where B is the analysis range. The total amount of data analyzed is then $T_{total} = n_d T$. Since the limiting operation T can never be obtained in practice, this

results in an estimate of the true value of the cross and auto-spectral densities:

$$\hat{G}_{12}(f) = \frac{2}{n_a t} \sum_{k=1}^{n_d} X_k^*(f,T)\, Y_k(f,T) \qquad (C.4)$$

$$G_{11}(f) = \frac{2}{n_d t} \sum_{k=1}^{n_d} X_k^*(f,T)\, X_k(f,T) \qquad (C.5)$$

These estimates are for discrete frequency intervals seperated in frequency $\Delta f = 1/T$ on account of the digital evaluation of the finite Fourier transforms. This interval is determined by the record length T of each sample taken and not the total amount of data analyzed $T_{total} = n_d T$.

If, when sampling pulses, the record length T is larger than the pulse length, a certain number of samples, either at the beginning or end of the sample block, will be equal to zero. In this case the actual resolution is determined by the pulse length $f = 1/T_p$. If the input data is not weighted, the values at intermediate frequency bins will simply be interpolated [33].

The above estimation process leads to two kinds of errors: random and bias errors. It should be mentioned that these errors are in addition to others that may occur during the experimental procedure. Random errors are a scattering of the analysis results from one sample to the next of the same random data, and are a result of the fact that the limiting procedure in Equations C.4 and C.5 is accomplished by taking a finite number of sample records n_d.

Generally, the random errors are inversely proportional to the square root of the number of records taken. Bias errors are consistent from measurement to measurement and are asssociated with windowing operations, such as that in Equation C.4 for the spectral density estimate. Bias errors can also arrise from nonlinearities in the system as well as from noise present at one input that does not pass through the system. The bias errors may be a significant problem when the data contains sharp spectral peaks.

Bendat and Piersol [34] discuss approximate error formulas to be used when estimating the transfer function $\bar{H}(f)$ by the formula $\hat{G}_{12}/\hat{G}_{11}$. Generally such an estimate will involve both random and bias errors. In most cases the coherence function, defined as:

$$\hat{\gamma}^2_{12}(f) = \frac{|\hat{G}_{12}(f)|}{\hat{G}_{11}(f)\ \hat{G}_{22}(f)} \tag{C.6}$$

will indicate the presence of such errors and is useful for evaluating their magnitude. Specifically, the normalized random error for the estimate of the transfer function $\tilde{H}(f)$ is given by:

$$\varepsilon[|H(f)|] \simeq \left[\frac{1 - \gamma^2_{12}(f)}{2n_d\ \gamma^2_{12}}\right]^{\frac{1}{2}} \tag{C.7}$$

for the magnitude estimate, and

$$\varepsilon[\phi(f)] \simeq \sin^{-1}\{\varepsilon[|H(f)|]\} \tag{C.8}$$

for the phase estimate.

Seybert and Soenarko [13] discuss the random and bias errors resulting form making impedance measurements in tubes using random excitation. Briefly, the bias errors can be minimized by keeping the analysis bandwidth small, and by keeping the microphone locations close to the sample surface. The random errors can be minimized by keeping the coherence high between the transducers (see Equation C.7). This can be accomplished by minimizing noise sources and by keeping the microphone spacing small. However, the accuracy at low frequency measurements will be reduced because of the decreased separation between the microphones. In addition, there will be a large drop in the coherence function when one of the microphone positions coincides with a node in the pressure field. They also report experimental results from Rapp [13], who found that the largest errors in measuring acoustic properties of materials using multiple microphones was due to the phase angle measurement uncertainty. The largest error occured when the phase angle was near zero or 180 degrees as for highly reflective surfaces.

APPENDIX D

PIEZOELECTRIC COEFFICIENTS AND TRANSDUCER SENSITIVITY

This appendix describes in more detail, the behavior of the various piezoelectric transducers considered in this thesis.

The piezoelectric coefficients most useful for describing the behavior of the transducers in underwater applications are the piezoelectric charge coefficients d_{31}, d_{32}, d_{33}, and the piezoelectric voltage coefficients g_{31}, g_{32}, and g_{33}. The subscripts refer to the three axes identifying orthogonal directions in the material, and are analogous to the X, Y, Z coordinates. The 3 axis is taken parallel to the direction of polarization in the material. The first subscript refers to the surfaces perpendicular to the axis on which the charge is collected. The second subscript refers to the surfaces perpendicular to the axis on which the force is impressed. The charge coefficients d_{ij} (coulombs/newton or meters/volt) relates the electric charge E_i generated per unit area to the force F_j applied per unit area (direct effect) or the mechanical strain S_j produced by an electric field E_i (inverse effect). The voltage coefficients g_{ij} relate the electric field E_i produced by an applied mechanical stress T_j. At frequencies far from any resonances, a piezoelectric material behaves as

a capacitor and the charge and voltage coefficients are related by the dielectric constant in the direction perpendicular to the electrodes.

Sessler [23] concludes from experimental data on the temperature dependence of the various coefficients, that the primary piezoelectric activity of PVDF is the longitudinal thickness effect, described by the 33 coefficients (see Figure 43). The transverse effect, described by the 31 and 32 coefficients is due to a lateral constraction of the film determined by Poisson's ratio in the 31 and 32 directions (see Figure 43).

The current application of the transducers is best described by the hydrostatic piezoelectric constant given by [23]:

$$-d_{3h} = d_{31} + d_{32} + d_{33} \qquad (D.1)$$

This constant takes into account the lateral contraction in the 1 and 2 direction experienced by the material as it expands in the 3 direction (longitudinal effect) in a hydrostatic field. As the 31 and 32 coefficients are of opposite sign to the 33 coefficient, the sensitivity will be lower than that calculated using the 33 coefficient only. The output voltage of the device is then given by $g_{3h}t$, where $g_{3h} = d_{3h}/\kappa_3\varepsilon_o$, and t is the thickness of the film. κ_3 is the relative dialectric constant in the 33 direction, and ε_0 is the permittivity constant.

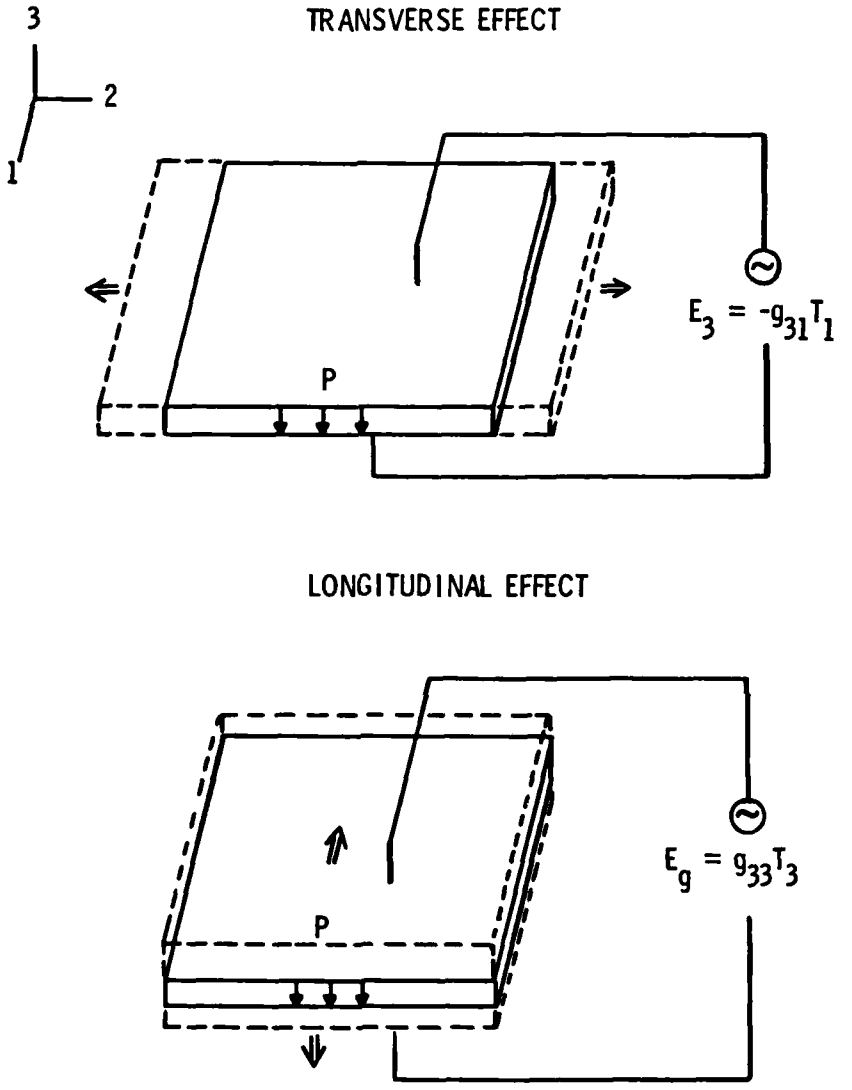

Figure 43. Illustration of the piezoelectric effect associated with the transverse (upper) and the longitudinal (lower) deformations.

The epoxy filling in the PZT composite transducers lessens the lateral contractions in the 1 and 2 directions as it expands in the 3 direction, thus enhancing the hydrostatic piezoelectric coefficient.

The equivalent electrical circuit of any piezoelectric transducer is a LCR series circuit for the motional impedance arm combined in parallel with a capacitance C_o in the electrical arm [35]. At low frequencies (well below the thickness expansion resonance), the circuit reduces to that shown in Figure 44. The voltage response $|E_o/p_b|$ is given by:

$$[C_{EM}/(C_o+C_{EM})]\ (S_y/\phi) = k^2\ (S_y/\phi_f) = g_{ij}t \qquad (D.2)$$

where k^2 is the ratio of the mechanical energy versus the total energy stored in the piezoelectric material. k^2 is called the electro-mechanical coupling coefficient and is equivilent to $g_{ij}t\,\phi_f/S_y$. ϕ_f is the transformation factor, and t is the thickness between the electrodes. The voltage response can then be written simply as $|E_o/p_b| = g_{ij}t$ as before.

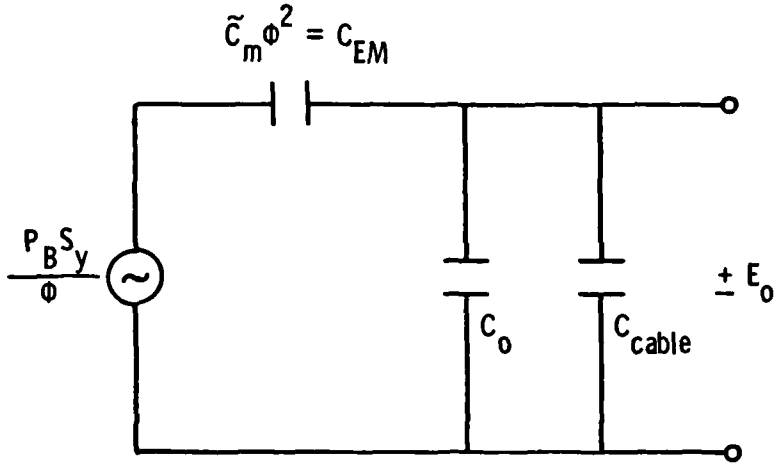

Figure 44. Low frequency equivalent circuit for a typical piezoelectric transducer, including the capacitance of the connecting cable.

DISTRIBUTION LIST FOR TM 82-246

Commander (NSEA 0342)
Naval Sea Systems Command
Department of the Navy
Washington, DC 20362 — Copies 1 and 2

Commander (NSEA 9961)
Naval Sea Systems Command
Department of the Navy
Washington, DC 20362 — Copies 3 and 4

Defense Technical Information Center
5010 Duke Street
Cameron Station
Alexandria, VA 22314 — Copies 5 through 10